LIN28B CONFERS CANCER STEM-LIKE PHENOTYPES FOR NEUROENDOCRINE

PROSTATE CANCER PROGRESSION

by

JESSICA MAGDALENA LOVNICKI

B.Sc. (Hon.), University of Guelph, 2017

A THESIS SUBMITTED IN PARTIAL FULFILLMENT OF

THE REQUIREMENTS FOR THE DEGREE OF

MASTER OF SCIENCE

in

THE FACULTY OF GRADUATE AND POSTDOCTORAL STUDIES

(Reproductive and Developmental Sciences)

THE UNIVERSITY OF BRITISH COLUMBIA

(Vancouver)

August 2019

The following individuals certify that they have read, and recommend to the Faculty of Graduate and Postdoctoral Studies for acceptance, a thesis entitled:

LIN28B CONFERS CANCER STEM-LIKE PHENOTYPES FOR NEUROENDOCRINE

PROSTATE CANCER PROGRESSION

Submitted by   Jessica Magdalena   in partial fulfillment of the requirements for

the degree of   Master of Science

in   Reproductive and Developmental Sciences

Examining Committee:

Xuesen Dong, Urological Sciences

Supervisor

Ralph Buttyan, Urological Sciences

Supervisory Committee Member

Nathan Lack, Urological Sciences

Supervisory Committee Member

Cathie Garnis, Integrative Oncology

External Committee Member

Abstract

Due to the increased utilization of next generation anti-androgens to treat prostate adenocarcinoma (AdPC), therapy-induced neuroendocrine prostate cancer (t-NEPC) has become more prevalent. Although the mechanisms by which t-NEPC is established are not fully understood, emerging evidence suggests that AdPC cells can gain an intermediate pluripotent stem cell (SC)-like phenotype that can promote t-NEPC development. However, it remains unclear whether the core embryonic stem cell genes (ESCs) (LIN28, POU5F1, SOX2, and NANOG) regulate the stem-like state of prostate cancer cells and the switch from luminal epithelial to neuroendocrine lineage during the transition from AdPC to t-NEPC. We hypothesize that LIN28B plays a key role in the transition from AdPC to t-NEPC, and that the overexpression of LIN28B may promote proliferation and trans-differentiation, which may contribute to t-NEPC progression.

By comparing the published RNA-seq data on AdPC and t-NEPC, we found that approximately 50% of t-NEPC patient tumors have gained LIN28B and SOX2 expression. Standard molecular and cellular biology techniques were applied to characterize the functions of LIN28B and its relationship with SOX2 using t-NEPC cell and xenograft models. We found that the mRNA levels of LIN28B and SOX2 are positively correlated in patient tumors, patient derived xenografts, transgenic mice, and multiple cell models. LIN28B and SOX2 expression was confirmed to be co-upregulated in a subset of t-NEPC patients by immunohistochemistry. Using our clinically relevant t-NEPC cell/xenograft model, DuNE, we demonstrated that LIN28B is essential for stem cell-like and neuroendocrine marker expression and cell morphology. LIN28B gene depletion by CRISPR inhibited DuNE xenograft initiation and tumor growth. These

LIN28B functions are mainly mediated by its inhibitory effects on the microRNA let-7d, which resulted in the upregulation of HMGA2 and HGMA2 mediated SOX2 transcription.

Overall, this thesis work adds to the understanding that the LIN28B/let-7/SOX2 axis is an important signaling pathway that regulates a cancer stem-like phenotype to promote t-NEPC development. Ultimately, this knowledge pertains to the clinical implications of LIN28B in informing future therapies that will be effective for managing t-NEPC.

Lay Summary

Prostate cancer is the most commonly diagnosed cancer among males and is the third leading cause of death from cancer in males in Canada. Currently, the primary treatment for advanced prostate cancer is hormonal therapy. However, recent findings indicate that this treatment can cause tumors to transform into a more aggressive cancer called treatment-induced neuroendocrine prostate cancer (t-NEPC). I investigated a novel mechanism where the development of a subset of t-NEPC tumors is driven by the gene LIN28B and the microRNA let-7d, which are known to contribute to embryogenesis and stem cell development. I also demonstrated a positive correlation between LIN28B and a gene called SOX2. LIN28B expression was sufficient to enhance SOX2 expression and stem cell properties in a prostate cancer cell model. I also identified the gene HMGA2 as a downstream effector of LIN28B and a key regulator of SOX2 expression.

Preface

All of the work presented henceforth was conducted in the Vancouver Coastal Health Research Institute at the Vancouver Prostate Centre, Jack Bell Research Centre, and Robert NH Ho buildings. All projects and associated methods were approved by the University of British Columbia Biosafety Committee (protocol #B13-0187). All animal procedures were performed in accordance with the guidelines and regulations of the Canadian Council on Animal Care and approved by the Institutional Animal Care and Use Committee at the University of British Columbia (protocol #A18-0065).

Dr. Xuesen Dong was the principal investigator of this study. The experimental design and data interpretation were done by myself, Dr. Yu Gan, and Dr. Xuesen Dong. Ning Xie trained me with molecular and cellular techniques with which I performed the experiments described in this thesis and assisted with technical support. Sonia Kung and Dr. Ladan Fazli from the Pathology Core of the Vancouver Prostate Centre prepared and conducted immunohistochemistry analyses, respectively. Mary Bowden from the Animal Model Core of the Vancouver Prostate Centre assisted with the xenograft studies.

Table of Contents

List of Tables

List of Figures

List of Abbreviations

7-AAD	7-Aminoactinomycin D
AUA	American Urological Association
AMH	Anti-Müllerian hormone
AR	Androgen receptor
ARPI	Androgen receptor pathway inhibition
ATCC	American Type Culture Collection
AURKA	Aurora kinase-A
BMI	Body mass index
BPH	Benign prostatic hyperplasia
CCHC	Cysteine cysteine histidine cysteine
CHGA	Chromogranin A
CHGB	Chromogranin B
CK	Cytokeratin
CRPC	Castration-resistant prostate cancer
CRPC-Ad	Castration-resistant prostate adenocarcinoma
CSC	Cancer stem cell
CSD	Cold shock domain
CSS	Charcoal stripped serum
CZ	Central zone
DBD	DNA binding domain
ddH$_2$O	Double-distilled water
DKO	Double knockout
DMEM	Dulbecco's Modified Eagle Medium
DTT	Dithiothreitol
EAU	European Association of Urology
EDTA	Ethylenediaminetetraacetic acid
EMT	Epithelial-mesenchymal transition
ESC	Embryonic stem cell
FACS	Fluorescence-activated cell sorter
FBS	Fetal bovine serum
FGF	Fibroblast growth factor
GEMM	Genetically engineered mouse model
GEO	Gene Expression Omnibus
GO	Gene oncology
gRNA	Guide RNA
GSEA	Gene set enrichment analysis
GWAS	Genome wide association studies
HCC	Human hepatocellular carcinoma
HPG	Hypothalamus-pituitary-gonadal
ICM	Inner cell mass

IF	Immunofluorescence
IGF2	Insulin-like growth factor 2
IHC	Immunohistochemistry
iPSCs	Induced pluripotent stem cells
LBD	Ligand binding domain
LE	Luminal epithelium
LIN28A	LIN-28 homolog A
LIN28B	LIN-28 homolog B
LN95	LNCaP95
LTL	Living tumor library
MAPK	Mitogen-activated protein kinase
miRNA	microRNA
mRNA	Messenger RNA
MSI1	Musashi 1
NCP	Nucleocapsid protein
NE	Neuroendocrine
NEdT	Neuroendocrine transdifferentiation
NEPC	Neuroendocrine prostate cancer
NLS	Nuclear localization signal
NoLS	Nucleolar localization signal
NSE	Neuron specific enolase
NTD	N-terminal domain
PCa	Prostate cancer
PDGF	Platelet derived growth factor
PSA	Prostate specific antigen
PVDF	Polyvinylidene difluoride
PZ	Peripheral zone
qPCR	Quantitative polymerase chain reaction
RB1	Retinoblastoma 1
RNA	Ribonucleic acid
RPMI-1640	Roswell Park Memorial Institute 1640
SC	Stem cell
SCLC	Small cell lung cancer
SCNC	Small neuroendocrine carcinoma
SDS	Sodium dodecyl sulfate
SKO	Single knockout
Spg-let-7	let-7 SPONGE
SRY	Sex determining region Y
SU2C	Stand Up 2 Cancer
SYP	Synaptophysin
TBS-T	Tris-buffered saline plus TWEEN-20

TKO	Triple knockout
TMA	Tissue microarray
t-NEPC or CRPC-NE	Treatment-induced neuroendocrine prostate cancer
TNM	Tumor, node, and metastasis
TP53	Tumor protein 53
TUT4	Terminal uridyl transferase 4
TUT7	Terminal uridyl transferase 7
TZ	Transition zone
UGM	Urogenital sinus mesenchyme
VPC	Vancouver Prostate Centre
WT	Wild type

Acknowledgements

First and foremost, I would like to thank my supervisor, Dr. Xuesen Dong, for providing me with the opportunity to complete my graduate studies under his supervision. Your mentorship and guidance have been invaluable, and I am grateful for all of the opportunities you have provided me with over the past two years. Our many stimulating discussions have shaped the way I think about problems and I thank you for your insight. I would also like to thank the members of my supervisory committee, Dr. Ralph Buttyan, Dr. Nathan Lack, and Dr. Cathie Garnis, as well as Dr. Ladan Fazli for their guidance, support, and constructive recommendations throughout my tenure at the Vancouver Prostate Centre.

I could never have completed this project without help from the members of the Dong lab: Ms. Ning Xie, Dr. Ahn Lee, Dr. Yinan Li, Dr. Yu Gan, and Miss Yuliia Kovalchuk. Being able to bounce ideas back and forth, troubleshoot, and collaborate made it a great lab to work in during my graduate studies. Your support and friendship are much appreciated.

My most sincere gratitude goes out to my family and friends who have supported me throughout this endeavor. To A.S. and R.H., thank you for your long-distance support throughout my many failing experiments. Your friendship and encouragement throughout my degree has kept me sane and allowed me to accomplish everything I could have ever imagined. To L.K., your ability to always make me laugh and to redirect my focus to opportunities on the horizon when I fixate on the challenges before me has truly helped me to become a better researcher and person, thank you.

To my parents, as well as to my sister and CeeCee, I am forever grateful for all the love and support you have given me not only during my graduate studies, but throughout my entire life in all the endeavours that I have pursued. As my mom and dad, you have taught me the value of hard work and how to strive to be the best person I can be. The completion of this thesis would not be possible without you, thank you.

Dedication

Success is a process for all of us, and as long as you are making consistent progress towards your goals - sincerely giving your best effort more often than not - then you are already successful and deserve to feel proud of yourself.

Hal Elrod

Chapter 1: Background, Hypothesis, and Objective

1.1 Prostate cancer

1.1.1 Overview

According to a 2018 report from Canadian Cancer Statistics, prostate cancer (PCa) is the most commonly diagnosed cancer among males and is the third leading cause of death from cancer in males in Canada (1). As of 2018, 1 in 7 Canadian men will develop PCa, and 1 in 29 will die from the disease (2). While the mortality rate of PCa has declined since the 1990s as a result of improved treatments and methods for early detection of the disease, PCa continues to place an immense financial burden not only on the patients themselves, but on their family members as well as society as a whole (3). As of 2000, the annual direct medical costs alone from PCa in Canada totalled $3.89 billion (4). This thesis aims to expand upon previously solidified knowledge on PCa to increase the scientific community's understanding of the disease.

1.1.2 The Prostate

The prostate is a small, walnut-sized gland that is part of the male reproductive system. It is located below the bladder, above the pelvic floor, and surrounds the urethra (Figure 1.1) (5). To initiate the process of sexual differentiation, the sex-determining region of the Y chromosome (SRY) directs a network of genes to begin testes development (6). During week six of embryonic development Leydig cells, which are located in the testes, secrete testosterone (6). Testosterone secretion then leads to the release of anti-Müllerian hormone (AMH) from the Sertoli cells during week seven of embryonic development, which in turn leads to the atrophy of the paramesonephric, or

Müllerian, ducts (6, 7). In humans, prostate development begins during week ten of gestation (5, 8). In order for the prostate to develop, the urogenital sinus mesenchyme (UGM) must first signal to the epithelium, which causes the formation of epithelial buds (5). Androgen receptors (AR) that are located in the UGM are stimulated by testosterone, which causes epithelial budding, morphogenesis, and differentiation into basal and epithelial subtypes (9, 10). By the end of week fifteen of gestation, the prostate is comprised of stromal and epithelium compartments, the latter of which consists of three fully distinguishable cells types: basal epithelial cells, luminal epithelial cells, and neuroendocrine cells (Figure 1.2) (8). Basal cells are located alongside the basement membrane, are AR negative, and express cytokeratin (CK) 5, CK14, CD44 and p63 (8). There is also evidence that basal cells are partially comprised of a regenerative stem cell population (11, 12). Luminal epithelium (LE) cells are found adjacent to basal cells, are tall and columnar, and express AR, prostate specific antigen (PSA), CK8, CK18, CD24, and CD26 (8). Neuroendocrine (NE) cells express chromogranin A (CHGA) and are characterized by their lack of AR and PSA (8).
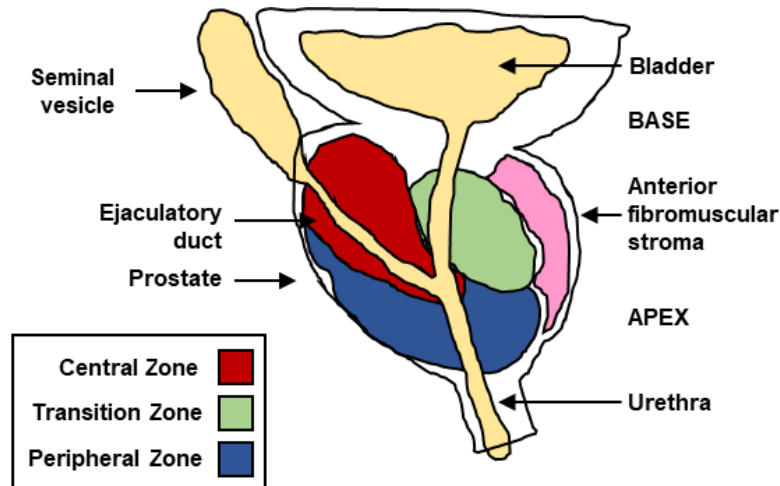
Figure 1.1 Human prostate location and zones. A depiction of the location of the prostate gland and its subdivided zones relative to the seminal vesicle and bladder. *Original drawing adapted from https://www.cancer.ca/en/cancer-information/cancer-type/prostate/prostate-cancer/the-prostate/?region=on.*
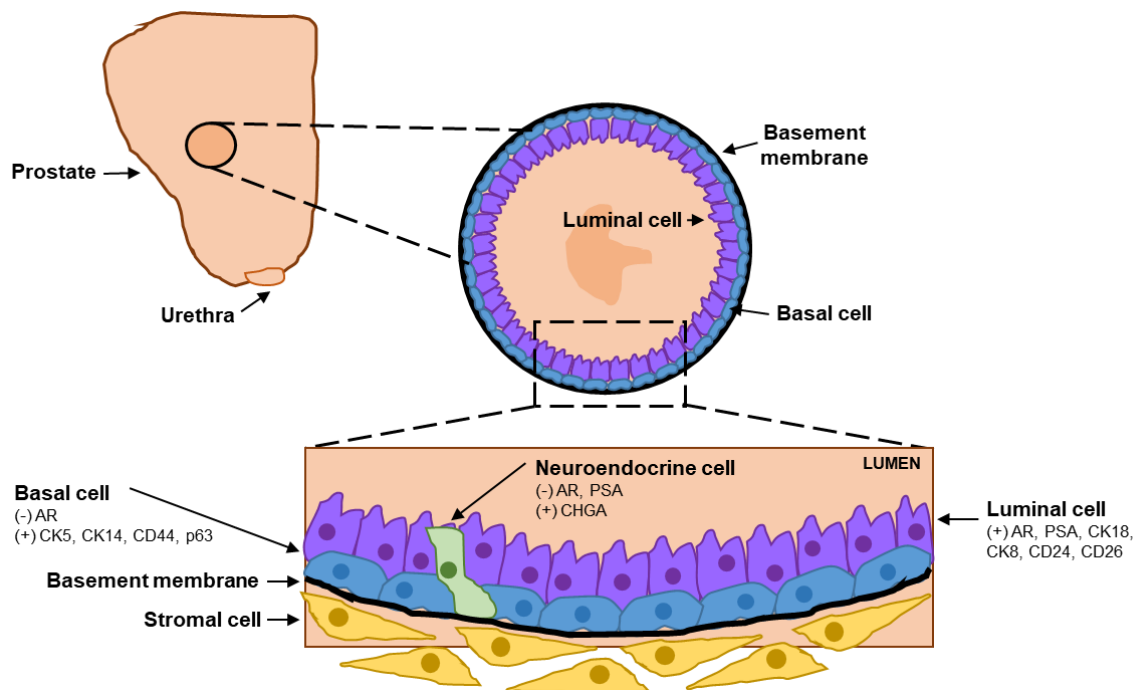
Figure 1.2 Prostate tissue structure. A depiction of cell types that are present in the prostate. *Original drawing adapted from Toivanen R and Shen M "Prostate organogenesis: tissue induction, hormonal regulation and cell type specification" (2017). Development (10.1242/dev.148270).*

In males 1 to 10 years of age, the average weight of the prostate is 2 grams (5). However, the prostate will continue to grow throughout a male's lifetime. At puberty, the prostate will grow exponentially to be approximately 20 grams (5). This increase in size is positively correlated with an increase in serum testosterone levels (5). Anatomically, the adult prostate is divided into three histological zones: the peripheral zone (PZ), central zone (CZ), and transition zone (TZ) (Figure 1.1) (13, 14). The PZ is derived from the urogenital sinus, comprises 70% of the prostatic tissue, and is the region where most PCa develops (15). The CZ is derived from the Wolffian duct, comprises 20-25% of the prostatic tissue, and has a very low incidence of PCa (16). Lastly, the TZ surrounds the urethra, is derived from epithelial cells and fibromuscular stroma, and is more likely to develop benign prostatic hyperplasia (BPH) (16).

Physiologically the prostate, along with the seminal vesicle, is primarily responsible for producing ejaculate as well as secretions that are related to semen gelation, coagulation, and liquefaction (5, 17). The secretory proteins that the prostate releases are involved in coating the ejaculated spermatozoa as a way to increase sperm motility (17). An important secretory glycoprotein that is released by the prostate gland is PSA, also known as kallikrein-3, which is used as a biomarker to diagnose PCa (8). PSA is a serine protease of the kallikrein-related peptidase family and is secreted from the epithelial cells of the prostate gland (8).

1.1.3   The Role of AR in the Prostate

As mentioned, the prostate gland will grow exponentially at puberty (5). This growth is regulated by the activation of the AR by steroid hormones, which are also known as androgens. AR is a ligand dependent transcription factor (18). As a member of the nuclear receptor family, the AR consists of a constitutively active N-terminal domain (NTD), DNA binding domain (DBD), and a ligand dependent C-terminal ligand binding domain (LBD) (18). The DBD binds the AR to promoter and enhancer regions of AR-regulated genes through DNA binding, which causes the activation of the NTD, LBD, and the subsequent transcription of AR-regulated genes (18).

In the adult prostate, AR-signalling occurs in the LE cells (19). Through the hypothalamus-pituitary-gonadal (HPG) axis, gonadotropin-releasing hormone (GnRH) is secreted from the hypothalamus, which in turn stimulates the anterior pituitary to secrete luteinizing hormone (LH) (19). LH then binds to receptors on Leydig cells in the testis which stimulates the release of testosterone (19). Testosterone is the main androgen found in males. Testosterone is then taken up by prostate stromal cells and is converted into dihydroxytestosterone (DHT). DHT will then bind to the AR in the cytoplasm of LE cells (18). The binding of DHT to AR will cause it to dimerize, activate, and translocate into the nucleus, where it will interact with chromatin remodeling complexes. Activated AR dimers will recruit co-factors and bind to androgen response elements within the enhancer regions of its target genes. This will then activate the transcription of AR-target genes that encode for growth factors and secretory proteins, such as PSA. During adulthood, AR-signaling is regulated in stromal cells, and its role is to maintain homeostasis of the prostate epithelial cells. Therefore, androgens and AR

signalling play a key role not only in the development of the prostate, but in the growth and survival of primary PCa.

1.1.4 Prostate Cancer

Currently, the confirmed risk factors that contribute to PCa development are age, race, genetics, and family history (20). After PSA screening was introduced, the average age of men diagnosed with PCa was 67 (21). There is a positive correlation between older age at diagnosis and high-risk prostate cancer (22). Based on a cohort study completed using a nationwide prostate cancer registry in the United States of America, approximately 25% of men older than 75 had feature that were characteristic of high-risk prostate cancer, whereas the proportion of men younger than 75 that presented with features associated with high-risk prostate cancer was less than 15% (22). Race and ethnicity have also been found to impact an individual's probability of developing PCa. Studies have reported that African-Americans or men of black African heritage have a higher incidence of the disease and are more likely to die from PCa compared to white males (21, 23). Despite these consistent observations, it is also known that the ability to access adequate medical care varies by geography and socioeconomic status (24). These variables confound the ability to make strong inferences about the relationship between race, ethnicity, geography, socioeconomic status, and prostate cancer diagnosis. Additional research should be completed to determine if socioeconomic status, race, and geography contribute to the disparity in PCa outcomes. Furthermore, having a family history of PCa may result in an increased risk of developing the disease (25). However this has been found to vary with the

degree of relatedness and the number of relatives that have been affected (25). Men with a family history of PCa have a 30%-60% probability of developing the disease by age 75, compared to a 4.8% probability in those who did not have a family history (26).

While obesity is not a confirmed risk factor that contributes to PCa development, recent studies have observed a causal relationship between diet, obesity, and a higher incidence of aggressive PCa. Obese men have a higher risk of being diagnosed with high-grade aggressive PCa, a higher incidence of PCa recurrence after surgery or radiation, and an increased risk of PCa-specific mortality (27, 28). Furthermore, epidemiological evidence suggests that men whose diets are high in saturated fats, red meats, and calcium have a higher probability of developing PCa (21). Other studies suggest that eating foods such as tomatoes, pink grapefruit, and watermelon are correlated with a decreased risk of PCa (29). However, more research needs to be completed to understand the underlying mechanisms and correlations between these specific foods and the development of PCa.

Like other cancers, PCa has an infinite potential to replicate its cells, resist apoptosis, invade local tissues, and spread to distant sites. One of the challenges of diagnosing PCa is that the early stages of the disease are usually asymptomatic due to the small size of the tumor (30). As the tumor grows in size, signs and symptoms will begin to appear such as changes in bladder habits (30). As the PCa becomes more invasive and metastatic, the signs and symptoms that are associated with the disease are difficultly urinating, blood in the urine, fatigue, and pain or stiffness of the hips, back, or chest. However, if an individual is tested regularly, early signs of PCa can be detected from digital rectal examinations or serum PSA levels (30, 31). As previously

mentioned, PSA is a glycoprotein made by the prostate gland that is mainly responsible for promoting sperm motility and dissolving cervical mucus (32). Elevated PSA levels have been hypothesized to be a result of the disruption of the prostate cellular architecture, which in turn results in the diffusion of PSA into circulation (33). If a patient is suspected to have PCa, both the American Urological Association (AUA) and the European Association of Urology (EAU) recommend that a prostate biopsy be performed and ten to twelve long narrow pieces of tissue called cores will be extracted and used to confirm a PCa diagnosis (30, 31). These cores should be taken bilaterally from the apex to the base of the prostate, and as far posteriorly and laterally as possible from the peripheral gland (30, 31). Pathologists will then evaluate the tissue samples from these biopsies via histological assessment (30, 31). Lastly, a urological pathologist will provide a report that includes information on histopathological type and Gleason grades (30, 31). The Gleason grading system is based on the histological arrangement of cancer cells in haematoxylin and eosin stained prostate tissue sections (34). The Gleason scoring system uses 5 grading categories (Gleason 1-5) (34). A primary grade is given to describe the cells in the largest area of the tumor and a secondary grade is given to describe the cells in the next largest area (34). The grades are then combined to obtain a Gleason score that ranges from 2-10 (34). For example, if a pathologist gave the cancer cells in the largest area of the tumor a 4, and the cancer cells in the next largest area a 2, then the total Gleason score would be 6. A patient with a Gleason score of 6 is considered to be low risk, Gleason 7 is intermediate risk, and Gleason 8-10 is high risk (35). Patients that have higher Gleason scores have undifferentiated cancer cells, poor prognosis, and an increase risk of metastasis (36). In addition to Gleason

groups, the Tumor Node Metastasis (TNM) system is used to describe the staging, location, and spread of the tumor (37). T (1-4) is used to describe the size and location of the tumor within and adjacent to the prostate, N (0-1) describes lymph node metastasis, and M (0-1) describes any metastasis to organs such as the lungs or to the bones (37). According to the newest guidelines, nucleotide-based tests such as PCA3 level, Genomic Prostate Score, and Cell Cycle Progression Score may also be taken into consideration when evaluation the PCa (38-43).

For patients with low and intermediate grade PCa with a Gleason score less than 6, the AUA and EAU recommend active surveillance, surgery, or radiation therapy (44). A physician will also monitor patients by testing their PSA levels either quarterly or semi-annually, as well as by completing annual prostate biopsies (44). For patients with high grade PCa with a Gleason score greater than or equal to 8, the AMA and EAU recommend that patients receive either radiation therapy with neoadjuvant androgen-deprivation therapy or a radical prostatectomy with salvage radiation therapy (45). Together, this information suggests that receiving various therapies in combination is more effective in cases of high risk PCa. Although surgery and radiation therapies effectively cure most localized PCa, some cases that undertake these therapies will reoccur and progress to advanced stages of the disease within 5 years (46). PCa reoccurrence is defined by re-rising PSA levels after radical prostatectomy or by metastasis of the disease (47-50). First line treatment for locally advanced, recurrent, or metastatic PCa is androgen receptor pathway inhibition (ARPI) (48-50). ARPI targets AR-mediated functions by suppressing androgen production or androgen binding to the AR ligand-binding domain to achieve medical or surgical castration (51-55).

Unfortunately, most patients with metastatic PCa will become unresponsive and resistant to ARPI within 2 to 3 years and will develop castration-resistant prostate cancer (CRPC) (55).

1.1.5 Castration Resistant Prostate Cancer

After patients are exposed to ARPIs for a prolonged period of time, relapse will inevitably occur and CRPC will emerge. Upon diagnosis, CRPC patients usually have a median survival rate of 18-24 months (56). At this stage, current therapies are limited to enzalutamide, abiraterone acetate, or taxane chemotherapies such as cabazitaxel (57). These CRPC tumors can emerge both as AR-dependent and AR-independent tumors.

To date, there are three main mechanisms through which CRPC tumors can evade first and second-line therapies: androgen-dependent AR signaling, receptor-dependent AR signaling, and the bypass of AR signaling. Tumor cells can restore the AR signalling pathway by increasing the amount of circulating androgens or by acquiring AR gene overexpression, amplification, or mutations which allow for AR activation (58-62). Tumor cells can also regain AR signalling through methods that are independent of androgen ligand-mediated activation of the AR by: (1) producing constitutively active splice variants of the AR (12, 63, 64); (2) altering the mode of actions of the AR in a receptor-dependent manner (65); or (3) relying on the downstream signaling of other hormone receptor pathways such as the glucocorticoid receptor (66). AR splice variants are alternatively spliced isoforms of the AR mRNA. While full-length AR and AR splice variants both have and NTD and a DBD, AR splice variants lack a LBD (67). Because there is no LBD, therapies such as enzalutamide and

abiraterone acetate, which use the LBD to block AR synthesis, are impractical (67).

Functionally, these isoforms can remain active and promote the expression of

endogenous AR-dependent genes (68). For example, the AR splice variant AR-v7,

which lacks a LBD, has been shown to be strongly associated with decreased success

when patients are treated with enzalutamide or abiraterone (69). CRPC tumors that can

restore their AR signalling pathways and maintain their LE lineage and AdPC phenotype

are known as castration-resistant prostate adenocarcinoma (CRPC-Ad) tumors.

However, a subset of tumor cells will develop mechanisms that will allow them to grow

and develop independently of AR signalling, and progress into AR "indifferent" tumors

(70). One subtype of AR-indifferent CRPC that was recently reported by Bluemn *et al.* is

double negative for AR and NE markers (41). These tumours have hyperactive

fibroblast growth factor (FGF) and mitogen-activated protein kinase (MAPK) pathways,

which have been reported to promote ARPI resistance and facilitate tumour

progression. However, the phenotype of this double-negative prostate cancer subtype

has not yet been characterized. Another subtype of AR-indifferent CRPC, which is

induced by the selection pressures of ARPI, chemotherapy, or radiation is called

treatment-induced neuroendocrine prostate cancer (t-NEPC), which is a subtype of

neuroendocrine prostate cancer (NEPC) (71-73).

1.2 Treatment-Induced Neuroendocrine Prostate Cancer

Primary, or *de novo,* NEPC is extremely rare and accounts for 0.50-2.0% of all

cases of PCa (74). T-NEPC is distinctive from *de novo* NEPC because patients with

these tumors usually have a history of typical prostate adenocarcinoma and have

received single or multiple rounds of ARPI. (75). It is estimated that t-NEPC accounts

for 13-17% of total CRPC cases (41,63). Current therapies for t-NEPC are limited to

platinum-based chemotherapies or etopside (57). However, targeted therapies such as

an aurora kinase-A (AUKRA) inhibitor and an EZH2 inhibitor are currently being studied.

These CRPC tumors can emerge both as AR-dependent and AR-independent tumors.

T-NEPC is an emerging clinical challenge for the following reasons. 1) T-NEPC is

under-diagnosed. The diagnosis of t-NEPC requires evaluating histological features and

NE markers using tumor biopsies. However, patients with metastatic PCa rarely

undergo biopsies. 2) T-NEPC is highly aggressive and metastatic. Once a patient's

diagnosis is confirmed, the median survival of said patient is only approximately 7

months (8). 3) T-NEPC is under studied. Because t-NEPC is under-diagnosed, the

disease has not been a focus of many research groups. The increasing frequency of an

aggressive and fatal disease with no effective detection or therapeutic regimens

emphasizes the need to understand the molecular underpinnings of t-NEPC

development.

Today, t-NEPC has not yet been clearly defined. In a clinical setting, a t-NEPC

diagnosis is confirmed based on the presence of low or no levels of PSA, aggressive

tumor growth, a history of typical prostate adenocarcinoma, and single or multiple

rounds of ARPI, radiation therapy, or chemotherapy (75). However, there have been

cases of t-NEPC that present with high PSA and AR, and yet are positive for and NE

markers. It is possible that these cases represent an early stage of NEPC development

that is nearing the end of an AR-dependent state (76). Pathologically, the definition of t-

NEPC is based on the presence of small neuroendocrine carcinoma (SCNC)

morphological features, such as a scant cytoplasm, finely granular "salt and pepper"

chromatin, absent or inconspicuous nucleoli, poorly defined borders, and a high mitotic

count (75, 77, 78). However, diagnosing t-NEPC using morphological characteristics

can be challenging because the transition from AdPC to t-NEPC is not an acute

process, and involves sequential molecular alternations, which ultimately results in

multiple intermediate transitional phenotypes. By utilizing immunohistochemistry (IHC),

t-NEPC tumors can also be defined by the expression of NE markers such as

synaptophysin (SYP), chromogranin A (CHGA), chromogranin B (CHGB), CD56, and

neuron-specific enolase (NSE) (62). T-NEPC is positive for one or more NE markers in

almost 90% of cases (79). Lastly, pathologists can use PSA levels to diagnose PCa.

Usually there is low, or no, PSA /AR expression in NEPC. However, during the NEPC

trans-differentiation process, AR and PSA can be positive (79).

Because PSA has a limited specificity, the need for biomarkers that can

distinguish between inactive and aggressive forms PCa are imperative. In recent years,

the prognostic capacity of CHGA as a biomarker of prostate cancer has been

extensively evaluated (80-87). In 2009, Appetecchia *et al.* analyzed the incidence of

preoperative CHGA levels in 486 patients with nonmetastatic prostate cancer and found

that preoperative CgA could supplement PSA in the selection of more aggressive cases

of prostate cancer, particularly in the presence of a high Gleason score (80). Overall,

these findings suggest that there may be a potential prognostic capacity for CHGA in

prostate cancer, however they also highlight the importance of identifying other reliable

NE markers of t-NEPC.

1.2.1 T-NEPC is Derived from AdPC

While it has been confirmed that NEPC is prostatic in origin, there is not a consensus on how t-NEPC is generated (88). Multiple hypotheses have been proposed suggesting that t-NEPC originates from either benign prostatic neuroendocrine cells that acquire tumorigenic capacity, AdPC cells that undergo NE differentiation followed by t-NEPC tumor establishment, or PCa stem-like cells that retain traits of self-renewal, invasion, and resistance to apoptosis under hormone therapy (79, 89-92). These mechanisms of therapeutic resistance and tumour cell heterogeneity can be facilitated by a cellular process termed lineage plasticity.

1.2.2 Lineage Plasticity in t-NEPC Development

Lineage plasticity can be defined as a fundamental developmental process that enables a single genotype to give rise to different phenotypes in response to environmental changes (93). Lineage plasticity can cause AdPC cells to dedifferentiate into a NE-like cell lineage (93). The mechanisms involved in lineage plasticity may utilize the dedifferentiation of AdPC to stem-like cells to NE-like cells, NE differentiation via a pluripotency network, or direct NE transdifferentiation of AdPC cells to NE-like cells (94).

Whole-genome sequencing has revealed that, compared to 15-40% of CRPC-Ad tumors, 55-75% of t-NEPC cases have concurrent functional mutations or deletions of the retinoblastoma 1 (*RB1)* and tumor protein 53 *(TP53)* genes (89, 95). It has been found that cancer cells that are RB1/TP53 deficient have the flexibility to adapt alternative lineages. For example, one of the genetically engineered mouse models

(GEMMs) of prostate cancer progression called TRAMP reveals how these genes played an important role in the emergence of t-NEPC tumors (96). TRAMP GEMMs mice express the transforming region of SV40 large T antigen, which inactivates Trp53 and Rb1 (97, 98). Researchers found that TRAMP mice spontaneously develop prostate cancer that closely resembled the characteristics and progression of metastatic CRPC-Ad to t-NEPC under castration conditions (96). Furthermore, a recent study by Mu *et al.* reported that the knockdown of the *RB1* and *TP53* genes in the human LNCaP AdPC cell line facilitated resistance to ARPI and promoted t-NEPC progression via a pluripotency gene network mediated by SOX2 (99). SOX2 is a putative developmental factor that is essential for self-renewal and pluripotency of embryonic stem cells. Moreover, they suggested that the SOX family of transcription factors (i.e. SOX2, SOX9, and SOX11) are temporally regulated to promote lineage plasticity of LE cells to the NE cell lineage fate in the emergence of t-NEPC (99). They also found that, in their LNCaP/AR and CWR22Pc-EP cells with a combined *TP53/RB1* shRNA knockdown, there was a significant enrichment of basal-signature genes (99). Ku *et al.* reported a similar resistance mechanism in their Pten/Rb1/Trp53 triple knock-out (TKO) GEMMs (100). Together, these findings led to a proposed model of lineage plasticity whereby LE cells undergo dedifferentiation reprogramming into a stem-like intermediate cell that can differentiate into NE, basal, or mesenchymal lineages.

Recently, our laboratory created the NEPC cell models LnNE and DuNE, which are unique SRRM4-driven transformations of LNCaP and DU145 AdPC cells to NEPC tumors, respectively (65, 101). The previously established LnNE model illustrates the long term progression from AdPC to t-NEPC as demonstrated by its gradual decrease

in PSA as well as its neuronal-like phenotype, whereas the DuNE model recapitulates the phenotypes of clinical t-NEPC tumors expressing stem-like characteristics (65, 101). We found that there was an increase in the expression of embryonic stem cell genes, such as SOX2, in the DuNE cell model (101). We also found distinct expression of SOX2 within a subgroup of t-NEPC tumors from the 2016 Beltran cohort (101). There were 5 t-NEPC tumors with low SOX2 expression, similar to that of CRPC-Ad tumors, while the remaining 10 t-NEPC tumors expressed a ~17.5-fold increase in SOX2 levels (101). These findings demonstrate that different subgroups of t-NEPC tumors exist, where a division of the two subgroups is evident based a robust difference in SOX2 expression levels. There are several possibilities for the development of two distinct subgroups of t-NEPC. One is that the upregulation and downregulation of these genes occurs because these cases of t-NEPC actually present at different stages of NEPC progression and are therefore presenting with different phenotypes. Another possible reason is that complex mechanism can overlap and work together to cause the increase and decrease in SOX2, which contributes to t-NEPC progression.

Currently, therapy induced plasticity of PCa cells falls into three categories: neuroendocrine transdifferentiation (NEdT), epithelial-mesenchymal transition (EMT), and basal cells that have stem-like potential. NEdT requires prostate adenocarcinoma cells to differentiate into a neuroendocrine-like cell without becoming an intermediate a stem cell (90). EMT is a process by which adherent cells with an epithelial phenotype develop more migratory and invasive properties through altered gene expression (102-104). EMT is characterized by the loss of epithelial markers, such as E-Cadherin and epithelial cytokeratins, the gain of mesenchymal markers such as N-Cadherin, vimentin,

and fibronectin, and Twist1, and the gain of transcriptional repressors of E-cadherin, such as Snai1, Snai2, Zeb1, and Zeb2 (66). Lastly PCa, like other human malignancies, can harbour a subset of tumour cells that display characteristics similar to those found in normal human stem cells. These characteristics include the expression of core embryonic developmental genes, such as NANOG, LIN28, POU5F1, SOX2, and the ability to proliferate in culture with an unattached spheroidal morphology (105-108). For these reasons, this subpopulation of cells are referred to as cancer stem-like cell (CSC) (11, 107). Currently, the origins of cancer stem-like cells are unknown. While some believe that they are remnants of an original oncogenic event that occurred in tissue stem cells, others believe that evidence suggests that they can arise through a process of de-differentiation from differentiated cancer cells (109).

While researchers generally agree that lineage plasticity contributes to the acquisition of the CSC-like phenotype, its involvement in t-NEPC development is contested. Currently, there is no direct evidence that supports the idea that t-NEPC arises from CSCs and/or neuroendocrine cells. However, acute androgen deprivation has been shown to drive the neuroendocrine transdifferentiation of AR-driven cell lines through an intermediary metastable stem-like state (109). Although this is not direct evidence of CSCs, neuroendocrine transdifferentiation from adenocarcinoma represents a similar phenotypic plasticity.

The selective expression of CD44, a cell surface marker for prostate CSCs, in NEPC further supports the idea that there is a relationship between lineage plasticity and neuroendocrine differentiation. CD44 was initially identified as a receptor for hyaluronic acid and as a lymphocyte-homing receptor (110, 111). Its expression has

since been correlated with cell invasion, cell migration, and the ability of cells to self-renew, thus connecting the EMT and CSC phenotypes (110, 111). For example, researchers found that knocking down the expression of EMT transcription factor ZEB1 in the PCa cell line DU145 decreased CD44 expression (110-112). Furthermore, analysis of PCa cell lines LNCaP, DU145, and PC3 found that CD44 expression is positively correlated with the expression of NSE, a neuroendocrine marker (103). While evidence has not been fully elucidated yet, there is clearly a relationship between NEdT, EMT, CSCs and t-NEPC.

1.2.3 Clinical Challenges

Currently, there are several challenges that prevent clinicians from effectively managing t-NEPC. First, because PSA is used as the "gold-standard" to monitor PCa progression, and t-NEPC tumors do not or express low levels of this biomarker, early detection of t-NEPC is difficult. Moreover, the heterogeneity of t-NEPC tumors is not fully understood due to the lack to biopsies that have been collected from CRPC patients. Recently, Beltran *et al.* found varied genomic, epigenetic, and transcriptomic characteristics among t-NEPC patients, which supports the idea of the complexity of the heterogeneity of t-NEPC (90). This also highlights the idea that there may be different mechanisms or stages when tumor biopsies were performed, which adds to the complex heterogeneity of the disease. The concept of many subtypes of t-NEPC suggest that many treatment options will be required to treat t-NEPC tumors, thus possibly hindering the development of t-NEPC treatment with high efficacy. Currently, treatment options are limited to platinum-based chemotherapies or etopside. The gravity

of an increasing frequency of an aggressive and fatal disease, whereby no effective

detection or therapeutic regimens have been defined, emphasizes a need for the

understanding of the molecular underpinnings of t-NEPC development.

1.3 LIN28B Pathway

1.3.1 LIN28B Gene and Protein Structure

The *Lin28* gene was first characterized in *Caenorhabditis elegans* and

Drosophila melanogaster as a highly conservative RNA-binding protein. There are two

Lin28 homologs in all vertebrates: lin-28 homolog a (*Lin28a)* and lin-28 homolog b

(*Lin28b)* (113, 114)*.* In humans, the LIN28A gene is located at chromosome 1p36 and

can be translated into a 209 amino acid protein, whereas the LIN28B gene is located at

chromosome 6q21 and can be translated into a 250 amino acid protein (115). LIN28A

and LIN28B proteins are highly conserved and share a high degree of homology in their

structural domain, as depicted in figure 1.3 (116). LIN28 proteins are unique in that they

are the only animal proteins that contain both a cold shock domain (CSD) and two

cysteine cysteine histidine cysteine (CCHC) zinc finger domains, both of which can bind

ribonucleic acid (RNA) (113, 116, 117). The CSD, which was first discovered in bacterial

cold shock proteins, binds to single-stranded nucleic acids to regulate ribosomal

translation, messenger RNA stability and degradation, transcription, and termination

(118). The CSD works with CCHC zinc finger domains, which were first identified in the

nucleocapsid protein (NCP) of HIV-1 virus, to increase the binding specificity and

enzymatic activity of LIN28B (80). Unique to LIN28B is a nucleolar localization signal

(NoLS) that is located between the CSD and the first zinc finger domain, as well as a

nuclear localization signal (NLS) at the C-terminus (119). Throughout an individual's lifetime, LIN28B is primarily expressed in undifferentiated, pluripotent cell types, as well as in the testis and placenta in males and females, respectively (93). LIN28 is primarily expressed in the cytoplasm and is associated with various organelles such as the ribosomes and stress granules (120). However, the subcellular distribution of LIN28B is not fully understood. To date, one report has demonstrated that in non-small cell lung cancer cells, LIN28B has distinct nucleolar and nuclear localization signals. However, many other studies have found that in neuroblastoma and hepatocellular carcinoma tissue arrays, LIN28B is a cytoplasmic protein that is shuttled into the nucleus in a cell-cycle dependent manner (116, 119-121). One study reported that the subcellular localization of LIN28B is cell-cycle regulated, where it is prominently expressed in the cytoplasm of G_1 phase cells and in the nucleus of S and G_2 phase cells (122). Additional studies should be completed to further elucidate the exact subcellular location of LIN28B, as it is hypothesized that it may vary depending on cell type.
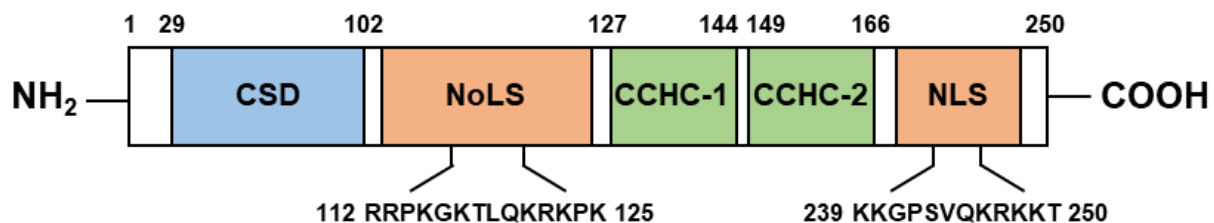
Figure 1.3 Schematic representation of LIN28B protein in humans. -NH$_2$, N terminus; -COOH, C terminus; CSD, cold shock domain; NoLS, nucleolar localization signal; NLS, nuclear localization signal. *Original drawing adapted from Balzeau et al "The LIN28/let-7 pathway in cancer" (2017). Frontiers in Genetics (10.3389/fgene.2017.00031).*

1.3.2 Biological Functions of LIN28B
1.3.2.1 Embryogenesis

In vertebrates, LIN28B is first expressed during the two-cell stage of embryogenesis (113, 123, 124). By embryonic day 6, LIN28B is not only expressed throughout the entire embryo, but also in the extra-embryonic tissue (124). Between embryonic days 42-63, LIN28B expression is significantly decreased (123). This decrease in LIN28B expression is concurrent with the onset of meiotic germ cell differentiation, and it remains low for the remainder of embryonic development (123). As the embryo continues to develop, progenitor cells begin to differentiation, and the previously broad expression of LIN28B becomes restricted to a subset of epithelial cells including those of the branchial arches, the lungs, the kidney, the cardiac muscle cells of the myocardium, and the neuroepithelium (124). The steadily decreasing expression of LIN28B allows for the formation of mature let-7 microRNAs (miRNAs). In turn, members of the *let-7* miRNA family bind to the 3′ UTR of LIN28 mRNA, which negatively regulates its expression. Thus, the introduction of let-7 inhibits the self-renewal of undifferentiated cells and promotes differentiation (125).

One population of cells that expresses high amounts of LIN28B are embryonic stem cells (ESCs). ESCs are pluripotent cells that are derived from the inner cell mass (ICM) of the preimplantation mammalian embryo and can become the cells and tissues of the three germ cell lineages of the developing embryo (126). Because of their pluripotent nature, ESCs can maintain their phenotype and genotype through self-renewal without losing their ability to differentiate. Along with SOX2, NANOG, and POU5F1, LIN28 has been cited as a marker of "stemness" where its expression is high in human and mouse ESCs and is dramatically decreases during ESC differentiation

(126-128). Strikingly, LIN28 is one of four genes (the others being OCT4, NANOG, and SOX2) that can reprogram human fibroblast cells into induced pluripotent stem cells (iPSCs) (129). Collectively referred to as Thompson Factors, Yu *et al.* found that these four genes in various combinations are necessary and sufficient to reprogram human ESC-derived somatic cells with a mesenchymal phenotype (129). Furthermore, in ESCs LIN28B is responsible for regulating growth, translation, cell number, and proliferation (120). LIN28 also regulates neural precursor cell proliferation promoted by MASH1 (ASCL1) via its inhibition of the miRNA let-7 (130). The proliferation of neural precursor cells is promoted by SOX2 through high LIN28B expression (130). Accordingly, the loss of LIN28 in neural progenitor cells results in fewer cells due to a reduction in proliferation (131).

At the organismal level, LIN28B expression causes an increase in body size which is associated with a proportional increase in organ size (114). This is likely due to an increase in cell number and proliferation (114). In contrast, LIN28B loss results in embryonic lethality, reduced growth and fat accumulation, and reduced brain size (131). Overall, LIN28B plays an important role in facilitating early embryonic growth and development, and maintaining ESC populations.

1.3.2.2 Stem Cell Pluripotency

As mentioned, LIN28B is highly expressed in undifferentiated ESCs and denotes part of a pluripotency network that is also made up by transcription factors such as LIN28A, SOX2, NANOG, and POU5F (132). When LIN28B expression decreases, this leads to a subsequent increase in miRNA let-7 expression which will in turn inhibit the

self-renewal properties of the undifferentiated cells and cause them to become differentiated (125). Furthermore, LIN28B is well known for its role in generating iPSCs by introducing the key pluripotency transcription factors into somatic cells (133, 134). This observation, along with evidence that inhibiting let-7 expression using antisense oligonucleotide inhibitors can reprogram mouse fibroblasts to iPSCs, demonstrates that LIN28B mediated inhibition of let-7 promotes cell de-differentiation during reprogramming (125). Additionally, the overexpression of LIN28B in mice in a tissue regeneration study resulted in increased digit repair, epidermal hair regrowth, and pinnal tissue regrowth (135). It is hypothesized that the ability for the tissue to regenerate is a result of LIN28B-mediated control of proliferation of stem cells and transit-amplifying populations, and the overexpression of LIN28B would lead to an increase in tissue size and regrowth of damaged regions (114). Together, these results suggest that the LIN28B/let-7 axis operates to maintain either a differentiated or undifferentiated ESC fate that can be manipulated in order to maintain cellular pluripotency.

1.3.2.3 Growth and Metabolism

Several recent reports have also discovered that LIN28B plays an important role in regulating growth. Regarding proliferative growth, LIN28B has been reported to increase the expression of a number of cell-cycle regulators by inhibiting microRNA let-7 expression, including MYC, RAS, cyclin D1/2, and HMGA2 (136-138). LIN28B has also been reported to control cellular growth via the regulation of ribosomal synthesis of proteins by binding directly to the messenger RNA (mRNA) of ribosomal peptides in human ESCs (139). When analyzing growth on a broader scale, genome wide association studies (GWAS) found that LIN28B was one of several genes that was

associated with human height, age of puberty onset, age of menopause, and body-mass index (BMI) (139-141). Generally, emerging evidence supports the idea that LIN28B plays an important role in the growth of not only individual cells, but of organisms as a whole.

LIN28B has also been reported to coordinate metabolism, both via the microRNA let-7 and by directly promoting mRNA translation. Through let-7, LIN28B has been reported to upregulate the insulin/PI3K, Ras, and Myc pathways, all of which are characteristic oncogenic regulators of metabolism (133). Related to the insulin/PI3K pathway, transgenic animals that overexpress LIN28B have been found to be more sensitive to insulin and to have reduced peripheral glucose levels (142). Additionally, LIN28B has been found to regulate glucose metabolism; its overexpression increased the ability of muscle cells to take up glucose, while its loss results in insulin resistance (142, 143). It seems that the association between LIN28B, let-7, and metabolism indicates that this axis is largely controlled through let-7 dependent pathways/regulations. Yet, in many of these experiments, the cellular basis and the mechanism of action of LIN28B are not fully understood, and further studies are required. Overall, given how growth signalling pathways are interrelated with cellular metabolism, it is not surprising that LIN28B influences self-renewal and reprogramming. Furthermore, while the LIN28B and let-7 pathway has been associated with rapid stem cell proliferation, the dysregulation of this regulatory pairing has been implicated in tumor development (144). Based on LIN28B's intricate role in cellular development, a new model has been proposed to argue that LIN28B programs metabolism and proliferative growth to regulate stem cell self-renewal (143).

1.3.3 LIN28B Signalling Pathways

There are two unique pathways through which LIN28B regulates its downstream targets. Here, these two pathways will be described, as well as illustrated in figure 1.4, to demonstrate how LIN28B downstream targets can be expressed or inhibited in the absence or presence of let-7, respectively.

1.3.3.1 The let-7 Dependent Pathway

Currently, the regulation of let-7 miRNAs is the best characterized mechanism of LIN28B. The let-7 gene was initially discovered as a developmental gene and as a miRNA in *C. elegans* (143, 145, 146). The mature let-7 family members are highly conserved, however the total number of let-7 genes varies between species (147). In humans, the let-7 family consists of: let-7a, let-7b, let-7c, let-7d, let-7e, let-7f, let-7g, let-7i, and mir-98 (148). In the human genome, the let-7 family members can be encoded individually or as clusters with other family members (149). In the human, let-7g and let-7i are located individually on chromosomes 3 and 12, respectively, while the other let-7 family members are distributed among four clusters (Table 1.1) (148). While it has been reported that let-7a and let-7c are involved in hematopoietic stem and progenitor cell homeostasis, the exact role of other let-7 family members in mammalian development has not yet been fully elucidated (150-153). This is due to the fact that it is technically difficult to knock out multiple let-7 family members at once (150-153).

One of the major functions of let-7 is to promote cell differentiation (129, 148, 154). This has been reported in *C. elegans*, where let-7 prevented the division of stem cells, which caused the cells to become fully differentiated (145). In more complex

species, let-7 levels rise during embryogenesis (152). In addition, a decrease in let-7 expression has been associated with human cancers and CSCs (129, 154). These findings have led scientists to propose that let-7 genes function to promote terminal differentiation in development and function as tumor suppressors.

Table 1.1 Genomic Location and Conserved Clusters of the let-7 Family in Humans

Let-7 Family Member	Genomic Location	Cluster #
hsa-let-7c	Chromosome 21: 16539828-16539911 +	1
hsa-let-7e	Chromosome 19: 51692786-51692864 +	
hsa-let-7a	Chromosome 9: 94175957-94176036 +	2
hsa-let-7d	Chromosome 9: 94178834-94178920 +	
hsa-let-7f	Chromosome 9: 94176347-94176433 +	
hsa-let-7b	Chromosome 22: 46113686-46113768 +	3
miR-98	Chromosome X: 53556223-53556341 −	4
hsa-let-7g	Chromosome 3: 52268278-52268361 −	
hsa-let-7i	Chromosome 12: 62603686-62603769 +	
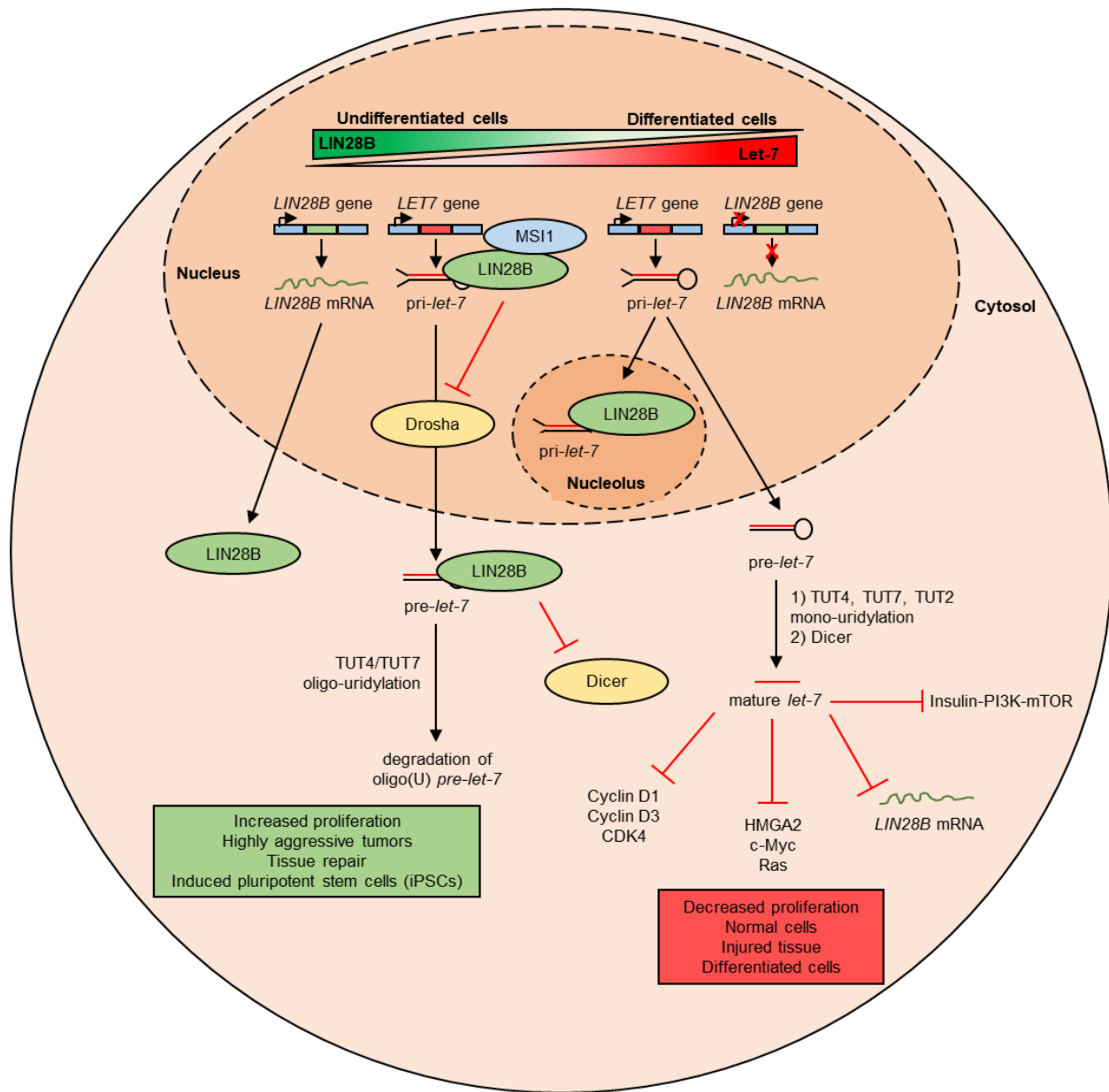
Figure 1.4 LIN28B/let-7 regulatory axis. In undifferentiated cells, LIN28B is highly expressed and blocks let-7 biogenesis by binding to pri-let-7 or pre-let-7, neither Drosha nor Dicer, respectively, can process let-7. LIN28B recruits TUT4/TUT7 to pre-let-7 and promotes its oligo-uridylation and degradation. When cells are differentiated LIN28B expression decreases, which leads to increased levels of mature let-7. The latter silences gene expression of proto-oncogenes (Ras, c-Myc, HMGA2), cell cycle progression factors (Cyclin D1 and D3, Cdk4), and components of the insulin-PI3K-mTOR pathway. *Original drawing adapted from Mayr F and Heinemann U "Mechanisms of Lin28-mediated miRNA and mRNA regulation – a structural and functional perspective" (2013). International Journal of Molecular Sciences. (10.3390/ijms140816532).*

The molecular mechanisms involved in the LIN28/let-7 axis have been studied in great detail and have been well documented (6, 155, 156). In brief, LIN28B can bind to both pri- and pre-let-7 and block their processing by binding to a conserved motif, GGAG, which is found in the let-7 stem loop (117, 155, 157, 158). In the nucleus, LIN28B can bind to pri-let-7 to inhibit it from being processed by the miRNA-processing enzyme Drosha (159). However, the mechanisms of let-7 suppression remain poorly understood, because LIN28B recognition depends on coordinated targeting by both the zinc knuckle domain and the CSD, whose binding sites have not been systematically characterized (113, 116, 117). Studies have also found that in human ESCs and neuronal stem/progenitor cells, the RNA-binding protein musashi 1 (MSI1) can enhance the localization of LIN28B to pri-let-7 found in the nucleus (160). LIN28B has also been found to localize in the nucleolus where it sequesters pri-let-7 and blocks its processing (119). In the cytoplasm, LIN28B binds to pre-let-7 to inhibit it from being processed by Dicer, and encourages terminal uridyl transferase 4 and 7 (TUT4, TUT7) to catalyze the oligo-uridylation and degradation of pre-let-7 (161, 162). Upon differentiation, when LIN28B expression is silenced, pri-let-7 is cut by Drosha and subsequently moved to the cytoplasm (156). Here Dicer, with the help of TUT4, TUT7, and TUT2, will create single stranded mature let-7 miRNAs (156). Let-7 will silence the expression of proto-oncogenes (Ras, c-Myc, HMGA2), cell cycle progression factors (Cyclin D1 and D3, CDK4), components of the insulin-PI3K-mTOR pathway, and LIN28B itself, thereby establishing a positive feedback loop (156).

1.3.3.2 The let-7 Independent Pathway

To date, a number of studies have found that LIN28B can operate through pathways that are independent of let-7. Zhu and colleagues found that transgenic mice with a LIN28 knockout presented with impaired glucose tolerance and insulin resistance, despite no significant change in let-7 levels (142). Furthermore, research completed by Peng *et al.* and Xu *et al.* showed that LIN28 promotes ESC proliferation in part by binding to, and increasing the translation of, cell cycle-related mRNAs (120, 163). Together, it is clear that let-7-independent roles of LIN28 are important in developmental contexts. However, the exact targets that are relevant for the biological function of LIN28, and more specifically LIN28B, and how LIN28 confers specificity when targeting these RNAs, is still unclear. While it has been noted that LIN28 primarily targets mature mRNAs in the gene ontology (GO) categories of cell cycle regulation, nuclear RNA-binding proteins, and genes involved in translation, further research must be completed to understand the LIN28B/let-7 independent pathway.

1.3.4 LIN28B/let-7 Pathway in Cancer

An oncogenic role for the LIN28B/let-7 pathway has been established in a number of cancers. Studies have demonstrated that an increase in LIN28B expression and a loss of let-7 expression is correlated with poor prognosis and advanced malignancies (164). In fact, studies have found that about 15% of cancers have high LIN28A/LIN28B and low let-7 expression, including glioblastoma, ovarian, gastric, prostate, and breast cancer (164-167). Acting as tumor suppressors, let-7 miRNAs repress several oncogenes such as K-RAS, C-MYC, HMGA2, and cell cycle factors

such as Cyclin D1 and D2 (148). When in a state of metastasis, the loss of let-7 expression triggers the de-repression of these oncogenes which leads to tumorigenesis, tumor growth, and advanced malignancy (164). This relationship between LIN28B and let-7 has been demonstrated in human leukemia cells, where the depletion of LIN28B caused a subsequent increase in let-7, which in turn decreased proliferation in the expression of the oncogene Myc (164).

Recent studies have implicated LIN28B upregulation in a growing list of cancers, and in some cases expression correlates with advanced tumor-stage and poor prognosis. For example in breast cancer, LIN28B expression is positively correlated with aggressive invasive ductal carcinoma (168). Furthermore, LIN28 can repress let-7a, inducing EMT and facilitating breast cancer metastasis (169). In human lung cancer cells, the overexpression of LIN28 has been found to encourage cell cycle progression and inhibit cell proliferation by mediating let-7-g repression (170). Multiple human hepatocellular carcinoma (HCC) cell lines and clinical patient samples have been reported to overexpress LIN28B (171). Hyperexpression of LIN28B correlated with decreased survival and increased tumor recurrence in patients with colorectal cancer (172). Furthermore, LIN28B can reportedly promote ovarian cancer cell growth by targeting insulin-like growth factor 2 (IGF2) (173). LIN28B was also found to promote cancer cell progression in head and neck cancer cells by repressing let-7 miRNAs and subsequently activating let-7 targets such as HMGA2, CCND2, IGF1R, and IGF2BP2 (174). Contrary to the reactivation of LIN28B in adult cancers, some cancers seen in children may be a consequence of cells that failed to silence LIN28B expression (115).

These childhood cancers include teratoid/rhabdoid tumors, pediatric CNSPNET, Wilms tumors, medulloblastoma, and neuroblastoma (115).

Emerging evidence suggests that the overexpression of LIN28B in pathological conditions plays an important role in the formation of CSCs. CSCs are cancer cells that have characteristics that are associated with normal stem cells which gives them the ability to initiate tumor relapse, promote metastasis, and become resistant to cancer therapies such as chemotherapy and radiation. CSCs have characteristic cell surface markers: $CD44^+$, $CD24^+$, and E-cadherin negative, with LIN28B being selectively expressed in these cells (175). CSCs acquire an EMT phenotype through the induction of SOX2, NANOG, OCT4, LIN28B and/or NOTCH1 expression. These cells also exhibit enhanced clonogenic and sphere forming ability and in vivo tumorigenicity (176). Further functional experiments have identified a double-negative feedback loop between LIN28 and let-7, in which LIN28 negatively regulated let-7 expression, and the decreased expression of let-7 in turn resulted in an increased expression of LIN28 (125). This suggests a "reprogramming-like" mechanism to be responsible for transforming CSCs (131).

1.3.5 LIN28B/let-7 Pathway in Prostate Cancer

The characteristics of the LIN28B/let-7 pathway in prostate cancer has not been studied in depth. While several papers have published research elucidating possible explanations on how the LIN28B/let-7 pathway promotes the development of prostate cancer, there are no conclusive theories agreed upon in the literature.

To date, LIN28A and LIN28B expression has been detected in some prostate cancer cell lines (154-156). While LIN28 is not normally expressed in prostate tissues, researchers have reported LIN28A and LIN28B expression in various prostate cancer cell lines such as PC3, DU145, C4-2B, LNCaP, and VCaP (177-179). However, LIN28B has only been detected in the PC3 cell line (178). While general consensus is that LIN28B acts through let-7 in prostate cancer, there has been some disagreement as to which let-7 miRNA is repressed. For example, while Albino *et al.* reported that pri-let-7b and let-7b expression was reduced when LIN28B expression was increased in Du145 cells, Kang *et al.* and Kong *et al.* reported that when LIN28B was overexpressed, there was a significantly decreased expression of all let-7 miRNA family members in PC3 cells (176, 178, 180). Furthermore, Fu *et al.* reported a decrease in let-7a and let-7c in Du145 cells and Nadiminty *et al.* found there to be a decrease in let-7c in C4-2B cells (176, 178, 180-182). However, a serious limitation to these experiments is that no researchers have ever determined the expression of the entire let-7 family. Further work needs to be performed to establish how the results from these various studies coincide, which may be elucidated by using a prostate cancer cell panel to determine the expression of the entire let-7 family.

Many hypothesis have been proposed to elucidate how LIN28B functions to promote prostate cancer growth. LIN28A/B staining is strong in benign prostate tissues is seen almost exclusively in the basal cell layer with no staining in the luminal epithelial compartment (179). This can be explained by the following: LIN28A/B is highly expressed in progenitor cells, and the basal cell compartment is generally considered to harbor putative prostate stem cells. Therefore, it is logical that the benign prostate gland

highly expresses LIN28A/B in the basal cell layer. Furthermore, a shift from mostly nuclear localization in benign prostate to a nuclear/ cytoplasmic or mostly cytoplasmic localization occurs in prostate cancer (179).

LIN28B expression has been reported to increase prostate cancer cell proliferation and promote prostate tumor growth through various downstream targets. For example, studies have reported that, through the upregulation of LIN28B and the repression of let-7, various downstream oncogenic markers such as c-Myc and cyclin D1 are upregulated (178, 179). Most notable is the finding that prostate cancer cells overexpressing platelet derived growth factor (PDGF), which contributes to an EMT phenotype, is strongly associated with cancer cell invasion and tumor metastasis, and is consistent with characteristics that are known to be associated with cancer stem-like cell (176). This study also found that the expressions of SOX2, NANOG, POU5F, and LIN28B were dramatically up-regulated in PC3 PDGF-D cells. More importantly, the knockdown of SOX2, NANOG, POU5F, and LIN28B by siRNA transfection repressed prostasphere-forming capacity of PC3 PDGF-D cells (176). Other studies have shown that, LIN28B expression is elevated in the CSC subpopulation of prostate cancer cell lines compared with the bulk tumor cell population (180).

1.4 Hypothesis

Analysis of the Beltran 2016 cohort of tumors from patients with NEPC, available through cBioPortal, allowed us to distinguish two classes of t-NEPC tumors; one with high LIN28B expression and the second with low LIN28B expression. Based on this information, as well as the theory that the transition from AdPC to NEPC may occur as a result of an intermediate stem-like phenotype, we hypothesized that LIN28B may promote proliferation and trans-differentiation, which contributes to t-NEPC progression. In this study, we aimed to investigate LIN28B expression in prostate cancer cells, as well as study the molecular mechanisms that may contribute to the overexpression of LIN28B in t-NEPC.

Aim 1: Investigate the expression of the LIN28B and let-7 gene in prostate tumors and cancer cells.

Aim 2: Determine the role of LIN28B in regulating SOX2 in neuroendocrine prostate cancer progression.

Aim 3: Determine the role of LIN28B in regulating key cancer stem-like properties in neuroendocrine prostate cancer progression.

Aim 4: Determine how LIN28B expression affects the development and growth of xenograft tumors.

Chapter 2: Materials and Methods

2.1 Cell Lines and Cell Culture

Human PCa cell lines C4-2, DU145, LNCaP, NCI-H660, PC-3, VCaP, and 22RV1 were purchased from American Type Culture Collection (ATCC; Manassas, VA, USA). The androgen-independent human PCa cell line LNCaP95 (LN95) was kindly provided by Dr. Alan Meeker (Johns Hopkins University; Baltimore, MD, USA). Human PCa cell line RWPE-1 and embryonic kidney cell line 293T were kindly provided by Dr. Michael Cox and Dr. Ralph Buttyan, respectively, from the Vancouver Prostate Centre (VPC; Vancouver, BC, Canada). The small cell lung cancer (SCLC) cell line NCI-H69 was kindly provided by Dr. YZ Wang from the VPC. The LnNE and DuNE cell models, along with their control cells, were previously established by our group (65, 101). To create these cell lines, lentiviral expression vectors (pFUGWBW) encoding Flag-SRRM4 and empty control vectors were used to package lentivirus in 293T cells and transduce target LNCaP and DU145 cells (65, 69). The transduced cells were then selected by blasticidin (Gibco Life Technologies), and the expression of SRRM4 was confirmed by real-time qPCR and immunoblotting assays (65, 69).

DU145, DuNE, PC-3, VCaP, and 293T cells were cultured in Dulbecco's Modified Eagle Medium, high Glucose/L-glutamine, (DMEM; Hyclone, Logan, UT, USA) with 10% fetal bovine serum (FBS; Gibico, Waltham, MA, USA). C4-2, LNCaP, and 22RV1 cells were cultured in Roswell Park Memorial Institute 1640 (RPMI-1640; Hyclone) medium with 10% FBS. LNP95 cells were cultured in phenol-free RPMI-1640 medium with 10% charcoalstripped serum (CSS; Hyclone). NCI-H660 cells were cultured in HITES medium (RPMI-1640 medium containing 0.005 mg/ml Insulin, 0.01 mg/ml transferrin, 30

nM sodium selenite, 10 nM hydrocortisone, 10 nM beta-estradiol, and 2 mM L-glutamine) with 10% FBS. NCI-H69 suspension cells were cultured in RPMI-1640 medium with 10% FBS, 100 μg/ml streptomycin, and 100 units/ml penicillin. RWPE-1 cells were cultured in Keratinocyte-SFM (1X) medium with human recombinant epidermal growth factor 1-53 and bovine pituitary extract supplements (Gibco). Cells were incubated in 5% CO_2 at 37°C. All cell lines used tested negative for mycoplasma contamination and were authenticated by short tandem repeat assays.

2.2 DNA and RNA Transfections

Cells were transfected with miRIDIAN microRNA human hsa-let-7d-5p mimic (cat#: C-300478-07-0002, Dharmacon; Lafayette, CO, USA), miRIDIAN microRNA mimic negative control (cat#: CN-001000-01, Dharmacon), or TRC LIN28B shRNA (cat#: RHS4533-EG389421, Dharmacon) using Lipofectamine 3000 (Life Techologies; Burlington, ON, Canada) according to the manufacturer's protocol. Transient DNA plasmid transfections also used Lipofectamine 3000. Detailed information on plasmid DNA and mimicRNA is listed in table 2.1.

Table 2.1 RNA and Plasmid Information

Reagent	Provider	Catalogue #
miRIDIAN microRNA human hsa-let-7d-5p mimic	Dharmacon	C-300478-07-0002
miRIDIAN microRNA mimic negative control	Dharmacon	CN-001000-01
TRC LIN28B shRNA	Dharmacon	RHS4533-EG389421
pcDNA3-FLAG-Lin28B	Addgene; pcDNA3-FLAG-Lin28B was a gift from Narry Kim	51373

pGL3-IRES-Lin28b-P3	Addgene; pGL3-IRES-Lin28b-P3 was a gift from Joshua Mendell	64794
MSCV puro let-7 sponge	Addgene: MSCV puro let-7 sponge was a gift from Phil Sharp	29766
pMXS-hs-HMGA2	Addgene; pMXS-hs-HMGA2 was a gift from Shinya Yamanaka	52727
pCCLc-U6-shHMGA2.3-PGK-dTomato	Addgene; pCCLc-U6-shHMGA2.3-PGK-dTomato was a gift from Fernando Fierro	89606
pGL3-Sox2	Addgene; pGL3-Sox2 was a gift from Yuh-Shan Jou	101761

2.3 qPCR

Gene expression was analyzed using real-time quantitative polymerase chain reactions (qPCR).

RNA Extraction: Total RNA was extracted using Trizol® (Ambion; Waltham, MA, USA) reagent according to the manufacturer's protocol. Specifically, cell medium was vacuumed and 1 mL of Trizol® reagent was added to the plate of cultured cells. After 5 minutes, the cell lysate and Trizol® mixture was transferred to a 1.50 mL Eppendorf tube and allowed to homogenize for 5 minutes at room temperature. Then, 200 µL of chloroform was added to the tube, and the tube was shaken by hand for 30 seconds. After incubating the tube at room temperature for 5 minutes, the cell lysates were centrifuged at 12,000 g for 15 minutes at 4°C. The upper aqueous phase was then removed and transferred to a new tube without disturbing the interphase or lower phase. Then, 500 µL of 100% isopropanol was added to the upper aqueous phase, incubated for 10 minutes at room temperature, and centrifuged at 12,000 g for 10

minutes at 4°C. After centrifuge, the supernatant was removed, and the RNA pellet was washed with 1 mL of 70% ethanol. After the ethanol was removed, the RNA pellet was allowed to air dry for 10 minutes or until becoming transparent. 20-50 µL of RNase-free water was added to each Eppendorf tube to dissolve the RNA pellet, followed by incubation for 10 minutes at 65°C. The RNA concentration and purity (260/280 > 1.9 and 260/230 > 2.0) was measured by NanoDrop2000.

Reverse Transcription: 2 µg of total RNA was reverse transcribed using 1 µL of 10 mM dNTP mix and 1 µL of 10 uM Random Hexamers. This solution was incubated at 65°C for 5 minutes. When reverse transcribing miRNA samples, 1 µL of a specifically designed 10 uM stem loop primer was added to the solution instead of the Random Hexomers. Then, a 7 µl of master mix containing 4 µL of 5X First Strand Buffer, 2 µL 0.1 M dithiothreitol (DTT), 0.5 µL SuperScript II Reverse Transcriptase (Invitrogen; Waltham, MA, USA), and 0.5 µL double-distilled water (ddH$_2$O) was added to the mixture to create cDNA.

Real-Time qPCR: Reactions were prepared using SYBR® Green reaction mix (Roche; Basel, Switzerland). Real-time qPCR was performed using an ABI ViiA7 machine (Applied Biosystems; Burlington, ON, Canada). The default cycle settings on the machine were used: 2 minutes at 50°C and 10 minutes at 95°C, followed by 40 cycles of 15 seconds at 95°C and 1 minute at 60°C. Relative quantification of gene transcription was measured by comparing the $\Delta\Delta$Ct values of the housekeeping gene GAPDH to the gene-of-interest. All real-time qPCR experiments were carried out with at least three technical replicates and three independent biological replicates. Primer information is listed in Table 2.2.

Table 2.2 RT-qPCR Primer Information

Primer Name	Forward Primer Sequence (5'-3')	Reverse Primer Sequence (5'-3')
ALDH1A2	TTGCAGGGCGTCATCAAAAC	ACACTCCAATGGGTTCATGTC
ASCL1	CCCAAGCAAGTCAAGCGACA	AAGCCGCTGAAGTTGAGCC
CCNF	AGGACAAGCGCTATGGAGAA	TCTGTCTTCCTGGAGGCTGT
CDH1	ATTTTTCCCTCGACACCCGAT	TCCCAGGCGTAGACCAAGA
CDH2	TGCGGTACAGTGTAACTGGG	GAAACCGGGCTATCTGCTCG
CDK6	CCAGATGGCTCTAACCTCAGT	AACTTCCACGAAAAAGAGGCTT
CHGA	TAAAGGGGATACCGAGGTGATG	TCGGAGTGTCTCAAAACATTCC
CHGB	CGAGGGGAAGATAGCAGTGAA	CAGCATGTGTTTCCGATCTGG
FOXC1	TGTTCGAGTCACAGAGGATCG	ACAGTCGTAGACGAAAGCTCC
FOXD3	TCACGCACCAATTCTAACGC	CACGGCTTGCTTACTGAAGG
GAPDH	GGACCTGACCTGCCGTCTAGAA	GGTGTCGCTGTTGAAGTCAGAG
HEY1	GTTCGGCTCTAGGTTCCATGT	CGTCGGCGCTTCTCAATTATTC
HMGA2	AGTCCCTCTAAAGCAGCTCAAAAG	GCCATTTCCTAGGTCTGCCTC
ID4	GGCCACTCAAGCAGCATTTG	TCTGGTTGCCTGGTTAGGAC
IGDCC3	TCATCGGCATCCACATCG	GAGGACCCTGCCCCTTTG
IGF2BP1	GGCCATCGAGAATTGTTGCAG	CCAGGGATCAGGTGAGACTG
INTS2	GTCTCTTGGTGGCCAATGTT	AGGGCCTGAGAAGGATTCAT
KRT8	TCCTCAGGCAGCTATATGAAGAG	GGTTGGCAATATCCTCGTACTGT
LIN28B	TGTAGTCTACCTCCTCAGCCAA	ATTCTGCTTCCTGTCTTCCCTG
miR-let-7a	CCAGCTGGGTGAGGTAGTAGGTTGT	CTGGTGTCGTGGAGTCGGCAATT
miR-let-7b	CCAGCTGGGTGAGGTAGTAGGTTGT	CTGGAGCTAGTTTCGTCGTAGGG
miR-let-7c	CCAGCTGGGTGAGGTAGTAGGTTGT	TCCAGTGCAGGGTCCGAGGTA
miR-let-7d	CCAGCTGGGAGAGGTAGTAGGTTGC	CTGGTGTCGTGGAGTCGGCAATT
miR-let-7e	CCAGCTGGGTGAGGTAGGAGGTTGT	CTGGTGTCGTGGAGTCGGCAATT
miR-let-7f1	CCAGCTGGGTGAGGTAGTAGATTGT	CTGGTGTCGTGGAGTCGGCAATT
miR-let-7g	CCAGCTGGGTGAGGTAGTAGTTTGT	CTGGTGTCGTGGAGTCGGCAATT
miR-let-7i	CCAGCTGGGTGAGGTAGTAGTTTGT	TCCAGTGCAGGGTCCGAGGTA
miR-98	CCAGCTGGGTGAGGTAGTAAGTTGT	CTGGTGTCGTGGAGTCGGCAATT
SCGN	GGCCATTTCTGAGGCTAAACT	GGGCTCCTGTTTTACTAACATCA

SIX2	AAGGCACACTACATCGAGGC	CACGCTGCGACTCTTTTCC
SOX2	GCCGAGTGGAAACTTTTGTCG	GGCAGCGTGTACTTATCCTTCT
SYP	TTAGTTGGGGACTACTCCTCG	GGCCCTTTGTTATTCTCTCGGTA
SYT4	ATGGGATACCCTACACCCAAAT	TCCCGAGAGAGGAATTAGAACTT
U6	GCTTCGGCAGCACATATACTAAAAT	CGCTTCACGAATTTGCGTGTCAT

Primer Name	Stem Loop Primer Sequence (5'-3')
miR-let-7a	CTCAACTGGTGTCGTGGAGTCGGCAATTCAGTTGAGAACTATAC
miR-let-7b	CTCAACTGGAGCTAGTTTCGTCGTAGGGCAGTTGAGAACCACAC
miR-let-7c	GTCGTATCCAGTGCAGGGTCCGAGGTATTCGCACTGGATACGACAACCAT
miR-let-7d	CTCAACTGGTGTCGTGGAGTCGGCAATTCAGTTGAGAACTATGC
miR-let-7e	CTCAACTGGTGTCGTGGAGTCGGCAATTCAGTTGAGAACTATAC
miR-let-7f1	CTCAACTGGTGTCGTGGAGTCGGCAATTCAGTTGAGAACTATAC
miR-let-7g	CTCAACTGGTGTCGTGGAGTCGGCAATTCAGTTGAGAACTGTAC
miR-let-7i	GTCGTATCCAGTGCAGGGTCCGAGGTATTCGCACTGGATACGACAACAGC
miR-98	CTCAACTGGTGTCGTGGAGTCGGCAATTCAGTTGAGAACAATAC
U6	CTCAACTGGTGTCGTGGAGTCGGCAATTCAGTTGAGAAAAATATG

2.4 Western Blot

After being washed with PBS and centrifuged at 8000 g for 3 minutes at 4°C,

cells were lysed in lysis buffer containing 50 mM Tris-HCl (pH 8.0), 150 mM NaCl, 1%

NP-40, 0.5% sodium deoxycholate, and 0.1% sodium dodecyl sulfate (SDS) with

proteinase and phosphatase inhibitors (Roche) in 1.50 mL Eppendorf tubes. The cell

lysate was then sonicated and centrifuged at 12,000 g for 10 minutes at 4°C. The

supernatant was then collected and transferred to a new 1.50 mL Eppendorf tube.

Protein concentration was then measured with the Pierce BCA Protein Assay Kit

(ThermoFisher Scientific; Missisauga, ON, Canada) according to the manufacturer's

protocol. Approximate equal weights of total protein (40-60 µg) were then mixed with

and denatured by SDS and boiled for 5 minutes at 95°C. Protein samples were loaded onto a 8-15% SDS polyacrylamide gel and separated by electrophoresis and transferred onto a polyvinylidene difluoride (PVDF) membrane (Millipore; Bedford, MA, USA). Transfers were performed using the semi-dry transfer method (40-60 minutes at 25 V at room temperature with the Trans-Blot® SD Semi-Dry Transfer Cell). Membranes were blocked with Odyssey Blocking Buffer for 1 hour at room temperature. The membranes were then immunoblotted with specific primary antibodies (1:500 to 1:2000 dilution) listed in table 2.3 overnight at 4°C. After 3 x 10 minute washes with the tris-buffered saline plus TWEEN-20 (TBS-T) buffer, the membranes were washed in secondary antibodies (rabbit/mouse IgG-HRP, Santa Cruz; Dallas, TX, USA) at a dilution of 1:10,000 for 1 hour at room temperature. After three additional 10 minute washes in TBS-T, the membranes were probed by Pierce ECL Western Blotting Substrate (ThermoFisher Scientific) and imaged and developed using autoradiography films and a film processor (EL-RAD; Vancouver, BC, Canada). All Western blot experiments were carried out with at least three technical replicates and three independent biological replicates.

Table 2.3 Antibody Information

Antibody	Vendor	Catalogue Number	Application	Dilution
CD44 APC	eBioscience	17-0441-82	FC	1:10
CD133 APC	Miltenyi Biotec	130-098-829	FC	1:10
E-Cadherin	Santa Cruz	Sc-7870	WB	1:1000
N-Cadherin	Abcam	ab76011	WB	1:1000
Histone H3	Abcam	ab1791	WB	1:1000
HMGA2	Thermo Fisher	PA5-21320	WB	1:1000
Lin28B	Proteintech	16178-1-AP	IF, IHC	1:25
Lin28B	Abcam	ab71415	WB	1:500
Snai2 (Slug)	Abcam	ab27568	WB	1:1000
Snail	Cell Signaling	3895	WB	1:1000
SOX2	Novus Biologicals	NB110-37235	IHC	1:25
SOX2	Cell Signaling	3579S	WB	1:1000
Tubulin	Abcam	ab18251	WB	1:1000
Vinculin	Sigma Aldrich	V9131-2ML	WB	1:2000
7-AAD	BD Pharmingen	51-68981E	FC	1:10

* FC = Flow Cytometry

* IF = Immunofluorescence

* IHC = Immunohistochemistry

* WB = Western blot

2.5 Luciferase Reporter Assay

DU145, DuNE, H69, LNCaP, and LnNE cells were transiently transfected with either pGL3-IRES-Lin28b-P3, pGL3-Sox2, or control, as well as a Renilla luciferase vector. 24 hours post transfection, cells were collected, washed with PBS, and lysed with passive lysis buffer. The luciferase activity of the cell lysates were determined using the Dual-Luciferase Reporter Assay System (Promega; Madison, WI, USA) on the Tecan Infinite 200 Pro (Tecan Group Ltd.; Männedorf, Switzerland) according to the manufacturer's protocol. Renilla values were used as transfection controls and transfection efficiency was normalized to renilla luciferase activities. All luciferase

reporter assays were carried out with at least three technical replicates and three independent biological replicates.

2.6 MTS Incorporation Assay

2D proliferation rates were measured using the CellTitre® 96 AqueousOne kit (Promega) according to the manufacturer's protocol. 2D-proliferation rates were measured at an OD of 490nm every other day for 9 days post-seeding. Each experiment contained six technical replicates, and three independent experiments were performed.

2.7 3D *In vitro* Tumorsphere Formation Assays

Matrigel® (Corning; New York, NY, USA) was thawed overnight on ice at 4°C. Using ice-cold DMEM medium with 10% FBS, Matrigel® was diluted to 5 mg/mL. Then, a 48-well plate was coated by adding 50 µL of Matrigel matrix to each well. The plate was then incubated at 37°C for 30 minutes to form a gel. During this time, following standing passaging protocol, cells were centrifuged into a pellet and re-suspended in DMEM medium with 10% FBS to adjust the cell density to $3x10^5$ cells/mL. 15 µL of the prepared cell suspension was then added to 135 µL of Matrigel® for a final density of $3x10^4$ cells/mL. 150 µL of the matrix cell mix was added into each well, and the plate was incubated at 37°C for 30 minutes, where 250 µL of DMEM medium with 10% FBS was added to each well. Cells were maintained in culture for 7 days, with the medium refreshed every 2 days. Tumorspheroids were imaged using the Zeiss AxioObserver Z1

light microscope (Carl Zeiss AG) at 35x magnification. Two technical replicates and three independent biological replicates were performed.

2.8 Flow Cytometry and Fluorescence-Activated Cell Sorting (FACS)

Flow Cytometry: Cells were first detached from 10.0 cm non-coated plates by adding 3.0 mL of 1 mM ethylenediaminetetraacetic acid (EDTA, Sigma-Aldrich; St. Louis, MI, USA) to the dish and subsequently incubating it for 2 minutes at 37°C. To ensure that each 1.50 mL Eppendorf tube had $1.0x10^6$ cells/mL in it, a TC20™ Automated Cell Counter (Bio-Rad Laboratories; Hercules, CA, USA) was used to count the cells. Eppendorf tubes were then labelled as one of the following: unstained control, isotype control (one tube with all isotypes), positive control(s) (one tube for each fluorophore), and 7-Aminoactinomycin D (7-AAD). A fluorophore is a fluorescent protein that is often co-expressed with the protein of interest. Antibodies that were used as positive controls are listen in table 2.3. Samples were then centrifuged at 1500 g for 5 minutes at 4°C, and the supernatant was suctioned off using a pipette to avoid damaging the cells. 400 µL of FACSWASH (0.5% BSA in PBS) was then added to each sample and the centrifugation process was repeated, with the supernatant suctioned off using a pipette. 10.0 µL of Fc Blocker (BD Biosciences; San Jose, CA, USA) was added to each sample, and the samples were incubated for 10 minutes at room temperature. Then, 50.0 µL of a 1:1600 dilution of Biotin-EpCAM (Abcam) was added to the positive control samples, and the Eppendorf tubes were incubated for 30 minutes on ice. While the samples were incubating, 1:10 positive control antibodies were made by diluting the antibodies with FACSWASH, and 40.0 µL of the antibody solution was added to each

sample and incubated for 30 minutes on ice. Cells were then washed three times with 300 μL of FACSWASH and subsequently resuspended in 400.0 μL of FACSWASH.

FACS Analysis: Relative DNA contents from 2.0×10^5 cells were analyzed by FACSCanto II flow cytometer (BD Biosciences) and data were analyzed using FlowJo software (TreeStar; Woodburn, OR, USA). Each experiment contained two technical replicates, and three independent experiments were performed.

2.9 Fluorescence Microscopy Immunofluorescence (IF)

2.0×10^4 DuNE cells were seeded on coverslips and fixed after 24 hours for immunofluorescence (IF). After the blocking solution was aspirated, diluted LIN28B (Proteintech) primary antibody was applied to the cells and incubated for 1.5 hours at room temperature. Antibody information is listed in table 2.3. After washing with 1x PBS 3 times for 3 minutes, Rhodamine-Goat anti-Rabbit IgG (Invitrogen) was applied to the cells and incubated for 1 hour at room temperature in a dark, moist environment. After washing with 1x PBS 3 times for 3 minutes, coverslips were mounted with Vectashield® mounting medium with DAPI (Vector Laboratories; Burlingame, CA, USA). Cells were imaged using the Zeiss AxioObserver Z1 (Carl Zeiss AG; Oberkochen, Germany) microscope. Each experiment contained two technical replicates, and three independent experiments were performed.

LIN28B subcellular localization was also confirmed by Western blotting nuclear and cytoplasmic extracts from cells transfected with Flag-tagged LIN28B using a nuclear protein extraction kit (Sigma) according to the manufacturer's instructions.

2.10 Tissue Microarray (TMA)

The CRPC tissue microarray (TMA) containing 100 tissue cores from 50 patients that had undergone hormonal therapy, chemotherapy, or radiotherapy was obtained from the tissue bank at VPC. This TMA was used for Chapter 3. The histopathology of the primary tumors (n=16), CRPC (n=54), and t-NEPC tumors (n=30) have been previously reported and characterized (65).

2.11 IHC Assays and Digital Image Analysis

IHC Assays: IHC staining was conducted with the Discovery XT autostainer (Ventana Medical Systems; Oro Valley, AZ, USA) and examined with their UltraMap^{TM} DAB kit (Ventana Medical Systems). Antibodies used for IHC are listed in table 2.3.

Digital Image Analysis: All stained slides were digitalized with the SL801 autoloader and Leica SCN400 scanning system (Leica Microsystems; Wetzlar, Germany) at a magnification equivalent to 40X (scale bar, 100 μm). The images were subsequently stored in the VPC SlidePath digital imaging hub (Leica Microsystems).

2.12 Ion AmpliSeq Transcriptome Sequencing and Gene Set Enrichment Analysis (GSEA)

Ion AmpliSeq Transcriptome Sequencing: DuNE shCntl and DuNE shLIN28B cells were extracted using the mirVana^{TM} RNA Isolation Kit (Ambion) according to the manufacturer's protocol. The quality of the RNA samples was assessed by Nanodrop^{TM} 2000 and 2100 Bioanalyzer (Caliper Life Sciences; Hopkinton, MA, USA). Samples were then sent for Ion AmpliSeq Transcriptome Sequencing. Next, Ion AmpliSeq transcriptome library preparation, sequencing, and primary analyses were completed by

the UBC-DMCBH Next Generation Sequencing Centre (Vancouver, BC, Canada)

following the protocol detailed by Li *et al.* (65). In summary, cDNA was synthesized from

100 ng of total RNA using the SuperScript® VILOTM cDNA Synthesis kit (Invitrogen)

and amplified with Ion AmpliSeqTM technology (ThermoFisher Scientific). cDNA libraries

were diluted to 100 pM and amplified on Ion Torren OneTouchTM 2 instrument

(ThermoFisher Scientific) using emulsion PCR. Templated libraries were then subjected

for sequencing of >20,000 RefSeq transcripts using the Ion Torrent ProtonTM

sequencing system (ThermoFisher Scientific).

Gene Set Enrichment Analysis (GSEA): GSEA was carried out to determine

whether a defined set of genes showed concordant enrichment between two sample

groups (e.g. shLIN28B vs Cntl) or two clinical phenotypes (e.g. t-NEPC with high vs low

LIN28B expression). The analyses in Chapter 3 were performed using the latest

MSigDB database for each gene set collection or using gene sets curated based on

published data. Heatmaps were constructed based on the results of the AmpliSeq data.

GSEA analyses in Chapter 3 used whole transcriptomic data with a *p*-value cut-off as

0.01.

2.13 Construction of prostate cancer cell lines by GeneArt™ CRISPR technology

DuNE cells with destructed exon 1 of LIN28B were generated using the

GeneArt™ Precision gRNA Synthesis Kit (Invitrogen A29377) and GeneArt™

Platinum™ Cas9 Nuclease (Invitrogen B25640) according to the manufacturer's

protocol. The sequences for the guide RNA (gRNA) synthesis were designed using the

GeneArt™ CRISPR Search and Design tool (thermofisher.com/crisprdesign). Cells

underwent selection for single cell colonies in 96 well plates. Successful depletion of LIN28B was confirmed by immunoblotting assays using LIN28B antibody and Sanger sequencing on PCR products amplified from genomic DNA extracted selected colonies.

2.14 Clinical and PDX Datasets

Clinical cohorts used in Chapter 3 include the following: RNA-seq data for the Beltran 2016 cohort (CRPC-Ad, n=34; t-NEPC, n=15) was from Weill Medical College of Cornell University (New York, NY, USA) and was accessed through cBioPortal (89). RNA-seq dataset of the DuNE and LnNE cell models were previously reported by our lab, and were accessed under the accession number GSE118104 and GSE86942 in the Gene Expression Omnibus (GEO) database, respectively (101, 183). cDNA samples from the LTL patient derived xenograft (PDX) models were shared by Dr. Yuzhuo Wang from the VPC and were accessed under the accession number GSE41193 in the GEO database. Microarray data from the Living Tumor Laboratory (LTL) 331-7 and 331-7-R castration time-series PDX model was accessed under the accession number GSE59986 from the GEO database (184). Sequencing data for the GEMMs including the Ku *et al.* (WT; wild-type, SKO; single knock-out, DKO; double knock-out, TKO; triple knock-out) (100) was accessed under the accession number GSE90891 and Zou *et al.* NPp53 cohorts (92) was accessed under the accession number GSE92721 from the GEO database. Lastly, RNA-seq dataset for the Stand Up 2 Cancer (SU2C) data was obtained from cBioPortal. Descriptions on how data was collected for each database and key findings from the studies are located in table 2.1.

Table 2.4 Clinical and PDX Dataset Information

Model	Description of Samples	Characteristics of Samples
Beltran 2016 Cohort	• Tumors and germline DNA was collected from 81 male subjects either from peripheral blood mononuclear cells or benign tissues	• Tumors were classified based on histomorphology as adenocarcinoma (A) or CRPC-NE (B–E) • A: Usual prostate adenocarcinoma without neuroendocrine differentiation • B: Usual prostate adenocarcinoma with >20% neuroendocrine differentiation • C: Small-cell carcinoma • D: Large-cell neuroendocrine carcinoma • E: Mixed small-cell carcinoma-adenocarcinoma
DuNE Cell Model	• Lentiviral expression vectors (pFUGWBW) encoding Flag-SRRM4 and empty control vector were used to package lentivirus in 293T cells and transduce Du145 cells • Transduced cells were selected by blasticidin • Expression of SRRM4 was confirmed by real-time qPCR and immunoblotting assays	• Reduced E-Cadherin and pan-cytokeratin levels, compared to its respective control • Strong expression of the NE marker SYP • Ki-67 positive • Cells grew in high density with minimal stromal components • The phenomenon that occurred are similar to what occurs when tumors form from NCI-H660 cells, which is a known NEPC model • The DuNE model represents a clinically relevant model to study the SRRM4-SOX2 axis during t-NEPC progression

LnNE Cell Model	• Lentiviral expression vectors (pFUGWBW) encoding Flag-SRRM4 and empty control vector were used to package lentivirus in 293T cells and transduce LNCaP cells • Transduced cells were selected by blasticidin • Expression of SRRM4 was confirmed by real-time qPCR and immunoblotting assays	• 30% decrease in REST, 130-fold increase in REST4 mRNA levels, compared to its respective control • Strong expression of the NE markers CHGB, SYP, SCG3, SCGN, NSE, ASCL1, and SYT4 • These results indicate that SRRM4 alternatively splices the *REST* gene, and that contributes additively to NEPC transdifferentiation
LTL PDX Model	• Fresh primary or metastatic prostate cancer samples were collected from 18 patients directly after surgery or biopsy and were transplanted into male SCID mice supplemented with testosterone • Tumor lines were established and expanded for a minimum of five generations of serial passaging • The two tumor lines with the shortest latency before line establishment and the fastest tumor volume doubling time were derived from metastatic NEPC • The remaining tumor lines represent adenocarcinoma	• The adenocarcinoma tumors preserved their glandular structure and retained AR and PSA expression • The NEPC tumors presented as oval tumor cells with minimal cytoplasm and frequent mitotic figures • The NEPC tumors were negative for AR and PSA but positive for CHGA and SYP
LTL331/331R AdPC-to-t-NEPC Model	• Upon host castration, primary adenocarcinoma (LTL331) initially regressed, but then relapsed as typical NEPC (LTL331R) .	• LTL331/331R is the first-PDX model of AdPC-to-NEPC transdifferentiation • The transdifferentiation process observed in the LTL331/331R model is predictive of disease progression and is recapitulated in the donor patient, which suggesting a strong clinical relevance
WT/SKO/ DKO/TKO GEMMs	• 27 mouse samples; 4 WT and 23 with floxed alleles	• SKO cancer was similar to human AdPC

	• The gene expression profile of prostate tumors from mice with different genotypes were compared using the following mice models: PBCre4:Ptenfl/fl, PBCre4:Ptenfl/fl:Rb1fl/fl, and PBCre4:Ptenfl/fl:Rb1fl/fl:Trp53fl/fl, where fl = floxed alleles of the indicated genes	• DKO and TKO cancers were similar to human NEPC • TKO mice developed aggressive prostate cancer with a median survival of 16 weeks • TKO mice expressed high SYP and low AR and AKT • These observations support the conclusion that *Rb1* and *Trp53* co-operate to suppress prostate cancer lineage plasticity, underlying the development of NEPC
NPp53 GEMMs Cohort	• Prostate tissue or tumor from: 9 month old Nkx3.1CreERT2/+ mice, 14 month old Nkx3.1CreERT2/+; Ptenflox/flox mice, 16 month old Nkx3.1CreERT2/+; Ptenflox/flox mice, 12 month old Nkx3.1CreERT2/+; Ptenflox/flox;P53flox/flox mice, 13 month old Nkx3.1CreERT2/+; Ptenflox/flox;P53flox/flox mice • Tissues or tumors were harvested, and snap frozen for subsequent molecular analysis	• *SOX11* expression was significantly up-regulated in high Gleason grade primary tumors, as well as in CRPC-NE relative to CRPC-Ad • CRPC-NE tumors had increased levels of NSE and SYP, relative to CRPC-Ad • Treatment-related *NPp53* CRPC phenotype shares molecular features in common with human CRPC-NE • Both focal and overt neuroendocrine differentiation arises by transdifferentiation of luminal prostate adenocarcinoma cells • *TP53* and *PTEN* inactivation plays a role in the progression of adenocarcinoma to CRPC-NE by transdifferentiation

SU2C 2015 Cohort	• High quality DNA and RNA was obtained from 150 bone or soft tissue biopsies • Central pathology revealed high-grade adenocarcinoma with four cases showing neuroendocrine differentiation	• Deviations in AR, TP53 and PTEN occurred in 40-60% of cases • TP53 and AR alterations were the highest in metastatic CRPC compared to primary prostate cancer

2.15 Statistics

Statistical analyses were carried out using R (version 3.3.2). All results are expressed as the mean ± SD. Statistical analyses were done using GraphPad Prism (version 6). One-way ANOVA or unpaired Student's *t*-tests were carried out to determine differences between groups. Correlation between two expression groups were measured by Pearson's *r* correlation coefficient. The level of significance was set at *P*<0.05, *P*<0.01, *P*<0.001, *P*<0.0001 denoted as *, **, ***, and **** respectively.

2.16 Technical Support

I would like to thank Ms. Sonia Kung for her help and persistence with the IHC staining. I would also like to thank Dr. Mannan Nouri for sharing his flow cytometry protocol and his expertise in analyzing FACS data.

Chapter 3: Results

3.1 LIN28B expression is positively correlated with t-NEPC progression

The relationship between LIN28B, plasticity, and stemness in cancer development has recently become an area of interest as its role in RNA regulation has been linked to altered miRNA expression during ESC differentiation and somatic cell reprograming (185). While other core embryonic stem cell factors, such as SOX2 and POU5F1, have been implicated in tumorigenesis, advanced malignancy, and stemness properties in prostate cancer, the role of LIN28B in t-NEPC development and how it relates to stemness is unclear (99, 186). We previously reported that, through the upregulation of a pluripotency gene network, there are distinct subgroups of t-NEPC tumors that express stem-like characteristics (101). To expand upon these findings and define the clinical relevance of these core ESC genes in t-NEPC development, we examined LIN28A, LIN28B, SOX2, POU5F1, and NANOG expression in the RNA-seq data of the Beltran 2016 patient cohort as well as in the NEPC cell models LnNE and DuNE (Fig. 3.1A). Tumors in the 2016 Beltran cohort could be distinguished by distinctive expression levels of LIN28B. There were 7 t-NEPC tumors with low LIN28B expression, t-NEPC(LIN28B^{low}), similar to that of the CRPC-Ad tumors, while the remaining 8 t-NEPC tumors expressed a ~98.6-fold increase in LIN28B expression, t-NEPC (LIN28B^{high}) (Fig. 3.1A, Appendix Ai). The t-NEPC(LIN28B^{high}) tumors overlapped with the previously reported t-NEPC(SOX2^{high}) tumors (101), but not with any of the other embryonic stem cell genes, signifying a potential positive correlation between LIN28B and SOX2 expression. We also found that the DuNE, but not the LnNE, cell model had a significant increase in both LIN28B and SOX2 expression, compared to their respective control cell lines (Fig. 3.1A). The previously established LnNE model

illustrates the long term progression from AdPC to NEPC as demonstrated by its gradual decrease in PSA as well as its neuronal-like phenotype, whereas the DuNE model recapitulates the phenotypes of clinical t-NEPC tumors expressing stem-like characteristics (65, 101). This data demonstrates that different subgroups of t-NEPC tumors exist, where the division of the two subgroups is evident based on the robust difference in LIN28B expression levels. While exploring RNA-seq data reported by Beltran *et al.* (2016) and SU2C from cBioPortal (2016), we observed a negative association between LIN28B and AR expression (Appendix Aii-iii). The LTL PDX model showed positive associations between NEPC and LIN28B expression (Fig. 3.1B), and the LTL331/331R PDX model that demonstrates the progression of AdPC to t-NEPC after castration surgery showed that LIN28B was positively correlated with SOX2 and SYP, but negatively correlated with AR expression (Fig. 3.1C). Furthermore, analyses of the recently reported WT/SKO/DKO/TKO GEMMs model by Ku *et al.* (2017) revealed that LIN28B was positively expressed in the TKO/DKO samples (Fig. 3.1D). In the NPp53 GEMMs model by Zou *et al.* (2017) LIN28B expression was significantly increased in the overt NE, but not the focal NE samples (Appendix Aiv). Interestingly, LIN28A expression was not statistically increased in the Beltran *et al.* (2016), cBioPortal (2016), or LTL331/331R PDX models (Appendix B).

We then analyzed and compared the expression level of LIN28B among prostate cancer cell lines. Absolute real-time qPCR, immunoblotting (Fig. 3.2A), luciferase assays (Fig. 3.2B), and IHC (Fig. 3.2C) showed that LIN28B expression was low in all AdPC cell lines, but high in the well-established NEPC cell model, NCI-H660, as well as in the SCLC cell line H69. This data is similar to that obtained from the Barretina cell

lines (2012) (Appendix Av). Interestingly, these results also demonstrated a significant

increase in LIN28B expression in the DuNE, but not the LnNE, cell model. Together

these findings support the idea that LIN28B is a major component of the intermediate

pluripotency stem cell network that develops in a subset of t-NEPC tumors.

Figure 3.1
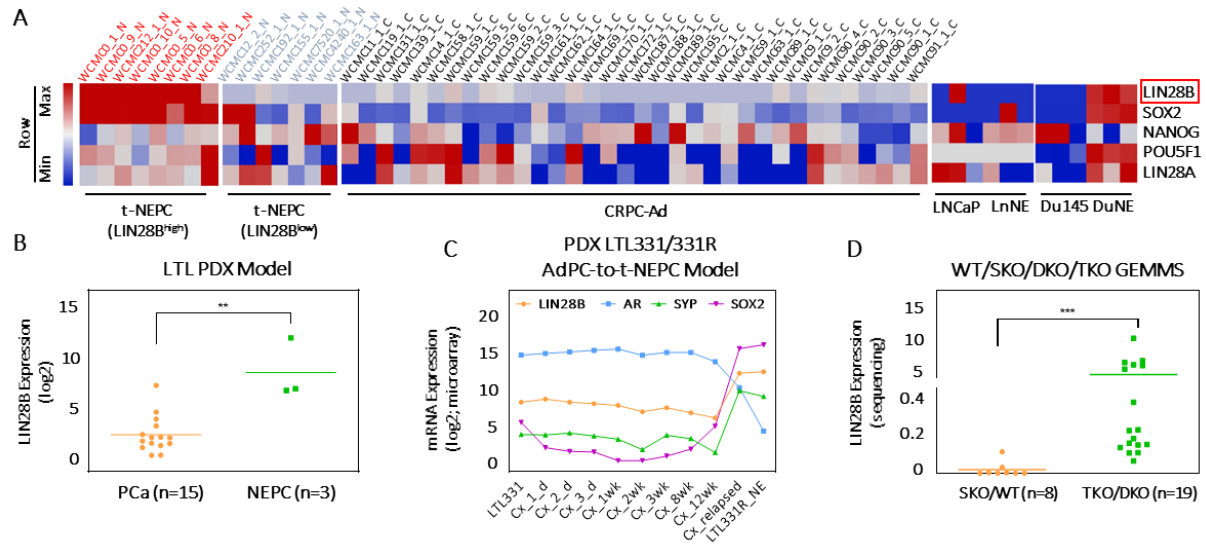
Figure 3.1 A subset of clinical t-NEPC tumors and the DuNE model have high LIN28B expression. (A) *LIN28B* expression was compared among CRPC tumor samples from the Beltran *et al.* (2016) cohort and separated into three groups: CRPC-Ad (n=34), t-NEPC expressing low levels of *LIN28B*, t-NEPC(LIN28B^low) (n=7), and t-NEPC expressing high levels of *LIN28B*, t-NEPC(LIN28B^high) (n=8). *LIN28B* expression was also compared among the LnNE and DuNE cell models and their respective control cell lines, LNCaP and Du145. Expressions of the core enrichment stem cell signatures genes in each patient sample (patient ID: "WCMC-") and cell line are indicated as high, red, or low, blue. **(B)** The expression of *LIN28B* during the progression of PCa (n=15) to NEPC (n=3) after castration in the LTL PDX model are shown. **(C)** The expressions of *LIN28B*, *SOX2*, *AR*, and *SYP* during the progression of AdPC (LTL331) to t-NEPC (LTL331R_NE) after castration in the PDX LTL331/331R model are shown. **(D)** *LIN28B* expression in WT/SKO/DKO/TKO GEMMs is shown. Statistical analyses were performed by one-way ANOVA or unpaired student's t test with **, ***, denoting *P*<0.01, *P*<0.001, respectively). AdPC, adenocarcinoma prostate cancer; CRPC-Ad, castration-resistant prostate adenocarcinoma; CRPC, castration-resistant prostate cancer; DKO, double knock-out; GEMMs, genetically engineered mouse models; PCa, prostate cancer, PDX, patient-derived xenograft; SKO, single knock-out; TKO, triple knock-out; t-NEPC, treatment-induced neuroendocrine prostate cancer; WT, wild-type.

Figure 3.2
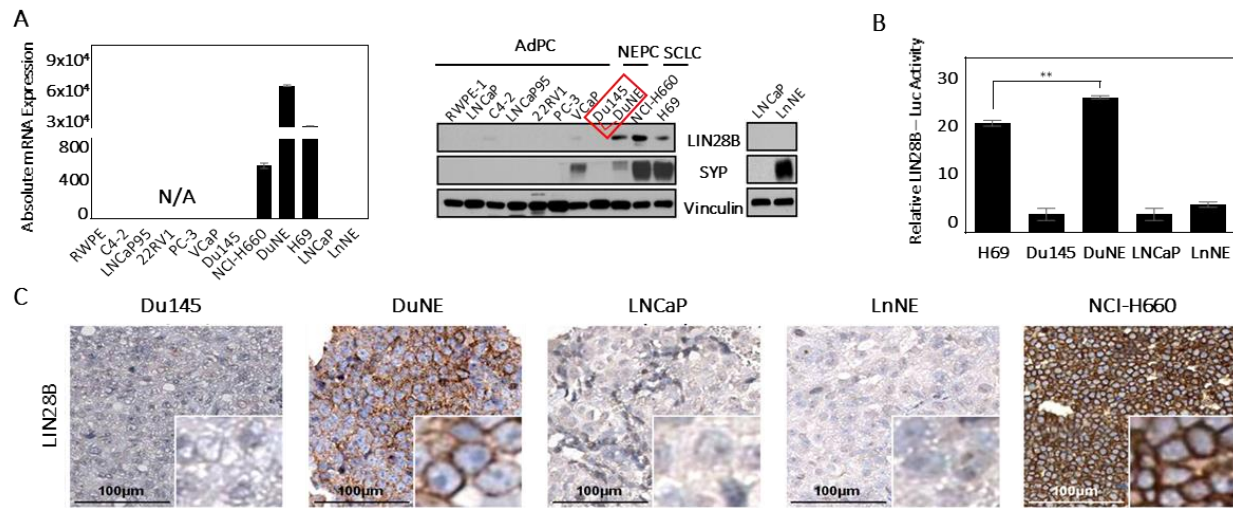
Figure 3.2 LIN28B expression is positively correlated with t-NEPC progression.
(A) The expression of *LIN28B* in AdPC, NEPC, and SCLC cell lines, as well as the newly established LnNE and DuNE models was measured by real-time qPCR for absolute quantification using a standard curve and immunoblotting. **(B)** H69, Du145, DuNE, LNCaP, and LnNE cell lines were transfected with *LIN28B* expression vector for 24 hours. Luciferase activities were measured and calibrated with Renilla luciferase activity. **(C)** AdPC, NEPC, and the LnNE and DuNE cell models were used to stain against *LIN28B* by IHC. Scale bars represent 100 µm. Three independent technical replicates were performed for each experiment. Only one set of the representative immunoblots is shown. All results are presented as mean ± SD. Statistical analyses were performed by unpaired student's t test with **, denoting *P*<0.01). AdPC, adenocarcinoma prostate cancer; NEPC, neuroendocrine prostate cancer; SCLC, small cell lung cancer; IHC, immunohistochemistry.

3.2 LIN28B and SOX2 expressions are positively correlated within a subgroup clinical NEPC tumors

It has been well documented that the transition from AdPC to t-NEPC can be through an intermediate SC-like state. Throughout this state, the expression of pluripotency genes, including SOX family members such as SOX2 and SOX11, is increased (92, 99-101, 187). These pluripotency genes are well known for their role in early embryogenesis, embryonic SC pluripotency, and neurogenesis (92, 99-101, 187). Furthermore, the proliferation of neural precursor cells is promoted by SOX2 through high LIN28B expression (130). Based on this information, we reasoned that co-expression of LIN28B and SOX2 may be vital for a subset of t-NEPC tumors to progress from and intermediate pluripotency phenotype to NE differentiation.

To study the association between LIN28B and SOX2 expression in t-NEPC, we applied IHC on a human CRPC TMA containing 100 cores: 16 primary tumors, 54 CRPC, and 30 t-NEPC (Fig 3.3A). We first confirmed that, in our prostate cancer model, LIN28B is expressed in the cytoplasm (Appendix Ci). Using the human CRPC TMA, we found that LIN28B and SOX2 were significantly reduced in the primary tumor and CRPC cores (Fig 3.3A). Statistical analyses indicated that the expression of both LIN28B and SOX2 were significantly increased in t-NEPC ($P < 0.001$) (Fig 3.3A-B). We found that LIN28B was expressed in 14 out of 30 t-NEPC tissue cores, whereas SOX2 was expressed in 15 out of 30 t-NEPC tissue cores (Fig 3.3A). Moreover, when the t-NEPC cores were subdivided into t-NEPC(LIN28B^{low}) and t-NEPC(LIN28B^{high}) groups, we found that both LIN28B and SOX2 expression were significantly higher in the t-NEPC(LIN28B^{high}) cores, and that their expression showed a significant positive correlation ($P < 0.001$) (Fig 3.3B). This finding was consistent with data from both

Beltran *et al.* (2016) and SU2C from cBioPortal (2016) (Appendix Cii-iii). Together, these findings support the idea that LIN28B and SOX2 are both part of a pluripotency network that promote CRPC progression to t-NEPC in a specific subset of tumors.

To further elucidate a relationship between LIN28B and SOX2 expression in t-NEPC we utilized the DuNE cell model which is AR- and PSA-negative, TP53- and RB1-null, exhibits striking neuronal-like morphologies, and mimics the molecular signatures of a subset of clinical t-NEPC (i.e. small-cell prostatic carcinoma) that present stem-like characteristics. While SOX2 was downregulated when the DuNE cells were challenged with LIN28B-targeted shRNA (Fig 3.3C), SOX2 overexpression in DU145 cells did not cause a significant increase in LIN28B expression (Appendix Civ). Collectively, these findings recognize two distinct subgroups of t-NEPC tumors classified by LIN28B and SOX2 expression. Our results support that t-NEPC development may be driven through different mechanisms, and that the upregulation of both LIN28B and SOX2 may be complimentary in inducing a pluripotent stem-like state.

Figure 3.3
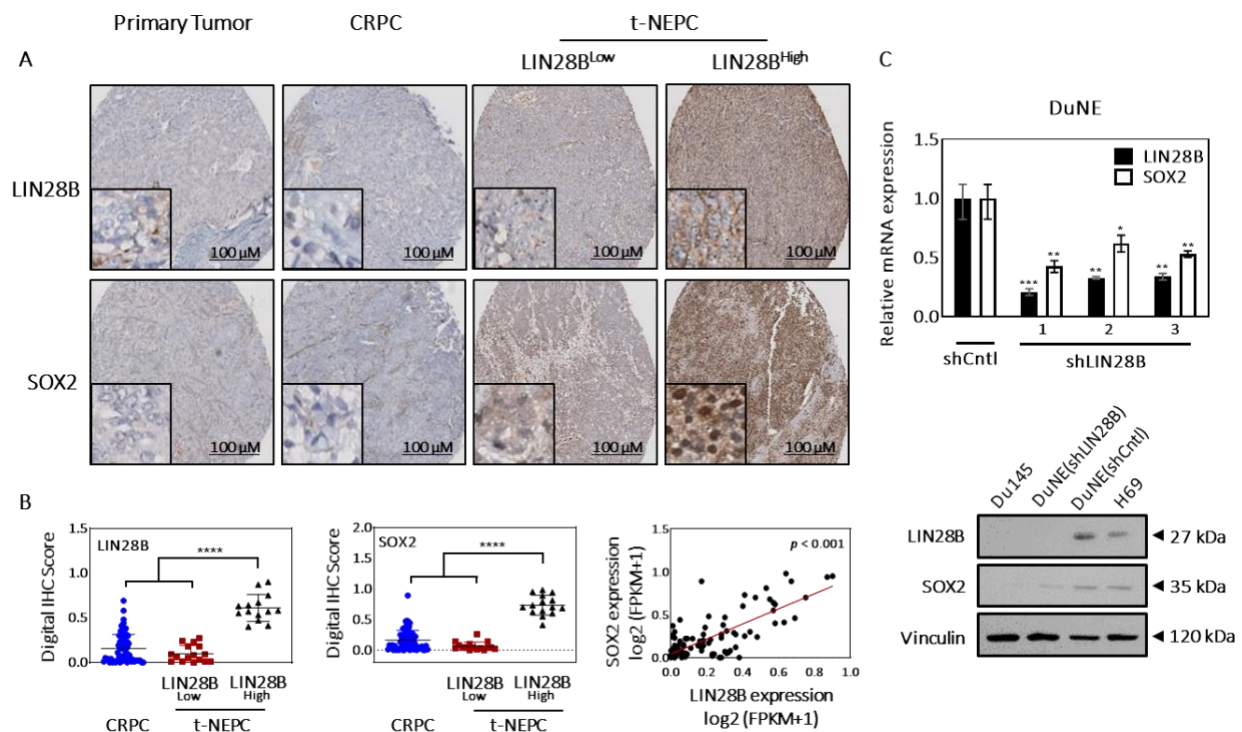
Figure 3.3 LIN28B and SOX2 expression are positively associated within a subgroup clinical NEPC tumors. (A) A human CRPC TMA (n=100 cores) was stained against *SOX2* and *LIN28B* by IHC. One representative core from each of the histologically diagnosed primary tumor (n=16), CRPC-Ad (n=54), t-NEPC(LIN28B^{low}) (n=16), and t-NEPC(LIN28B^{high}) (n=14) cores is shown. Scale bars represent 100 μm. **(B)** Average IHC scores within the tumor subtypes CRPC, t-NEPC(LIN28B^{low}) and t-NEPC(LIN28B^{high}) are shown as well as the Pearson's *r* correlation coefficient (0.60) between *LIN28B* and *SOX2* expressions. **(C)** DuNE cells were transfected with control or shLIN28B and extracted for RNA and protein to detect the expression levels of indicated genes using qPCR and immunoblotting assays. Three independent technical replicates were performed for each experiment. Only one set of the representative immunoblots is shown. All results are presented as mean ± SD. Statistical analyses were performed by one-way Anova or unpaired student's *t* test with *, **, ***, **** denoting *P*<0.05, *P*<0.01, *P*<0.001, *P*<0.0001, respectively). CRPC-Ad, castration-resistant prostate adenocarcinoma; CRPC, castration-resistant prostate cancer; IHC, immunohistochemistry; TMA, tissue microarray; t-NEPC, treatment-induced neuroendocrine prostate cancer.

3.3 LIN28B pathway promotes the development of a stem-like pluripotency gene network in DuNE model

Stem cells and cancer stem cells share similar properties such as their ability to self-renew and express core embryonic stem cell signatures (134), which have been found to promote the induction of cancer stem–like properties and tumor development (188-190). Based on this information, Yu *et al.* (2003) reported that by using a combination of the core embryonic stem cell signature genes, human somatic cells can be reprogrammed into induced pluripotent stem cells (129). Due to the fact that SOX2 mediates the ESC/stem-like transition, we investigated the role of LIN28B signaling by inducing a pluripotent stem-like state in DuNE cells.

To understand which signaling networks are regulated by LIN28B expression, we developed a CRISPR/Cas9 knock-in strategy in DuNE cells to inhibit LIN28B expression and confirmed its deletion by immunoblotting and Sanger sequencing (Appendix Di-ii). Using Ion AmpliSeq Transcriptome analyses, we profiled and compared the DuNE(gLIN28B) transcriptome to the Beltran t-NEPC(LIN28B[Low]) subgroup (n=3291 and 3302 genes, respectively; Fig 3.4A). The transcriptomes were mostly distinct, with the exception of 550 genes in common (Fig 3.4A). To investigate the biological differences between the DuNE(gControl) and DuNE(gLIN28B) transcriptomes, we carried out GSEA and compared the two phenotypes. We found that the DuNE(gLIN28B) transcriptome had a reduction in the expression of gene sets related to cell lineage plasticity and embryogenesis (Fig 3.4B). For example, the silencing of LIN28B was negatively associated with well-defined gene sets named "Oishi Cholangioma Stem Cell Like Up", "Ramalho Stemness Up", and "Benporath ES 2" (Fig 3.4B). Furthermore, the top 10 genes that were associated with the DuNE(gLIN28B) cell lines were also

associated with the Beltran t-NEPC(LIN28B^{Low}) subgroup (Fig 3.4B; Appendix Diii). Together, these findings further suggest that LIN28B plays a role in reprogramming the AdPC phenotype towards a stem cell-mediated phenotype by activating a pluripotency gene network.

To determine the functional significance of LIN28B, we used flow cytometry and our DuNE(gLIN28B) CRISPR cell line and found that, in comparison to the control cells, removing LIN28B decreased the percentage of CD44$^+$CD133$^+$ cells (Fig 3.5A). To assess the effects of LIN28B on cellular tumor initiation and growth, we employed 3D sphere formation and MTS assays which indicated that knocking down LIN28B expression reversed the ability for LIN28B to create spheroids and maintain cell viability, resulting in a decrease of sphere formation and survival, respectively (Fig 3.5B-C).We then validated the mRNA expression of 10 genes, including SOX2, using qPCR (Fig 3.5D). LIN28B depletion resulted in the reduced expression of several pluripotency genes and NE markers (Fig 3.5E). These results demonstrated that LIN28B mediates the regulation of tumorigenesis and stemness-derived reprogramming properties in DuNE cells. Western blot results demonstrate that depleting LIN28B caused a decrease in N-cadherin and Snai2, and an increase in E-cadherin, suggesting that LIN28B causes an EMT in DuNE cells (Fig 3.5F). These results demonstrate that LIN28B regulates a pluripotency gene network in the DuNE model.

Figure 3.4
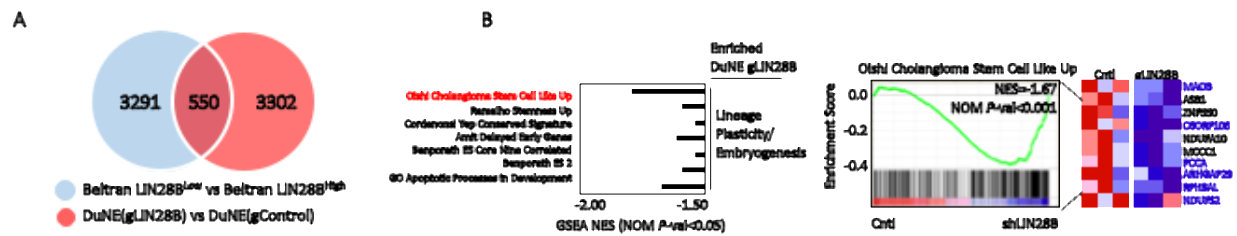
Figure 3.4 LIN28B mediates stemness properties in the DuNE cell line. (A) Compared to control, genes unique to the transcriptomes of DuNE(gLIN28B) (n=3291) or Beltran LIN28B^{Low} (n=3302) overlapped (n=550) using a fold change threshold of 1.5 and *P*<0.05 cut-off. **(B)** Transcriptome data of the DuNE(gLIN28B) cell model and its respective control, DuNE (p-value cut-off as 0.01) were analyzed by GSEA based on the latest MSigDB database for each collection. GSEA revealed a decreased enrichment of genes associated with lineage plasticity/embryogenesis when *LIN28B* expression was knocked down in the DuNE cells. Genes that are blue indicates that the expression of these genes is also upregulated in the LIN28B^{low} cohort from Beltran *et al.* (2016). GSEA, gene set enrichment analysis; GO, gene ontology; NES, normalized enrichment score.

Figure 3.5
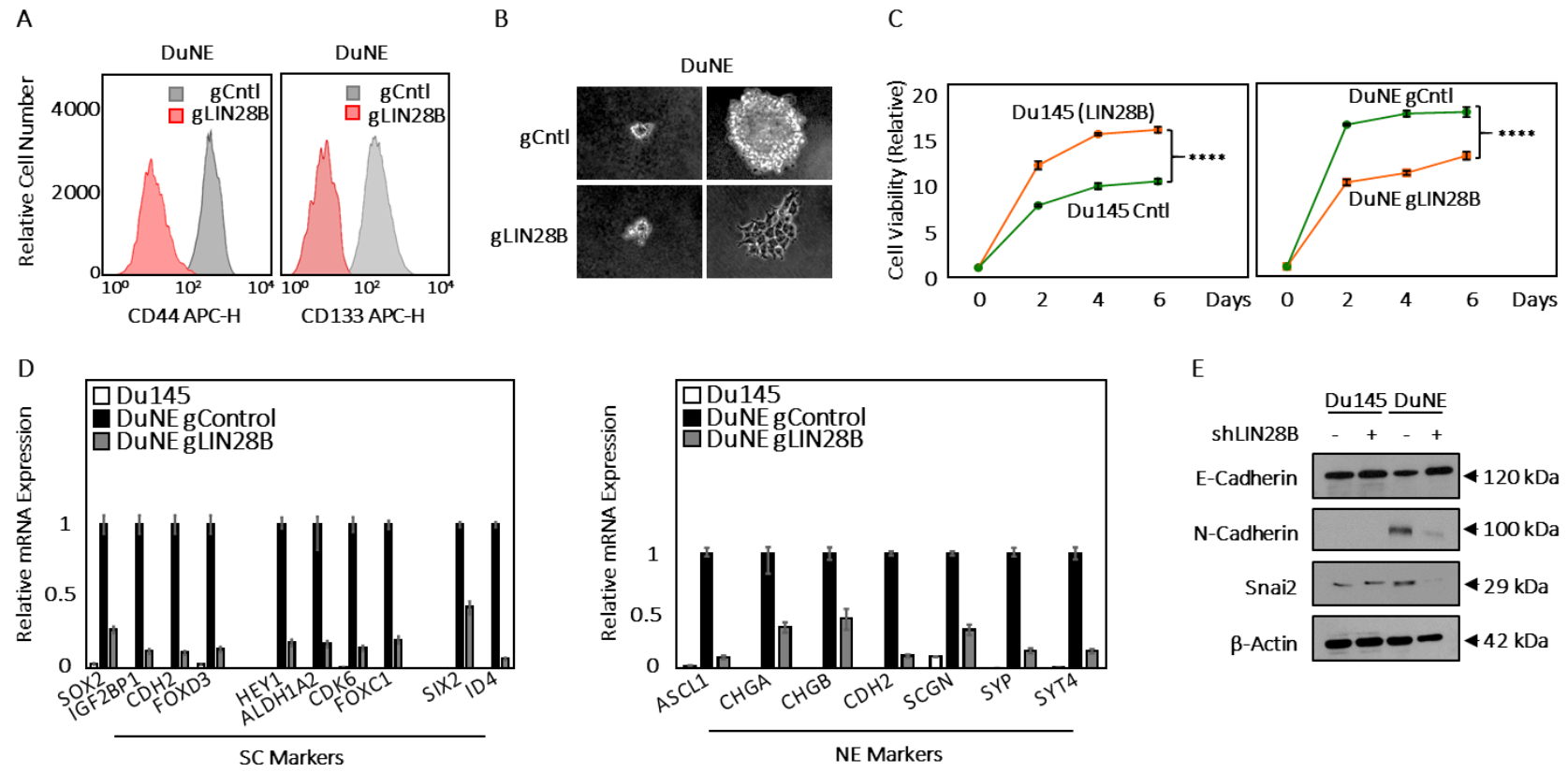
Figure 3.5 LIN28B mediates stemness and tumorigenic properties in NEPC. (A)
FACS analyses indicate that removing LIN28B expression decreases the population of
CD44$^+$ and CD133$^+$ cells. **(B)** The DuNE(gLIN28B) cells and its respective control cells
were seeded in 3D Matrigel. Representative phase-contrast images of DuNE(gControl)
and DuNE(gLIN28B) spheroids after 4-days of culture. Scale bars represent 100 μm.
(C) The DuNE(gLIN28B) cells and its respective control cells, as well as Du145 cells
transiently transfected with 4 ug *LIN28B* and its respective control cells were seeded in
a 96-well plate for MTS assays to determine cell viability over a 7-day time course. **(D)**
DuNE(gLIN28B) cells and its respective control cells and were cultured and RNA was
extracted to detect expression levels of ten SC- or pluripotency-related genes that were
selected from the leading-edge groups associated with the DuNE phenotype in the
GSEA gene sets under the 'lineage plasticity' subgroup. **(E)**DuNE(gLIN28B) cells and its
respective control were cultured, and RNA was extracted to perform real-time qPCR to
measure the expression of NE markers. **(F)** Cell protein lysate from DuNE(gLIN28B)
and its respective control were extracted to measure E-Cadherin, N-Cadherin, Slug, and
Snail protein levels by immunoblotting. Three independent technical replicates were
performed for each experiment. Only one set of the representative immunoblots is
shown. FACS, fluorescent activated cell sorting; NE, neuroendocrine; SC, stem cell.

3.4 LIN28B accelerates xenograft tumor take and formation

It is well known that, in PCa, cancer stem cells have the ability to initiate tumorigenesis, stimulate invasion, and promote metastasis (191, 192). Furthermore, cancer stem cells and their progeny have significant plasticity, which has been proposed as a means for cells to maintain their resistance to treatments (192, 193). We determined that high *LIN28B* expression was correlated with poor prognosis in patients after receiving hormone therapies in both the TCGA provisional and the Grasso *et al.* (2012) CRPC cohorts (Fig 3.6A), which were obtained from cBioPortal (194). To study the impact of LIN28B on tumor take, we transplanted DuNE(gControl) or DuNE(gLIN28B) cells subcutaneously into immunocompromised mice (n=16). Compared to the DuNE(gControl) mice, it took a significantly longer time for the DuNE(gLIN28B) tumors to begin to grow (Fig 3.7A). The difference between these two groups might be attributed to the fact that LIN28B expression was only partially supressed in the CRISPR knockout cell lines (Appendix Di). Interestingly, 6 of the DuNE(gLIN28B) cell injections failed to develop into tumors. It is possible that the number of cells transplanted into the mice was less than expected. This would cause the injection to fall below a critical number whereby a tumor would not form. This may possibly account for the differences in the 10 gLIN28B tumors that grew, albeit at a slower rate, and the 6 gLIN28B tumors that did not grow. Once the control tumors formed, they grew from 100 mm^3 to 200 mm^3 in 4 days, which was significantly faster than the time it took the DuNE(gLIN28B) tumors to grow from 100 mm^3 to 200mm^3, which was 7.5 days (p<0.001) (Fig 3.7B-C). The control tumors also doubled in volume from 200mm3 to 400mm3 significantly faster than the DuNE(gLIN28B) tumors did (p>0.05) (Fig 3.7B-C). Immunoblotting assays validated that exogenous LIN28B

expression was decreased in the DuNE(gLIN28B) xenografts and found that if the

gLIN28B tumors were actually established, it expressed a lower amount of LIN28B (Fig

3.7D). We also confirmed that the LIN28B depletion in xenografts was associated with a

reduced expression of NE maker SYP and stem cell marker CD44 (Fig 3.7E). Taken

together with the results from figure 3.6, these results confirm that LIN28B promotes

prostate xenograft take and formation.

Figure 3.6
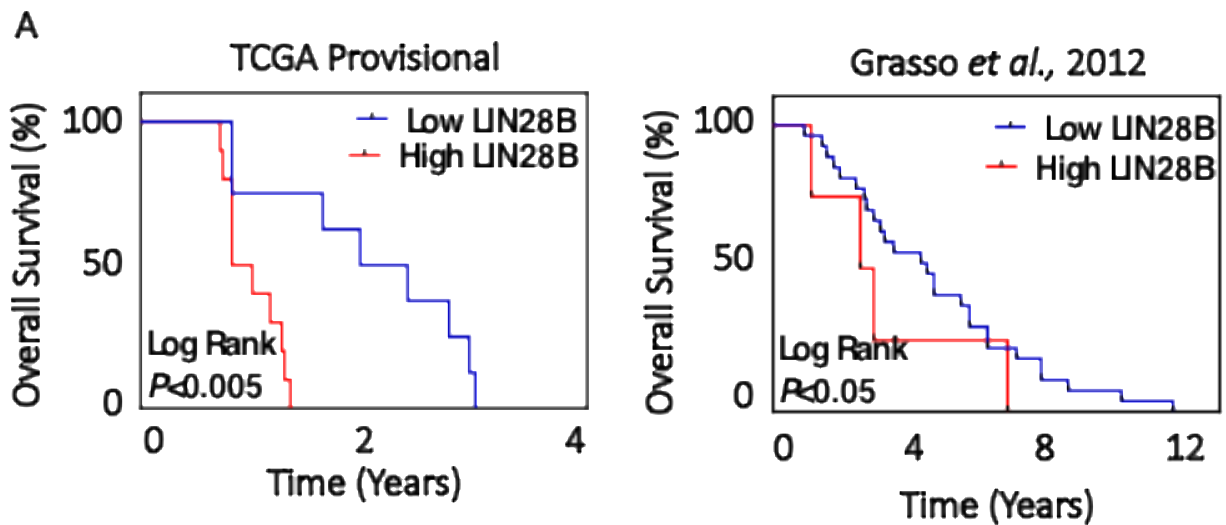
Figure 3.6 LIN28B decreases overall survival (A) Overall survival Kaplan-Meier between low and high expression of *LIN28B* in CRPC tumors from the TCGA provisional cohort and Grasso *et al.* (2012) were analyzed using cBioportal.Statistical analyses were performed by one-way ANOVA followed by Tukey test was used in pairwise comparison among different groups. CRPC, castration resistant prostate cancer; TCGA, The Cancer Genome Atlas.

Figure 3.7
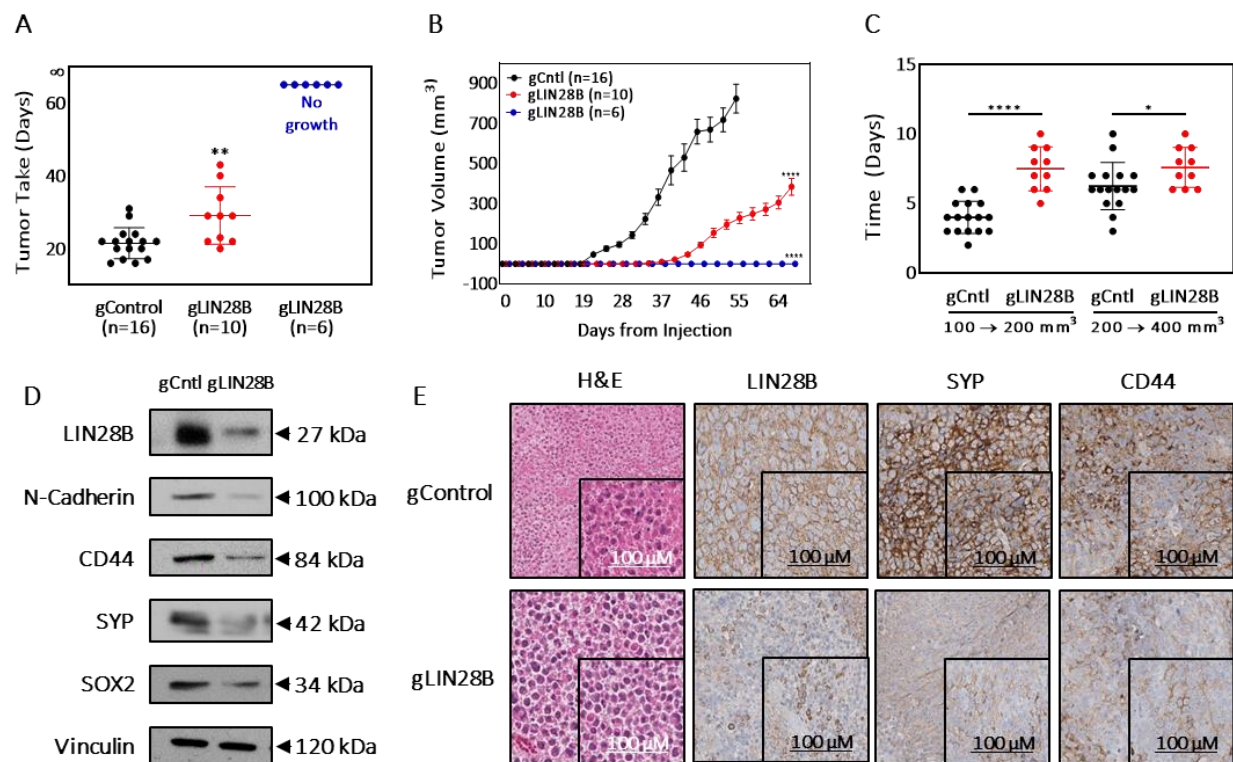
Figure 3.7 LIN28B accelerates xenograft tumor take and formation. Control DuNE(gControl) or DuNE(gLIN28B) cells cells were transplanted subcutaneously in two sites of immunocompromised mice (n=16; each mouse was injected by 1.0×10^6 cells). **(A)** Tumor take and **(B)** Tumor volumes of the xenografts (mean tumor volume cm^3 ± SEM) were measured by a caliper and monitored up to 9 weeks. **(C)** Tumor doubling time was calculated during tumor growth from 100 to $200mm^3$ and from 200 to 400 mm^3. **(D)** Total protein lyses were collected from DuNE(gControl) and DuNE(gLIN28B) xenografts. LIN28B, SOX2, SYP, CD44, and N-Cadherin expressions were confirmed by immunoblotting assays. **(E)** IHC detected LIN28B, N-Cadherin, and SYP expression in DuNE(gControl) and DuNE(gLIN28B) xenografts. Three independent technical replicates were performed for each experiment. Only one set of the representative immunoblots is shown. All results are presented as mean ± SD. Statistical analyses were performed student *t* test was used to compare results between two groups with *, **** denoting *P*<0.05, *P*<0.0001, respectively). IHC, immunohistochemistry.
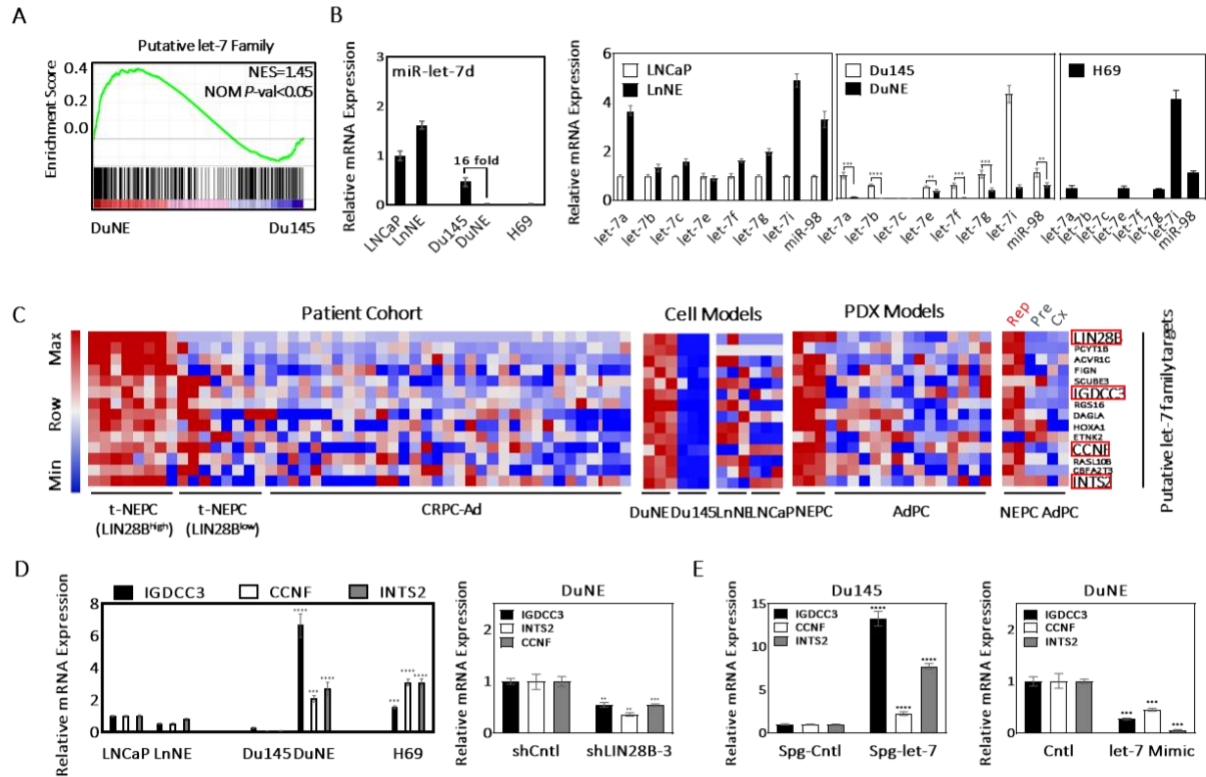
3.5 Let-7d is a negative downstream effector of LIN28B in NEPC

An oncogenic role for the LIN28B/let-7 pathway has been established in a number of cancers (164-167). Studies have demonstrated that an increase in LIN28B expression and a loss of let-7 expression is correlated with poor prognosis and advanced malignancies (164). Furthermore, LIN28B-mediated inhibition of let-7 has been reported to play a critical role in regulating tumor-initiating and self-renewal properties of CSCs in human cancers (130, 195-197). We investigated whether let-7 is one of the major downstream effectors of LIN28B in regulating CSC-like properties and a pluripotency network in NEPC. To first elucidate if the let-7 miRNA was repressed in NEPC, we used Beltran *et al.* (2016) miRNAseq datasets to determine that there was substantial downregulation of let-7 (Fig 3.8A; Appendix Ei). Consistent with the results of microarray analyses, we analyzed the expression of nine members of the let-7 family (let-7a, let-7b, let-7c, let7d, let-7e, let-7f1, let-7g, let-7i, miR-98) using qPCR and confirmed that the expression of let-7d was the most significantly reduced (Fig 3.8B). Interestingly, we also found that the inhibition of let-7 consequently caused the upregulation of its downstream targets such as IGDCC3, CCNF, and INTS2 in the Beltran 2016 patient cohort, LTL PDX model, LTL331/331R PDX model, and, most importantly, the DuNE cell model (Fig 3.8C). We discovered that the expression of these three downstream targets was only de-repressed in the cell models that had increased LIN28B and decreased let-7 expression - DuNE, and H69, which served as our positive control (Fig 3.8D). Furthermore, we confirmed that depleting LIN28B in DuNE cells by transfecting them with LIN28B shRNA resulted in an increased expression of let-7d and a decreased expression of the let-7 targets (Fig 3.8D). A

similar relationship was observed when we transfected DU145 and DuNE cells with let-7 SPONGE (spg-let-7), which "absorbs" let-7 in cells and relieves the targets of let-7 from being suppressed, or a let-7d mimic, respectively. qPCR results indicate that the LIN28B-elevated mRNA levels of IGDCC3, CCNF, and INTS2 were increased upon the transfection of the let-7 sponge, and that the delivery of the let-7d mimic had opposite results (Fig 3.8E, Appendix Eii-iv). These results demonstrated that let-7d is one of the key downstream effectors of LIN28B in NEPC.
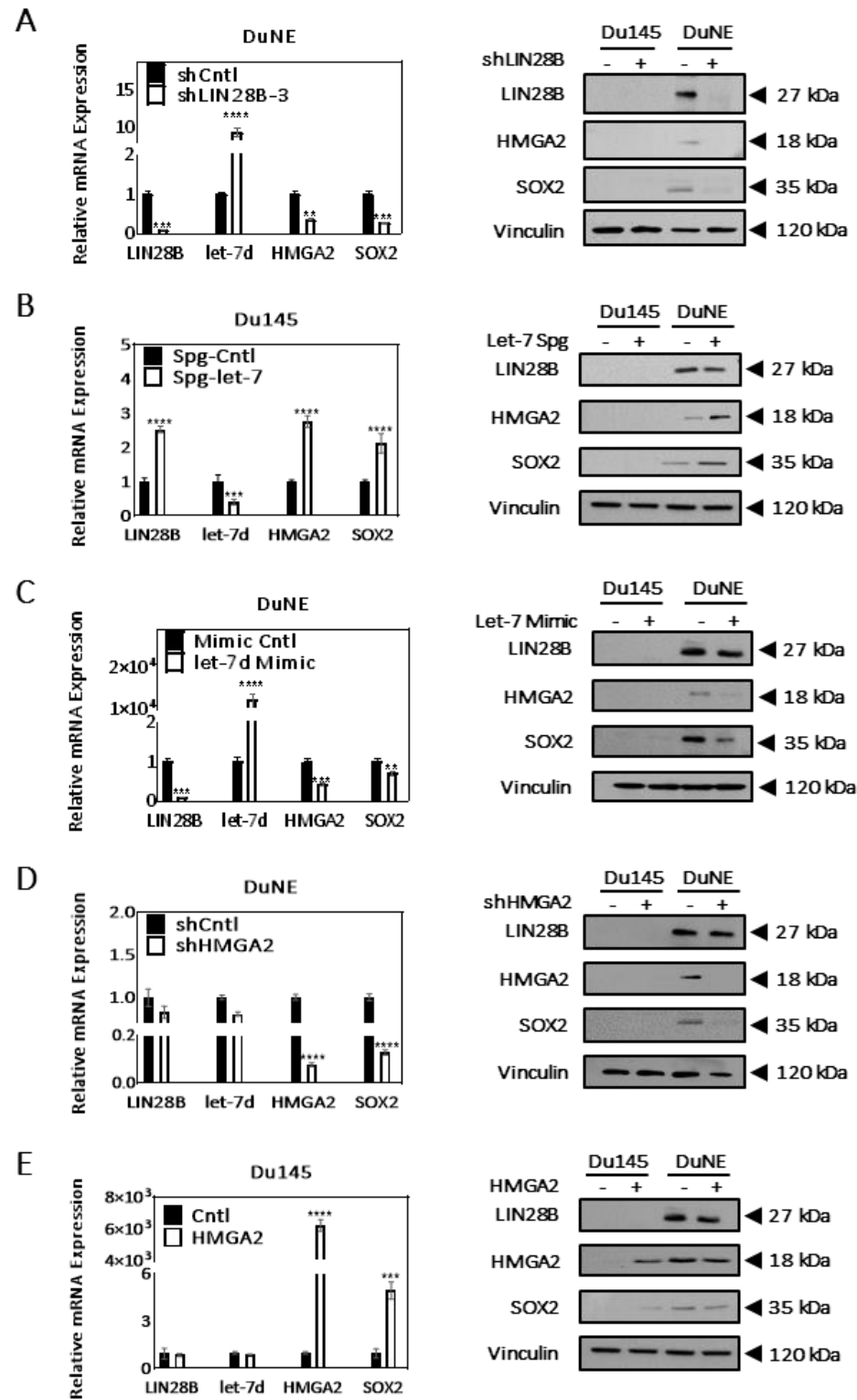
Figure 3.8

Figure 3.8 Let-7d is a negative downstream effector of LIN28B in NEPC. (A) GSEA revealed that "Putative let-7 family" is enriched in the DuNE model **(B)** The relative expression of let-7 family members was profiled using AdPC, SCNC, and the LnNE and DuNE models. **(C)** The expression of putative let-7 family targets, specifically LIN28B, IGDCC3, CCNF, and INTS2, was compared among CRPC tumor samples from the Beltran *et al.* (2016) cohort and separated into three groups, CRPC-Ad (n=34), t-NEPC expressing low level of LIN28B, t-NEPC (LIN28B^low) (n=7), and t-NEPC expressing high level of LIN28B, t-NEPC(LIN28B^high) (n=8). The expression of putative let-7 family targets was compared among the LnNE and DuNE cell models and their respective controls, LNCaP and Du145, and in the LTL PDX model. Expressions of the putative let-7 family targets is indicated as high, red, or low, blue. **(D)** The expressions of IGDCC3, CCNF, and INTS2 in AdPC, NEPC, and SCNC cell lines were measured by qPCR. DuNE cells were transfected with control or shLIN28B expression vector and RNA was extracted to detect the expression levels of indicated genes using qPCR. **(E)** Du145 cells were transfected with sponge-control or sponge-let-7 expression vector and extracted for RNA to detect the expression levels of indicated genes using qPCR. **(F)** DuNE cells were transfected with control or let-7d mimic expression vector and extracted for RNA to detect the expression levels of indicated genes using qPCR. All results are presented as mean ± SD. Statistical analyses were performed by student's *t*-test with **, ***, ****, denoting *P*<0.01, *P*<0.001, *P*<0.0001, respectively.

3.6 HMGA2 is a downstream target of LIN28B/let-7 signaling that regulates SOX2 in NEPC

After determining that there was a relationship between LIN28B and SOX2, we sought to determine the mechanism by which LIN28B may mediate the expression of the important stemness factor. Currently, there are specific pathways that are known to be target oncogenic signalling pathways of let-7 including HMGA, MYC, RAS, EZH2, and REST (162, 198-201). We then utilized our let-7 SPONGE to see if the expression of any of these genes would increase in the DuNE model when let-7d expression was decreased (Appendix F). We identified HMGA2, which is a member of the high-mobility group AT-hook protein family and a reported let-7 target (196) that directly binds to the SOX2 promoter in glioblastoma cells to induce SOX2 expression (202). HMGA2 is also an oncofetal protein that is highly expressed during embryonic development and is expressed minimally in normal adult tissues. HMGA2 has been demonstrated to be involved in tumor cell development and differentiation, stem cell self-renewal of cancer stem cells, and EMT (203). To validate this hypothesis, we first treated DU145 and DuNE cells with shLIN28B or spg-let-7. We found that, in DuNE cells, the depletion of LIN28B decreased the protein and mRNA levels of HMGA2 and SOX2, and decreased the levels of let-7d (Fig 3.9A), whereas the loss of let-7 increased the expression of LIN28B, HMGA2 and SOX2, (Fig 3.9B). Overexpressing let-7d mimic in DuNE cells dramatically decreased the expression of the three molecules, but it did not alter the expression of SC and NE markers (Fig. 3.9C; Appendix G). Moreover, we dissected the regulatory causal effects between HMGA2 and SOX2 by enhancing and knocking down HMGA2 expression. Overexpression of HMGA2 in DuNE cells enhanced the protein and mRNA levels SOX2, whereas the overexpression of SOX2 did not affect the levels

of HMGA2 (Fig. 3.9E, Appendix Ciii). Knockdown of HMGA2 in DuNE cells supressed

SOX2 expression (Fig. 3.9D). To investigate whether HMGA2 directly regulates SOX2

expression through direct promoter binding, we used luciferase reporter plasmids to

confirm that HMGA2 bound to and increased the activity of SOX2 promoter (Fig 3.9E).

Furthermore, when HMGA2 expression was knocked down, there was a decrease in the

activity of SOX2 promoter (Fig 3.9E). Collectively, these findings recognise two distinct

groups of t-NEPC tumors that arise from the same AdPC tumors after treatments with

APRIs (Fig 3.9F). Taken together, these results demonstrate the causal effect of

LIN28B/ let-7d driven HMGA2-SOX2 pathway in NEPC.

Figure 3.9

Figure 3.9 Let7 is a negative downstream effector of LIN28B in the regulation of HMGA2/SOX2 in NEPC. (A) Du145 and DuNE cells were transfected with control or shLIN28B and extracted for RNA or protein to assess the expression level of LIN28B, HMGA2, SOX2, and vinculin using real-time qPCR and immunoblotting assays, respectively. **(B)** Du145 and DuNE cells were transfected with control-spg or let-7-spg and extracted for RNA or protein to assess the expression level of LIN28B, HMGA2, SOX2, and vinculin using qPCR and immunoblotting assays, respectively. **(C)** Du145 and DuNE cells were transfected with scrambled miR-mimic control or Let -7-mimic and extracted for RNA or protein to assess the expression level of LIN28B, HMGA2, SOX2, and vinculin using qPCR and immunoblotting assays, respectively. **(D)** Du145 and DuNE cells were transfected with control or shHMGA2 and extracted for RNA or protein to assess the expression level of LIN28B, HMGA2, SOX2, and vinculin using qPCR and immunoblotting assays, respectively. **(E)** Du145 and DuNE cells were transfected with control or HMGA2 and extracted for RNA or protein to assess the expression level of LIN28B, HMGA2, SOX2, and vinculin using qPCR and immunoblotting assays, respectively. Three independent technical replicates were performed for each experiment. Only one set of the representative immunoblots is shown. All results are presented as mean ± SD. Statistical analyses were performed by one-way ANOVA or unpaired student's t test with **, ***, **** denoting $P<0.01$, $P<0.001$, $P<0.0001$, respectively). AdPC, prostate adenocarcinoma; ARPI, androgen receptor pathway inhibitors; t-NEPC, treatment-induced neuroendocrine prostate cancer.

Chapter 4: Discussion

Within this study we found that a subgroup of t-NEPC tumors in the Beltran *et al.* (2016) cohort could be distinguished by the expression of LIN28B (Fig. 3.1A). We also found that LIN28B expression was significantly increased in the DuNE cell model, when compared to other PCa cell models, which recapitulates the phenotypes of clinical t-NEPC tumors that promote lineage plasticity and express stem-like characteristics (Fig. 3.1A; 3.2A-C). Furthermore, SOX2 expression was increased within the same subgroup of t-NEPC tumors (Fig. 3.1A). IHC was used to determine that LIN28B and SOX2 were expressed in the same subgroup of t-NEPC tumors from a human CRPC TMA (Fig. 3.3A-B). Together, our findings suggest that LIN28B and SOX2 may be complimentary in inducing a pluripotent stem-like state. We then identified an inverse relationship between LIN28B and let-7d in DuNE cells; increased LIN28B expression causes a subsequent decrease in let-7d expression (Fig. 3.8). Furthermore, we demonstrated that the LIN28B/ let-7d pathway regulates cancer stemness, viability, and an EMT phenotype in DuNE cells (Fig. 3.5A-F). Our data also confirmed that let-7d targets HMGA2, which upregulates SOX2 expression through its promoter in response to LIN28B overexpression (Fig. 3.9). While the importance of SOX2 and its role in promoting lineage plasticity have been well documented, none have comprehensively determined a signal pathway upstream of SOX2 that provides further insight on the complex stemness regulatory network (99, 101, 204).

To date, clinical evidence suggests that cancer cells with stem cell-like characteristics may contribute to the failure of conventional therapy options, since stem

cells are more resistant to these therapies than differentiated tumor cells (193, 205-207). Studies have shown that stem cell-like characteristics, such as the ability to self-renew, promote EMT, and maintain pluripotency are analogous to that of ESCs, indicating that stem cell reprogramming factors may function as regulators to induce a temporary pluripotent stem cell-like state during the transition from AdPC to t-NEPC (204, 208, 209). While the upregulation of SOX2 has been well documented when p53 and Rb1 expressions are lost (99, 101), our novel finding suggests that the co-expression of LIN28B and SOX2 is sufficient to promote NEPC development and the gain a pluripotency phenotype. While LIN28B and SOX2 upregulation has been well documented in other cancers that progress in a similar manner to prostate neuroendocrine tumors, such as hepatocellular and oral squamous cell carcinoma (195, 210), this is the first time that increased expression of the LIN28B/SOX2 axis is associated with NEPC progression. The fact that LIN28B and SOX2 are only upregulated in half of clinical samples suggests that there are multiple pathways through which AdPC cells can develop into NEPC. Perhaps LIN28B and SOX2 act as regulators that push AdPC cells that are subjected to APRIs towards a pathway that promotes NE differentiation rather than transdifferentiation as a means to develop into t-NEPC (Fig 6G). While the AdPC cells begin as a heterogeneous population, the selective pressures that they face will drive the cells towards a pathway that will most promote their survival. Furthermore, the upregulation of LIN28B and SOX2 expression only occurs in the AR-/RB1-/TP53- DuNE model, but not the AR+/Rb1+/Trp53+ LnNE cell model. Furthermore, AR-/TP53-null PC-3 cells do not demonstrate the same results, indicating that additional complex mechanisms may contribute to the t-NEPC

progression driven by a pluripotency gene network. This data demonstrates that different subgroups of t-NEPC tumors exist, where a division of two subgroups is evident based on a robust difference in LIN28B expression levels. Lastly, knocking down LIN28B expression demonstrated a dynamic exchange of stem-like and non–stem-like states in the DuNE and DuNE knockout cells, respectively (Fig 3.4). The role of LIN28B signaling in stemness pathways and pluripotency regulation during cell reprogramming echoes its role in cancer stemness, and it would be interesting to investigate the demethylation mechanism of stemness gene promoters in the LIN28B-modulated reprogramming process.

While AdPC and t-NEPC are very similar genomically, treatment with ARPIs, genomic abnormality, and transcription reprogramming may create many transcriptional differences between the tumors and result in the development of a NE differentiation. These transcriptional differences may also be a result of epigenetic or post-transcriptional modifications, such as those brought about by microRNAs (miRNAs). An interesting aspect about miRNAs acting as key post-transcriptional regulators is that their role in altering cellular pathways is dynamic, yet reversible. There is also evidence suggesting that some miRNAs could upregulate gene expression in specific cell types and conditions with distinct transcripts and proteins. Let-7, which was identified originally in *C. elegans,* is a highly conserved miRNA, and the role of let-7 as a tumor suppressor has been reported because its defects can result in over-proliferation and lack of terminal differentiation in human cancers. Our results provide the first evidence of a correlation between high expression of LIN28B and down-regulation of let-7d in a prostate cancer plasticity model (DuNE). While we demonstrated that let-7d was integral

in regulating downstream factor HMGA2 that is not to say other members of the let-7 family may not play a role in t-NEPC progression. While the downregulation of let-7d was the most significant in the DuNE model, let-7a, b, and f were also downregulated. Perhaps these let-7 family members could play a role in regulating other targets such as EZH2, REST, and MYC.

In conclusion, the LIN28B-let-7d pathway is upregulated in a subset of clinical t-NEPC tumors that express stem-like characteristics through HMGA2-mediated SOX2 signaling. This pathway increases the ESC-stemness properties, viability, pluripotency, and EMT characteristics of t-NEPC. Together, this data greatly contributes to a deeper understanding of cancer reprogramming and ESC-stemness acquisition in t-NEPC and the complex nature in which AdPC progresses to t-NEPC.

Chapter 5: Conclusions

5.1 Summary of Findings

While primary *de novo* NEPC is rare and accounts for approximately 1% of PCa cases, it is becoming increasingly prevalent in patients who have a history of AdPC and receive radiation, chemo-, or hormone therapy (71-73, 161). T-NEPC is highly aggressive and metastatic, and accounts for approximately 25% of prostate cancer related deaths (71). Currently, there are no targeted therapies available to treat patients with t-NEPC, which reflects the limited knowledge on the molecular underpinnings of t-NEPC progression. Given the increasing occurrence of t-NEPC it is necessary to develop novel therapeutic agents that can be used to treat the disease.

In chapter 3, the idea that the transition from AdPC to t-NEPC can be through an intermediate pluripotent SC-like state was further developed. By comparing the whole transcriptomes of AdPC and t-NEPC tumors, a subset of t-NEPC tumors that express elevated levels of core embryonic stem cell genes SOX2 and LIN28B was identified. I demonstrated a novel positive correlation between LIN28B and SOX2 in clinical data as well as in the DuNE cell model. LIN28B expression was sufficient to enhance both SOX2 expression in CRPC-TMAs and stem cell properties in DuNE cells. HMGA2 was identified as a downstream effector of LIN28B/let-7d signaling that regulated SOX2 expression. In conclusion, I discovered a novel signalling pathways in a subset of clinical t-NEPC tumors that is upstream of SOX2 and expresses stem-like characteristics through HMGA2-mediated SOX2 signaling. This pathway increases the stemness properties, pluripotency, and EMT characteristics of t-NEPC. Together, this data greatly contributes to a deeper understanding of cancer reprogramming and ESC-

stemness acquisition in t-NEPC and the complex nature in which AdPC progresses to t-
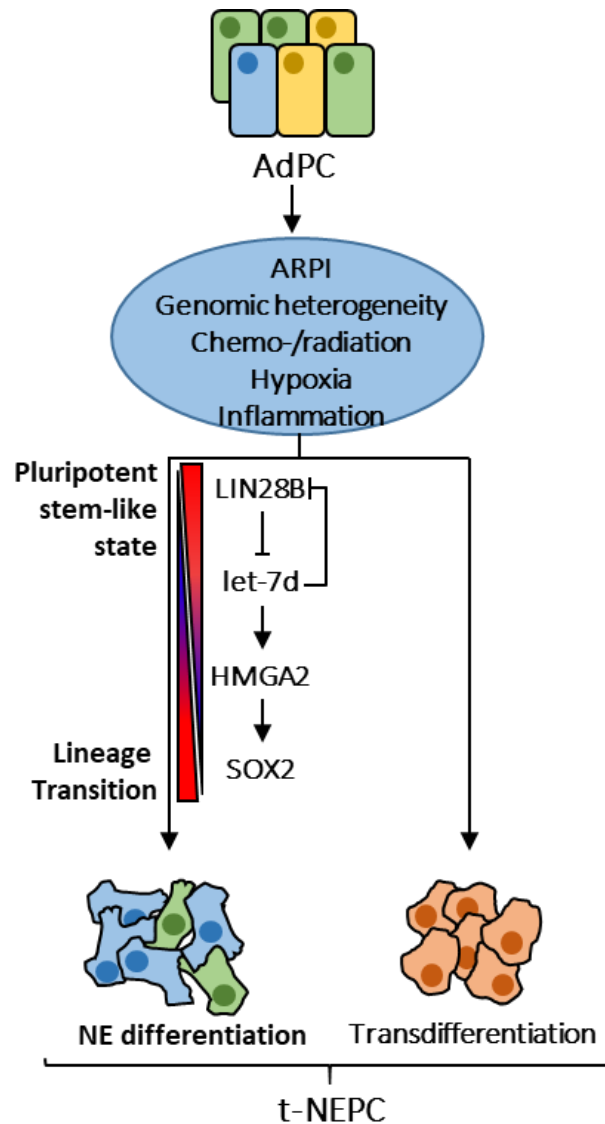
NEPC.

Figure 5.1 Schematic representing a graphical summary of the thesis.

5.2 Limitations

Currently, there are a limited number of *in vitro* NEPC cell models that can be used to study the molecular mechanisms that advance AdPC to NEPC. NCI-H660 is the only bona fide NEPC cell line that is derived from a patient and is available for *in vitro* study. The NCI-H660 cell line grows slowly as floating attached clusters with an approximate doubling time of 100 hours (211). Recent publications state that instead of passaging the cells, new medium should be added to flasks as the cell density increases and that the medium should be renewed every 2-3 days (211). The fact that the NCI-H660 cells are very difficult to culture makes regular *in vitro* cell assays such as transfections, proliferation assays, and colony formation assays very challenging to perform. While I found that it I could substitute the NCI-H660 cell line for the small cell lung cancer cell line NCI-H69 when performing *in vitro* experiments, it would improve future study results if there were a way to utilize the clinically relevant NCI-H660 cell model.

One of the biggest challenges in understanding the molecular mechanisms of t-NEPC development is the fact that the transition from AdPC to t-NEPC is a chronic process that involves many intermediate phenotypes and molecular events. Even if the molecular underpinnings of the disease were to be delineated, the role epigenetic modifications and the microenvironment play in inducing lineage plasticity and differentiation makes fully understanding the disease a near impossible task (212). The heterogeneity of patient samples that have been collected suggests that there are many complex mechanisms involved in the development of t-NEPC. Furthermore, the disease

progression of t-NEPC is difficult to monitor due to the short survival expectancy after diagnosis (213).

Another limitation is the fact that the CRISPR cell lines that were created did not completely eliminate LIN28B expression. Even after single cell selection was completed, LIN28B was still expressed in the cell model. Therefore, a completely LIN28B independent system was not created. There are multiple ways through which a complete LIN28B knockout could be achieved. One option would be to repeat single cell selection again. The colonies that do not express any LIN28B should be selected for and cultured. Another method that could be applied is the Lenti CRISPR lentiviral CRISPR/Cas9 system. The Lenti CRISPR lentiviral CRISPR/Cas9 system works by utilizing an integrated lentiviral vector. Unlike the short term transient transfection approach, cell lines that are generated from lentiviral vectors are ideal for long-term protein expression studies. Moreover, repeating experiments in a stable cell line as opposed to transiently-transfected cells increases reproducibility, as it eliminates the variation associated with repeated transient transfection.

5.3 Future Directions

5.3.1. Drug Development

In the future, developing a small molecular weight inhibitor may be a useful therapeutic tool for NEPC patients. While LIN28 has been widely researched, there is currently only one LIN28 inhibitor, Lin28 1632, available, and there are no small-molecule inhibitors that are specific for LIN28B (214). Hypothetically, this inhibitor blocks LIN28 from binding to let-7 pre-micro RNA, which in turn inhibits stemness,

inhibits growth of tumor cell lines and tumor-sphere formation *in vitro*, and induces

differentiation of ESCs (214). However, since this drug was developed in 2016 there

have been no publications on LIN28 that have used this inhibitor. This suggests that this

drug may have been effective for preclinical cancer models, however its effectiveness in

cellular models remains unclear. Preliminary experiments in our laboratory confirmed

that, when transiently transfected at a concentration of 8 uM, the Lin28 inhibitor 1632

did in fact increase let-7d mRNA and let-7-luciferase reporter activity in DuNE cells

(Figure 5.2). By taking advantage of the available crystal structure of the LIN28B/let-7

complex, we can utilize an *in silico* guided drug design method to screen potential

chemicals that could inhibit or interfere with LIN28B/let-7 interactions. As completed by

Roos *et al.*, we too can perform RNA ELISA, protein target capture using biotinylated

chemical of interest, luciferase assays, and RT-qPCR to ensure that our develop drug

effectively inhibits LIN28B and subsequently increases let-7d expression (214).
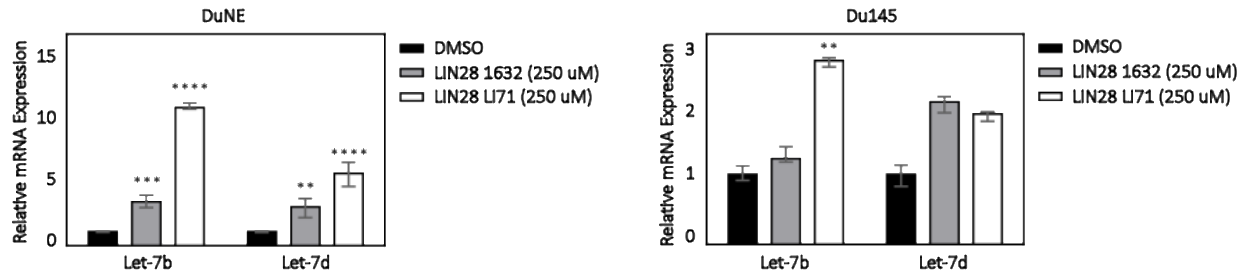
Figure 5.2 Impact of small molecule inhibitors Lin28 1632 and Lin28 LI71 on let-7 expression. DuNE and Du145 cells were treated with 250 uM of Lin28 inhibitors Lin28 1632 and Lin28 LI71 for 48 hours. Relative expression levels of let-7b and let-7d were measured by real time q-PCR.

5.3.2 Elucidating the Role of Other Let-7 Downstream Targets

In this research, I perused studying HMGA2 because it was reported to be a let-7 target that directly binds to the SOX2 promoter in glioblastoma cells to induce SOX2 expression (196, 202). Furthermore, HMGA2 is also an oncofetal protein that is highly expressed during embryonic development, and the oncogenic properties of HMGA2 have been shown to be involved in tumor cell development, cancer stem-like cell self-renewal, and EMT (203). However, as mentioned in chapter one, there are many downstream targets of let-7. It would be interesting to expand upon this research and study other known let-7 targets that are upregulated in other neuroendocrine cancers, as well as how both the let-7 dependent and independent pathways may contribute to NEPC progression and pluripotency. For example, one of the well-known downstream targets of let-7 is c-Myc. While c-Myc is not constitutively expressed in NEPC, other studies have shown that c-MYC helps to regulate ductal-neuroendocrine plasticity of pancreatic ductal adenocarcinoma, and that it supports a colon cancer cell line, COLO 320, to develop neuroendocrine properties (215, 216). By studying how c-Myc

expression, or other well established let-7 targets, are influenced by LIN28B in other neuroendocrine cancers, we may be able to further elucidate important let-7 targets that are important in NEPC development. Furthermore, it would be interesting to modify let-7d expression and investigate how it could be used as a therapeutic to reduce tumor growth. Overall, there are many future directions that can be taken to improve upon and expand this research project.

5.4 Overall Significance

In summary, we report a novel finding that the LIN28B-let-7d pathway is upregulated in a subset of clinical t-NEPC tumors that express stem-like characteristics through HMGA2-mediated SOX2 signaling. This pathway increases the ESC-stemness properties, viability, pluripotency, and EMT characteristics of t-NEPC. Together, this data greatly contributes to a deeper understanding of cancer reprogramming and ESC-stemness acquisition in t-NEPC and the complex nature in which AdPC progresses to t-NEPC.

References

1.   Public Health Agency of C, Canadian Cancer S. Release notice - Canadian Cancer Statistics. Health Promot Chronic Dis Prev Can. 2018;38(7-8):306.

2.   Gomella LG. Prostate Cancer Statistics: Anything You Want Them To Be. Can J Urol. 2017;24(1):8603-4.

3.   Torre LA, Siegel RL, Ward EM, Jemal A. Global Cancer Incidence and Mortality Rates and Trends--An Update. Cancer Epidemiol Biomarkers Prev. 2016;25(1):16-27.

4.   Grover SA, Coupal L, Zowall H, Rajan R, Trachtenberg J, Elhilali M, et al. The economic burden of prostate cancer in Canada: forecasts from the Montreal Prostate Cancer Model. CMAJ. 2000;162(7):987-92.

5.   Hayward SW, Cunha GR. The prostate: development and physiology. Radiol Clin North Am. 2000;38(1):1-14.

6.   Rey RA, Grinspon RP. Normal male sexual differentiation and aetiology of disorders of sex development. Best Pract Res Clin Endocrinol Metab. 2011;25(2):221-38.

7.   Rey R, Lukas-Croisier C, Lasala C, Bedecarras P. AMH/MIS: what we know already about the gene, the protein and its regulation. Mol Cell Endocrinol. 2003;211(1-2):21-31.

8.   Wang Y, Hayward S, Cao M, Thayer K, Cunha G. Cell differentiation lineage in the prostate. Differentiation. 2001;68(4-5):270-9.

9.   Cunha GR, Donjacour AA, Cooke PS, Mee S, Bigsby RM, Higgins SJ, et al. The endocrinology and developmental biology of the prostate. Endocr Rev. 1987;8(3):338-62.

10.   Cunha GR. Role of mesenchymal-epithelial interactions in normal and abnormal development of the mammary gland and prostate. Cancer. 1994;74(3 Suppl):1030-44.

11.   Collins AT, Habib FK, Maitland NJ, Neal DE. Identification and isolation of human prostate epithelial stem cells based on alpha(2)beta(1)-integrin expression. J Cell Sci. 2001;114(Pt 21):3865-72.

12.   Goldstein AS, Huang J, Guo C, Garraway IP, Witte ON. Identification of a cell of origin for human prostate cancer. Science. 2010;329(5991):568-71.

13.   McNeal JE. The zonal anatomy of the prostate. Prostate. 1981;2(1):35-49.

14. McNeal JE. Normal histology of the prostate. Am J Surg Pathol. 1988;12(8):619-33.

15. McNeal JE. Origin and development of carcinoma in the prostate. Cancer. 1969;23(1):24-34.

16. Shen MM, Abate-Shen C. Molecular genetics of prostate cancer: new prospects for old challenges. Genes Dev. 2010;24(18):1967-2000.

17. Aumuller G, Seitz J. Protein secretion and secretory processes in male accessory sex glands. Int Rev Cytol. 1990;121:127-231.

18. Tan MH, Li J, Xu HE, Melcher K, Yong EL. Androgen receptor: structure, role in prostate cancer and drug discovery. Acta Pharmacol Sin. 2015;36(1):3-23.

19. Zhou Y, Bolton EC, Jones JO. Androgens and androgen receptor signaling in prostate tumorigenesis. J Mol Endocrinol. 2015;54(1):R15-29.

20. Zhu X, Albertsen PC, Andriole GL, Roobol MJ, Schroder FH, Vickers AJ. Risk-based prostate cancer screening. Eur Urol. 2012;61(4):652-61.

21. Brawley OW. Prostate cancer epidemiology in the United States. World J Urol. 2012;30(2):195-200.

22. Bechis SK, Carroll PR, Cooperberg MR. Impact of age at diagnosis on prostate cancer treatment and survival. J Clin Oncol. 2011;29(2):235-41.

23. Virnig BA, Baxter NN, Habermann EB, Feldman RD, Bradley CJ. A matter of race: early-versus late-stage cancer diagnosis. Health Aff (Millwood). 2009;28(1):160-8.

24. Rebbeck TR. Prostate Cancer Disparities by Race and Ethnicity: From Nucleotide to Neighborhood. Cold Spring Harb Perspect Med. 2018;8(9).

25. Glass AS, Cary KC, Cooperberg MR. Risk-based prostate cancer screening: who and how? Curr Urol Rep. 2013;14(3):192-8.

26. Ventimiglia E, Salonia A, Briganti A, Montorsi F. Re: Family History and Probability of Prostate Cancer, Differentiated by Risk Category - A Nationwide Population-based Study. Eur Urol. 2017;71(1):143-4.

27. Allott EH, Masko EM, Freedland SJ. Obesity and prostate cancer: weighing the evidence. Eur Urol. 2013;63(5):800-9.

28. Calle EE, Rodriguez C, Walker-Thurmond K, Thun MJ. Overweight, obesity, and mortality from cancer in a prospectively studied cohort of U.S. adults. N Engl J Med. 2003;348(17):1625-38.

29. Giovannucci E. Tomatoes, tomato-based products, lycopene, and cancer: review of the epidemiologic literature. J Natl Cancer Inst. 1999;91(4):317-31.

30. Mottet N, Bellmunt J, Bolla M, Briers E, Cumberbatch MG, De Santis M, et al. EAU-ESTRO-SIOG Guidelines on Prostate Cancer. Part 1: Screening, Diagnosis, and Local Treatment with Curative Intent. Eur Urol. 2017;71(4):618-29.

31. Carter HB, Albertsen PC, Barry MJ, Etzioni R, Freedland SJ, Greene KL, et al. Early detection of prostate cancer: AUA Guideline. J Urol. 2013;190(2):419-26.

32. Pezaro C, Woo HH, Davis ID. Prostate cancer: measuring PSA. Intern Med J. 2014;44(5):433-40.

33. Stamey TA, Yang N, Hay AR, McNeal JE, Freiha FS, Redwine E. Prostate-specific antigen as a serum marker for adenocarcinoma of the prostate. N Engl J Med. 1987;317(15):909-16.

34. Gleason DF, Mellinger GT. Prediction of prognosis for prostatic adenocarcinoma by combined histological grading and clinical staging. J Urol. 1974;111(1):58-64.

35. van Poppel H. Locally advanced and high risk prostate cancer: The best indication for initial radical prostatectomy? Asian J Urol. 2014;1(1):40-5.

36. Brimo F, Montironi R, Egevad L, Erbersdobler A, Lin DW, Nelson JB, et al. Contemporary grading for prostate cancer: implications for patient care. Eur Urol. 2013;63(5):892-901.

37. Tombal B, Alcaraz A, James N, Valdagni R, Irani J. Can we improve the definition of high-risk, hormone naive, non-metastatic prostate cancer? BJU Int. 2014;113(2):189-99.

38. Cuzick J, Swanson GP, Fisher G, Brothman AR, Berney DM, Reid JE, et al. Prognostic value of an RNA expression signature derived from cell cycle proliferation genes in patients with prostate cancer: a retrospective study. Lancet Oncol. 2011;12(3):245-55.

39. Knezevic D, Goddard AD, Natraj N, Cherbavaz DB, Clark-Langone KM, Snable J, et al. Analytical validation of the Oncotype DX prostate cancer assay - a clinical RT-PCR assay optimized for prostate needle biopsies. BMC Genomics. 2013;14:690.

40.   Neves AF, Araujo TG, Biase WK, Meola J, Alcantara TM, Freitas DG, et al. Combined analysis of multiple mRNA markers by RT-PCR assay for prostate cancer diagnosis. Clin Biochem. 2008;41(14-15):1191-8.

41.   Nguyen HG, Welty CJ, Cooperberg MR. Diagnostic associations of gene expression signatures in prostate cancer tissue. Curr Opin Urol. 2015;25(1):65-70.

42.   Ramos CG, Valdevenito R, Vergara I, Anabalon P, Sanchez C, Fulla J. PCA3 sensitivity and specificity for prostate cancer detection in patients with abnormal PSA and/or suspicious digital rectal examination. First Latin American experience. Urol Oncol. 2013;31(8):1522-6.

43.   Schroder FH, Hermanek P, Denis L, Fair WR, Gospodarowicz MK, Pavone-Macaluso M. The TNM classification of prostate cancer. Prostate Suppl. 1992;4:129-38.

44.   Wilt TJ, Brawer MK, Jones KM, Barry MJ, Aronson WJ, Fox S, et al. Radical prostatectomy versus observation for localized prostate cancer. N Engl J Med. 2012;367(3):203-13.

45.   Chang AJ, Autio KA, Roach M, 3rd, Scher HI. High-risk prostate cancer-classification and therapy. Nat Rev Clin Oncol. 2014;11(6):308-23.

46.   Bubendorf L, Schopfer A, Wagner U, Sauter G, Moch H, Willi N, et al. Metastatic patterns of prostate cancer: an autopsy study of 1,589 patients. Hum Pathol. 2000;31(5):578-83.

47.   Amling CL, Blute ML, Bergstralh EJ, Seay TM, Slezak J, Zincke H. Long-term hazard of progression after radical prostatectomy for clinically localized prostate cancer: continued risk of biochemical failure after 5 years. J Urol. 2000;164(1):101-5.

48.   Cookson MS, Roth BJ, Dahm P, Engstrom C, Freedland SJ, Hussain M, et al. Castration-resistant prostate cancer: AUA Guideline. J Urol. 2013;190(2):429-38.

49.   Cornford P, Bellmunt J, Bolla M, Briers E, De Santis M, Gross T, et al. EAU-ESTRO-SIOG Guidelines on Prostate Cancer. Part II: Treatment of Relapsing, Metastatic, and Castration-Resistant Prostate Cancer. Eur Urol. 2017;71(4):630-42.

50.   Sharifi N, Gulley JL, Dahut WL. Androgen deprivation therapy for prostate cancer. JAMA. 2005;294(2):238-44.

51.   Beer TM, Tombal B. Enzalutamide in metastatic prostate cancer before chemotherapy. N Engl J Med. 2014;371(18):1755-6.

52.   Elsada A, Pearce F, George E, Adler A. NICE guidance on enzalutamide for metastatic hormone-relapsed prostate cancer. Lancet Oncol. 2014;15(10):1058-9.

53.   Pal SK, Sartor O. Prostate cancer: the best fit for enzalutamide in metastatic prostate cancer. Nat Rev Clin Oncol. 2014;11(9):504-6.

54.   Raymond LW, Carr JP, Only C. Abiraterone in metastatic prostate cancer. N Engl J Med. 2013;368(15):1457-8.

55.   Ryan CJ, Molina A, Griffin T. Abiraterone in metastatic prostate cancer. N Engl J Med. 2013;368(15):1458-9.

56.   Afshar M, Evison F, James ND, Patel P. Shifting paradigms in the estimation of survival for castration-resistant prostate cancer: A tertiary academic center experience. Urol Oncol. 2015;33(8):338 e1-7.

57.   Sridhar SS, Freedland SJ, Gleave ME, Higano C, Mulders P, Parker C, et al. Castration-resistant prostate cancer: from new pathophysiology to new treatment. Eur Urol. 2014;65(2):289-99.

58.   Korpal M, Korn JM, Gao X, Rakiec DP, Ruddy DA, Doshi S, et al. An F876L mutation in androgen receptor confers genetic and phenotypic resistance to MDV3100 (enzalutamide). Cancer Discov. 2013;3(9):1030-43.

59.   Linja MJ, Savinainen KJ, Saramaki OR, Tammela TL, Vessella RL, Visakorpi T. Amplification and overexpression of androgen receptor gene in hormone-refractory prostate cancer. Cancer Res. 2001;61(9):3550-5.

60.   Marcelli M, Ittmann M, Mariani S, Sutherland R, Nigam R, Murthy L, et al. Androgen receptor mutations in prostate cancer. Cancer Res. 2000;60(4):944-9.

61.   Nelson WG, De Marzo AM, Yegnasubramanian S. Epigenetic alterations in human prostate cancers. Endocrinology. 2009;150(9):3991-4002.

62.   Visakorpi T, Hyytinen E, Koivisto P, Tanner M, Keinanen R, Palmberg C, et al. In vivo amplification of the androgen receptor gene and progression of human prostate cancer. Nat Genet. 1995;9(4):401-6.

63.   Hu R, Dunn TA, Wei S, Isharwal S, Veltri RW, Humphreys E, et al. Ligand-independent androgen receptor variants derived from splicing of cryptic exons signify hormone-refractory prostate cancer. Cancer Res. 2009;69(1):16-22.

64.   Linn DE, Yang X, Sun F, Xie Y, Chen H, Jiang R, et al. A Role for OCT4 in Tumor Initiation of Drug-Resistant Prostate Cancer Cells. Genes Cancer. 2010;1(9):908-16.

65. Li Y, Donmez N, Sahinalp C, Xie N, Wang Y, Xue H, et al. SRRM4 Drives Neuroendocrine Transdifferentiation of Prostate Adenocarcinoma Under Androgen Receptor Pathway Inhibition. Eur Urol. 2017;71(1):68-78.

66. Jia S, Gao X, Lee SH, Maira SM, Wu X, Stack EC, et al. Opposing effects of androgen deprivation and targeted therapy on prostate cancer prevention. Cancer Discov. 2013;3(1):44-51.

67. Kallio HML, Hieta R, Latonen L, Brofeldt A, Annala M, Kivinummi K, et al. Constitutively active androgen receptor splice variants AR-V3, AR-V7 and AR-V9 are co-expressed in castration-resistant prostate cancer metastases. Br J Cancer. 2018;119(3):347-56.

68. Dehm SM, Schmidt LJ, Heemers HV, Vessella RL, Tindall DJ. Splicing of a novel androgen receptor exon generates a constitutively active androgen receptor that mediates prostate cancer therapy resistance. Cancer Res. 2008;68(13):5469-77.

69. Antonarakis ES, Lu C, Wang H, Luber B, Nakazawa M, Roeser JC, et al. AR-V7 and resistance to enzalutamide and abiraterone in prostate cancer. N Engl J Med. 2014;371(11):1028-38.

70. Bluemn EG, Coleman IM, Lucas JM, Coleman RT, Hernandez-Lopez S, Tharakan R, et al. Androgen Receptor Pathway-Independent Prostate Cancer Is Sustained through FGF Signaling. Cancer Cell. 2017;32(4):474-89 e6.

71. Aparicio A, Logothetis CJ, Maity SN. Understanding the lethal variant of prostate cancer: power of examining extremes. Cancer Discov. 2011;1(6):466-8.

72. Hirano D, Okada Y, Minei S, Takimoto Y, Nemoto N. Neuroendocrine differentiation in hormone refractory prostate cancer following androgen deprivation therapy. Eur Urol. 2004;45(5):586-92; discussion 92.

73. Sasaki T, Komiya A, Suzuki H, Shimbo M, Ueda T, Akakura K, et al. Changes in chromogranin a serum levels during endocrine therapy in metastatic prostate cancer patients. Eur Urol. 2005;48(2):224-9; discussion 9-30.

74. Helpap B, Kollermann J, Oehler U. Neuroendocrine differentiation in prostatic carcinomas: histogenesis, biology, clinical relevance, and future therapeutical perspectives. Urol Int. 1999;62(3):133-8.

75. Parimi V, Goyal R, Poropatich K, Yang XJ. Neuroendocrine differentiation of prostate cancer: a review. Am J Clin Exp Urol. 2014;2(4):273-85.

76. Conteduca V, Scarpi E, Salvi S, Casadio V, Lolli C, Gurioli G, et al. Plasma androgen receptor and serum chromogranin A in advanced prostate cancer. Sci Rep. 2018;8(1):15442.

77.   Epstein JI, Amin MB, Beltran H, Lotan TL, Mosquera JM, Reuter VE, et al. Proposed morphologic classification of prostate cancer with neuroendocrine differentiation. Am J Surg Pathol. 2014;38(6):756-67.

78.   Santoni M, Conti A, Burattini L, Berardi R, Scarpelli M, Cheng L, et al. Neuroendocrine differentiation in prostate cancer: novel morphological insights and future therapeutic perspectives. Biochim Biophys Acta. 2014;1846(2):630-7.

79.   Klimstra DS, Beltran H, Lilenbaum R, Bergsland E. The spectrum of neuroendocrine tumors: histologic classification, unique features and areas of overlap. Am Soc Clin Oncol Educ Book. 2015:92-103.

80.   Appetecchia M, Mecule A, Pasimeni G, Iannucci CV, De Carli P, Baldelli R, et al. Incidence of high chromogranin A serum levels in patients with non metastatic prostate adenocarcinoma. J Exp Clin Cancer Res. 2010;29:166.

81.   De Nunzio C, Albisinni S, Presicce F, Lombardo R, Cancrini F, Tubaro A. Serum levels of chromogranin A are not predictive of high-grade, poorly differentiated prostate cancer: results from an Italian biopsy cohort. Urol Oncol. 2014;32(2):80-4.

82.   Esfahani M, Ataei N, Panjehpour M. Biomarkers for evaluation of prostate cancer prognosis. Asian Pac J Cancer Prev. 2015;16(7):2601-11.

83.   Fan L, Wang Y, Chi C, Pan J, Xun S, Xin Z, et al. Chromogranin A and neurone-specific enolase variations during the first 3 months of abiraterone therapy predict outcomes in patients with metastatic castration-resistant prostate cancer. BJU Int. 2017;120(2):226-32.

84.   Grigore AD, Ben-Jacob E, Farach-Carson MC. Prostate cancer and neuroendocrine differentiation: more neuronal, less endocrine? Front Oncol. 2015;5:37.

85.   Heck MM, Thaler MA, Schmid SC, Seitz AK, Tauber R, Kubler H, et al. Chromogranin A and neurone-specific enolase serum levels as predictors of treatment outcome in patients with metastatic castration-resistant prostate cancer undergoing abiraterone therapy. BJU Int. 2017;119(1):30-7.

86.   Mitsui Y, Arichi N, Hiraki M, Harada Y, Yasumoto H, Shiina H. Tissue Chromogranin A Expression during Prostate Cancer Progression: Prediction of Chemosensitivity. Urol J. 2015;12(3):2165-72.

87.   Niedworok C, Tschirdewahn S, Reis H, Lehmann N, Szucs M, Nyirady P, et al. Serum Chromogranin A as a Complementary Marker for the Prediction of Prostate Cancer-Specific Survival. Pathol Oncol Res. 2017;23(3):643-50.

88.   Lotan TL, Gupta NS, Wang W, Toubaji A, Haffner MC, Chaux A, et al. ERG gene rearrangements are common in prostatic small cell carcinomas. Mod Pathol. 2011;24(6):820-8.

89.   Beltran H, Prandi D, Mosquera JM, Benelli M, Puca L, Cyrta J, et al. Divergent clonal evolution of castration-resistant neuroendocrine prostate cancer. Nat Med. 2016;22(3):298-305.

90.   Lin D, Wyatt AW, Xue H, Wang Y, Dong X, Haegert A, et al. High fidelity patient-derived xenografts for accelerating prostate cancer discovery and drug development. Cancer Res. 2014;74(4):1272-83.

91.   Smith BA, Sokolov A, Uzunangelov V, Baertsch R, Newton Y, Graim K, et al. A basal stem cell signature identifies aggressive prostate cancer phenotypes. Proc Natl Acad Sci U S A. 2015;112(47):E6544-52.

92.   Zou M, Toivanen R, Mitrofanova A, Floch N, Hayati S, Sun Y, et al. Transdifferentiation as a Mechanism of Treatment Resistance in a Mouse Model of Castration-Resistant Prostate Cancer. Cancer Discov. 2017;7(7):736-49.

93.   Gronberg H. Prostate cancer epidemiology. Lancet. 2003;361(9360):859-64.

94.   Davies AH, Beltran H, Zoubeidi A. Cellular plasticity and the neuroendocrine phenotype in prostate cancer. Nat Rev Urol. 2018;15(5):271-86.

95.   Aparicio AM, Shen L, Tapia EL, Lu JF, Chen HC, Zhang J, et al. Combined Tumor Suppressor Defects Characterize Clinically Defined Aggressive Variant Prostate Cancers. Clin Cancer Res. 2016;22(6):1520-30.

96.   Greenberg NM, DeMayo F, Finegold MJ, Medina D, Tilley WD, Aspinall JO, et al. Prostate cancer in a transgenic mouse. Proc Natl Acad Sci U S A. 1995;92(8):3439-43.

97.   DeCaprio JA, Ludlow JW, Figge J, Shew JY, Huang CM, Lee WH, et al. SV40 large tumor antigen forms a specific complex with the product of the retinoblastoma susceptibility gene. Cell. 1988;54(2):275-83.

98.   Linzer DI, Levine AJ. Characterization of a 54K dalton cellular SV40 tumor antigen present in SV40-transformed cells and uninfected embryonal carcinoma cells. Cell. 1979;17(1):43-52.

99.   Mu P, Zhang Z, Benelli M, Karthaus WR, Hoover E, Chen CC, et al. SOX2 promotes lineage plasticity and antiandrogen resistance in TP53- and RB1-deficient prostate cancer. Science. 2017;355(6320):84-8.

100. Ku SY, Rosario S, Wang Y, Mu P, Seshadri M, Goodrich ZW, et al. Rb1 and Trp53 cooperate to suppress prostate cancer lineage plasticity, metastasis, and antiandrogen resistance. Science. 2017;355(6320):78-83.

101. Lee AR, Gan Y, Tang Y, Dong X. A novel mechanism of SRRM4 in promoting neuroendocrine prostate cancer development via a pluripotency gene network. EBioMedicine. 2018;35:167-77.

102. Aktas B, Tewes M, Fehm T, Hauch S, Kimmig R, Kasimir-Bauer S. Stem cell and epithelial-mesenchymal transition markers are frequently overexpressed in circulating tumor cells of metastatic breast cancer patients. Breast Cancer Res. 2009;11(4):R46.

103. Chaffer CL, Thompson EW, Williams ED. Mesenchymal to epithelial transition in development and disease. Cells Tissues Organs. 2007;185(1-3):7-19.

104. Thompson EW, Williams ED. EMT and MET in carcinoma--clinical observations, regulatory pathways and new models. Clin Exp Metastasis. 2008;25(6):591-2.

105. Amini S, Fathi F, Mobalegi J, Sofimajidpour H, Ghadimi T. The expressions of stem cell markers: Oct4, Nanog, Sox2, nucleostemin, Bmi, Zfx, Tcl1, Tbx3, Dppa4, and Esrrb in bladder, colon, and prostate cancer, and certain cancer cell lines. Anat Cell Biol. 2014;47(1):1-11.

106. Bae KM, Su Z, Frye C, McClellan S, Allan RW, Andrejewski JT, et al. Expression of pluripotent stem cell reprogramming factors by prostate tumor initiating cells. J Urol. 2010;183(5):2045-53.

107. Jeter CR, Liu B, Liu X, Chen X, Liu C, Calhoun-Davis T, et al. NANOG promotes cancer stem cell characteristics and prostate cancer resistance to androgen deprivation. Oncogene. 2011;30(36):3833-45.

108. Weiswald LB, Bellet D, Dangles-Marie V. Spherical cancer models in tumor biology. Neoplasia. 2015;17(1):1-15.

109. Gupta PB, Chaffer CL, Weinberg RA. Cancer stem cells: mirage or reality? Nat Med. 2009;15(9):1010-2.

110. Aruffo A, Stamenkovic I, Melnick M, Underhill CB, Seed B. CD44 is the principal cell surface receptor for hyaluronate. Cell. 1990;61(7):1303-13.

111. Shang J, Gu J, Han Q, Xu Y, Yu X, Wang K. Chemoradiotherapy is superior to radiotherapy alone after surgery in advanced squamous cell carcinoma of the head and neck: a systematic review and meta-analysis. Int J Clin Exp Med. 2014;7(9):2478-87.

112. Marin-Aguilera M, Codony-Servat J, Reig O, Lozano JJ, Fernandez PL, Pereira MV, et al. Epithelial-to-mesenchymal transition mediates docetaxel resistance and high risk of relapse in prostate cancer. Mol Cancer Ther. 2014;13(5):1270-84.

113. Moss EG, Tang L. Conservation of the heterochronic regulator Lin-28, its developmental expression and microRNA complementary sites. Dev Biol. 2003;258(2):432-42.

114. Tsialikas J, Romer-Seibert J. LIN28: roles and regulation in development and beyond. Development. 2015;142(14):2397-404.

115. Balzeau J, Menezes MR, Cao S, Hagan JP. The LIN28/let-7 Pathway in Cancer. Front Genet. 2017;8:31.

116. Guo Y, Chen Y, Ito H, Watanabe A, Ge X, Kodama T, et al. Identification and characterization of lin-28 homolog B (LIN28B) in human hepatocellular carcinoma. Gene. 2006;384:51-61.

117. Viswanathan SR, Daley GQ. Lin28: A microRNA regulator with a macro role. Cell. 2010;140(4):445-9.

118. Mihailovich M, Militti C, Gabaldon T, Gebauer F. Eukaryotic cold shock domain proteins: highly versatile regulators of gene expression. Bioessays. 2010;32(2):109-18.

119. Piskounova E, Polytarchou C, Thornton JE, LaPierre RJ, Pothoulakis C, Hagan JP, et al. Lin28A and Lin28B inhibit let-7 microRNA biogenesis by distinct mechanisms. Cell. 2011;147(5):1066-79.

120. Xu B, Zhang K, Huang Y. Lin28 modulates cell growth and associates with a subset of cell cycle regulator mRNAs in mouse embryonic stem cells. RNA. 2009;15(3):357-61.

121. Molenaar JJ, Domingo-Fernandez R, Ebus ME, Lindner S, Koster J, Drabek K, et al. LIN28B induces neuroblastoma and enhances MYCN levels via let-7 suppression. Nat Genet. 2012;44(11):1199-206.

122. Hafner M, Max KE, Bandaru P, Morozov P, Gerstberger S, Brown M, et al. Identification of mRNAs bound and regulated by human LIN28 proteins and molecular requirements for RNA recognition. RNA. 2013;19(5):613-26.

123. Vogt EJ, Meglicki M, Hartung KI, Borsuk E, Behr R. Importance of the pluripotency factor LIN28 in the mammalian nucleolus during early embryonic development. Development. 2012;139(24):4514-23.

124. Yang DH, Moss EG. Temporally regulated expression of Lin-28 in diverse tissues of the developing mouse. Gene Expr Patterns. 2003;3(6):719-26.

125. Melton C, Judson RL, Blelloch R. Opposing microRNA families regulate self-renewal in mouse embryonic stem cells. Nature. 2010;463(7281):621-6.

126. Evans MJ, Kaufman MH. Establishment in culture of pluripotential cells from mouse embryos. Nature. 1981;292(5819):154-6.

127. Darr H, Benvenisty N. Genetic analysis of the role of the reprogramming gene LIN-28 in human embryonic stem cells. Stem Cells. 2009;27(2):352-62.

128. Reubinoff BE, Pera MF, Fong CY, Trounson A, Bongso A. Embryonic stem cell lines from human blastocysts: somatic differentiation in vitro. Nat Biotechnol. 2000;18(4):399-404.

129. Yu J, Vodyanik MA, Smuga-Otto K, Antosiewicz-Bourget J, Frane JL, Tian S, et al. Induced pluripotent stem cell lines derived from human somatic cells. Science. 2007;318(5858):1917-20.

130. Cimadamore F, Amador-Arjona A, Chen C, Huang CT, Terskikh AV. SOX2-LIN28/let-7 pathway regulates proliferation and neurogenesis in neural precursors. Proc Natl Acad Sci U S A. 2013;110(32):E3017-26.

131. Yang M, Yang SL, Herrlinger S, Liang C, Dzieciatkowska M, Hansen KC, et al. Lin28 promotes the proliferative capacity of neural progenitor cells in brain development. Development. 2015;142(9):1616-27.

132. Marson A, Levine SS, Cole MF, Frampton GM, Brambrink T, Johnstone S, et al. Connecting microRNA genes to the core transcriptional regulatory circuitry of embryonic stem cells. Cell. 2008;134(3):521-33.

133. Stadtfeld M, Hochedlinger K. Induced pluripotency: history, mechanisms, and applications. Genes Dev. 2010;24(20):2239-63.

134. Takahashi K, Yamanaka S. Induction of pluripotent stem cells from mouse embryonic and adult fibroblast cultures by defined factors. Cell. 2006;126(4):663-76.

135. Shyh-Chang N, Zhu H, Yvanka de Soysa T, Shinoda G, Seligson MT, Tsanov KM, et al. Lin28 enhances tissue repair by reprogramming cellular metabolism. Cell. 2013;155(4):778-92.

136. Johnson CD, Esquela-Kerscher A, Stefani G, Byrom M, Kelnar K, Ovcharenko D, et al. The let-7 microRNA represses cell proliferation pathways in human cells. Cancer Res. 2007;67(16):7713-22.

137. Mayr C, Hemann MT, Bartel DP. Disrupting the pairing between let-7 and Hmga2 enhances oncogenic transformation. Science. 2007;315(5818):1576-9.

138. Nishino J, Kim I, Chada K, Morrison SJ. Hmga2 promotes neural stem cell self-renewal in young but not old mice by reducing p16Ink4a and p19Arf Expression. Cell. 2008;135(2):227-39.

139. Sulem P, Gudbjartsson DF, Rafnar T, Holm H, Olafsdottir EJ, Olafsdottir GH, et al. Genome-wide association study identifies sequence variants on 6q21 associated with age at menarche. Nat Genet. 2009;41(6):734-8.

140. Lettre G, Jackson AU, Gieger C, Schumacher FR, Berndt SI, Sanna S, et al. Identification of ten loci associated with height highlights new biological pathways in human growth. Nat Genet. 2008;40(5):584-91.

141. Ong KL, Tso AW, Cherny SS, Sham PC, Lam KS, Jiang CQ, et al. A genetic variant in the gene encoding fibrinogen beta chain predicted development of hypertension in Chinese men. Thromb Haemost. 2010;103(4):728-35.

142. Zhu H, Shyh-Chang N, Segre AV, Shinoda G, Shah SP, Einhorn WS, et al. The Lin28/let-7 axis regulates glucose metabolism. Cell. 2011;147(1):81-94.

143. Zhu H, Shah S, Shyh-Chang N, Shinoda G, Einhorn WS, Viswanathan SR, et al. Lin28a transgenic mice manifest size and puberty phenotypes identified in human genetic association studies. Nat Genet. 2010;42(7):626-30.

144. Rehfeld F, Rohde AM, Nguyen DT, Wulczyn FG. Lin28 and let-7: ancient milestones on the road from pluripotency to neurogenesis. Cell Tissue Res. 2015;359(1):145-60.

145. Reinhart BJ, Slack FJ, Basson M, Pasquinelli AE, Bettinger JC, Rougvie AE, et al. The 21-nucleotide let-7 RNA regulates developmental timing in Caenorhabditis elegans. Nature. 2000;403(6772):901-6.

146. Sulston JE, Horvitz HR. Post-embryonic cell lineages of the nematode, Caenorhabditis elegans. Dev Biol. 1977;56(1):110-56.

147. Lee YS, Dutta A. The tumor suppressor microRNA let-7 represses the HMGA2 oncogene. Genes Dev. 2007;21(9):1025-30.

148. Roush S, Slack FJ. The let-7 family of microRNAs. Trends Cell Biol. 2008;18(10):505-16.

149. Lee H, Han S, Kwon CS, Lee D. Biogenesis and regulation of the let-7 miRNAs and their functional implications. Protein Cell. 2016;7(2):100-13.

150. Emmrich S, Rasche M, Schoning J, Reimer C, Keihani S, Maroz A, et al. miR-99a/100~125b tricistrons regulate hematopoietic stem and progenitor cell homeostasis by shifting the balance between TGFbeta and Wnt signaling. Genes Dev. 2014;28(8):858-74.

151. Lancman JJ, Caruccio NC, Harfe BD, Pasquinelli AE, Schageman JJ, Pertsemlidis A, et al. Analysis of the regulation of lin-41 during chick and mouse limb development. Dev Dyn. 2005;234(4):948-60.

152. Schulman BR, Esquela-Kerscher A, Slack FJ. Reciprocal expression of lin-41 and the microRNAs let-7 and mir-125 during mouse embryogenesis. Dev Dyn. 2005;234(4):1046-54.

153. Wulczyn FG, Smirnova L, Rybak A, Brandt C, Kwidzinski E, Ninnemann O, et al. Post-transcriptional regulation of the let-7 microRNA during neural cell specification. FASEB J. 2007;21(2):415-26.

154. Esquela-Kerscher A, Slack FJ. Oncomirs - microRNAs with a role in cancer. Nat Rev Cancer. 2006;6(4):259-69.

155. Loughlin FE, Gebert LF, Towbin H, Brunschweiger A, Hall J, Allain FH. Structural basis of pre-let-7 miRNA recognition by the zinc knuckles of pluripotency factor Lin28. Nat Struct Mol Biol. 2011;19(1):84-9.

156. Mayr F, Heinemann U. Mechanisms of Lin28-mediated miRNA and mRNA regulation--a structural and functional perspective. Int J Mol Sci. 2013;14(8):16532-53.

157. Newman MA, Thomson JM, Hammond SM. Lin-28 interaction with the Let-7 precursor loop mediates regulated microRNA processing. RNA. 2008;14(8):1539-49.

158. Rybak A, Fuchs H, Smirnova L, Brandt C, Pohl EE, Nitsch R, et al. A feedback loop comprising lin-28 and let-7 controls pre-let-7 maturation during neural stem-cell commitment. Nat Cell Biol. 2008;10(8):987-93.

159. Van Wynsberghe PM, Kai ZS, Massirer KB, Burton VH, Yeo GW, Pasquinelli AE. LIN-28 co-transcriptionally binds primary let-7 to regulate miRNA maturation in Caenorhabditis elegans. Nat Struct Mol Biol. 2011;18(3):302-8.

160. Kawahara H, Okada Y, Imai T, Iwanami A, Mischel PS, Okano H. Musashi1 cooperates in abnormal cell lineage protein 28 (Lin28)-mediated let-7 family microRNA biogenesis in early neural differentiation. J Biol Chem. 2011;286(18):16121-30.

161. Hagan JP, Piskounova E, Gregory RI. Lin28 recruits the TUTase Zcchc11 to inhibit let-7 maturation in mouse embryonic stem cells. Nat Struct Mol Biol. 2009;16(10):1021-5.

162. Thornton JE, Gregory RI. How does Lin28 let-7 control development and disease? Trends Cell Biol. 2012;22(9):474-82.

163. Peng S, Chen LL, Lei XX, Yang L, Lin H, Carmichael GG, et al. Genome-wide studies reveal that Lin28 enhances the translation of genes important for growth and survival of human embryonic stem cells. Stem Cells. 2011;29(3):496-504.

164. Viswanathan SR, Powers JT, Einhorn W, Hoshida Y, Ng TL, Toffanin S, et al. Lin28 promotes transformation and is associated with advanced human malignancies. Nat Genet. 2009;41(7):843-8.

165. Cai J, Yang C, Yang Q, Ding H, Jia J, Guo J, et al. Deregulation of let-7e in epithelial ovarian cancer promotes the development of resistance to cisplatin. Oncogenesis. 2013;2:e75.

166. Dahiya N, Morin PJ. MicroRNAs in ovarian carcinomas. Endocr Relat Cancer. 2010;17(1):F77-89.

167. Qin N, Yang F, Li A, Prifti E, Chen Y, Shao L, et al. Alterations of the human gut microbiome in liver cirrhosis. Nature. 2014;513(7516):59-64.

168. Xie R, Wang Y, Nie W, Huang W, Song W, Wang Z, et al. Lin28B expression correlates with aggressive clinicopathological characteristics in breast invasive ductal carcinoma. Cancer Biother Radiopharm. 2014;29(5):215-20.

169. Liu Y, Li H, Feng J, Cui X, Huang W, Li Y, et al. Lin28 induces epithelial-to-mesenchymal transition and stemness via downregulation of let-7a in breast cancer cells. PLoS One. 2013;8(12):e83083.

170. Yu F, Yao H, Zhu P, Zhang X, Pan Q, Gong C, et al. let-7 regulates self renewal and tumorigenicity of breast cancer cells. Cell. 2007;131(6):1109-23.

171. Qiu C, Ma Y, Wang J, Peng S, Huang Y. Lin28-mediated post-transcriptional regulation of Oct4 expression in human embryonic stem cells. Nucleic Acids Res. 2010;38(4):1240-8.

172. King CE, Cuatrecasas M, Castells A, Sepulveda AR, Lee JS, Rustgi AK. LIN28B promotes colon cancer progression and metastasis. Cancer Res. 2011;71(12):4260-8.

173. Hsu KF, Shen MR, Huang YF, Cheng YM, Lin SH, Chow NH, et al. Overexpression of the RNA-binding proteins Lin28B and IGF2BP3 (IMP3) is

associated with chemoresistance and poor disease outcome in ovarian cancer. Br J Cancer. 2015;113(3):414-24.

174. Alajez NM, Shi W, Wong D, Lenarduzzi M, Waldron J, Weinreb I, et al. Lin28b promotes head and neck cancer progression via modulation of the insulin-like growth factor survival pathway. Oncotarget. 2012;3(12):1641-52.

175. Meirelles K, Benedict LA, Dombkowski D, Pepin D, Preffer FI, Teixeira J, et al. Human ovarian cancer stem/progenitor cells are stimulated by doxorubicin but inhibited by Mullerian inhibiting substance. Proc Natl Acad Sci U S A. 2012;109(7):2358-63.

176. Kong D, Banerjee S, Ahmad A, Li Y, Wang Z, Sethi S, et al. Epithelial to mesenchymal transition is mechanistically linked with stem cell signatures in prostate cancer cells. PLoS One. 2010;5(8):e12445.

177. Borrego-Diaz E, Powers BC, Azizov V, Lovell S, Reyes R, Chapman B, et al. A potential regulatory loop between Lin28B:miR212 in androgen-independent prostate cancer. Int J Oncol. 2014;45(6):2421-9.

178. Kang M, Lee KH, Lee HS, Jeong CW, Ku JH, Kim HH, et al. Concurrent treatment with simvastatin and NF-kappaB inhibitor in human castration-resistant prostate cancer cells exerts synergistic anti-cancer effects via control of the NF-kappaB/LIN28/let-7 miRNA signaling pathway. PLoS One. 2017;12(9):e0184644.

179. Tummala R, Nadiminty N, Lou W, Zhu Y, Gandour-Edwards R, Chen HW, et al. Lin28 promotes growth of prostate cancer cells and activates the androgen receptor. Am J Pathol. 2013;183(1):288-95.

180. Albino D, Civenni G, Dallavalle C, Roos M, Jahns H, Curti L, et al. Activation of the Lin28/let-7 Axis by Loss of ESE3/EHF Promotes a Tumorigenic and Stem-like Phenotype in Prostate Cancer. Cancer Res. 2016;76(12):3629-43.

181. Fu X, Meng Z, Liang W, Tian Y, Wang X, Han W, et al. miR-26a enhances miRNA biogenesis by targeting Lin28B and Zcchc11 to suppress tumor growth and metastasis. Oncogene. 2014;33(34):4296-306.

182. Nadiminty N, Tummala R, Lou W, Zhu Y, Shi XB, Zou JX, et al. MicroRNA let-7c is downregulated in prostate cancer and suppresses prostate cancer growth. PLoS One. 2012;7(3):e32832.

183. Li Y, Chen R, Bowden M, Mo F, Lin YY, Gleave M, et al. Establishment of a neuroendocrine prostate cancer model driven by the RNA splicing factor SRRM4. Oncotarget. 2017;8(40):66878-88.

184. Akamatsu S, Wyatt AW, Lin D, Lysakowski S, Zhang F, Kim S, et al. The Placental Gene PEG10 Promotes Progression of Neuroendocrine Prostate Cancer. Cell Rep. 2015;12(6):922-36.

185. Ma T, Xie M, Laurent T, Ding S. Progress in the reprogramming of somatic cells. Circ Res. 2013;112(3):562-74.

186. Prieto-Vila M, Takahashi RU, Usuba W, Kohama I, Ochiya T. Drug Resistance Driven by Cancer Stem Cells and Their Niche. Int J Mol Sci. 2017;18(12).

187. Kregel S, Kiriluk KJ, Rosen AM, Cai Y, Reyes EE, Otto KB, et al. Sox2 is an androgen receptor-repressed gene that promotes castration-resistant prostate cancer. PLoS One. 2013;8(1):e53701.

188. Bass AJ, Watanabe H, Mermel CH, Yu S, Perner S, Verhaak RG, et al. SOX2 is an amplified lineage-survival oncogene in lung and esophageal squamous cell carcinomas. Nat Genet. 2009;41(11):1238-42.

189. Ben-David U, Benvenisty N. The tumorigenicity of human embryonic and induced pluripotent stem cells. Nat Rev Cancer. 2011;11(4):268-77.

190. Rudin CM, Durinck S, Stawiski EW, Poirier JT, Modrusan Z, Shames DS, et al. Comprehensive genomic analysis identifies SOX2 as a frequently amplified gene in small-cell lung cancer. Nat Genet. 2012;44(10):1111-6.

191. Rycaj K, Tang DG. Molecular determinants of prostate cancer metastasis. Oncotarget. 2017;8(50):88211-31.

192. Zhang D, Tang DG, Rycaj K. Cancer stem cells: Regulation programs, immunological properties and immunotherapy. Semin Cancer Biol. 2018;52(Pt 2):94-106.

193. Tang DG. Understanding cancer stem cell heterogeneity and plasticity. Cell Res. 2012;22(3):457-72.

194. Grasso CS, Wu YM, Robinson DR, Cao X, Dhanasekaran SM, Khan AP, et al. The mutational landscape of lethal castration-resistant prostate cancer. Nature. 2012;487(7406):239-43.

195. Chien CS, Wang ML, Chu PY, Chang YL, Liu WH, Yu CC, et al. Lin28B/Let-7 Regulates Expression of Oct4 and Sox2 and Reprograms Oral Squamous Cell Carcinoma Cells to a Stem-like State. Cancer Res. 2015;75(12):2553-65.

196. Copley MR, Babovic S, Benz C, Knapp DJ, Beer PA, Kent DG, et al. The Lin28b-let-7-Hmga2 axis determines the higher self-renewal potential of fetal haematopoietic stem cells. Nat Cell Biol. 2013;15(8):916-25.

197. Zhou J, Ng SB, Chng WJ. LIN28/LIN28B: an emerging oncogenic driver in cancer stem cells. Int J Biochem Cell Biol. 2013;45(5):973-8.

198. Bussing I, Slack FJ, Grosshans H. let-7 microRNAs in development, stem cells and cancer. Trends Mol Med. 2008;14(9):400-9.

199. Heo I, Joo C, Cho J, Ha M, Han J, Kim VN. Lin28 mediates the terminal uridylation of let-7 precursor MicroRNA. Mol Cell. 2008;32(2):276-84.

200. Kong D, Heath E, Chen W, Cher ML, Powell I, Heilbrun L, et al. Loss of let-7 up-regulates EZH2 in prostate cancer consistent with the acquisition of cancer stem cell signatures that are attenuated by BR-DIM. PLoS One. 2012;7(3):e33729.

201. Luu HN, Lin HY, Sorensen KD, Ogunwobi OO, Kumar N, Chornokur G, et al. miRNAs associated with prostate cancer risk and progression. BMC Urol. 2017;17(1):18.

202. Chiou SH, Dorsch M, Kusch E, Naranjo S, Kozak MM, Koong AC, et al. Hmga2 is dispensable for pancreatic cancer development, metastasis, and therapy resistance. Sci Rep. 2018;8(1):14008.

203. Venkatesan N, Krishnakumar S, Deepa PR, Deepa M, Khetan V, Reddy MA. Molecular deregulation induced by silencing of the high mobility group protein A2 gene in retinoblastoma cells. Mol Vis. 2012;18:2420-37.

204. Mei W, Lin X, Kapoor A, Gu Y, Zhao K, Tang D. The Contributions of Prostate Cancer Stem Cells in Prostate Cancer Initiation and Metastasis. Cancers (Basel). 2019;11(4).

205. Li X, Lewis MT, Huang J, Gutierrez C, Osborne CK, Wu MF, et al. Intrinsic resistance of tumorigenic breast cancer cells to chemotherapy. J Natl Cancer Inst. 2008;100(9):672-9.

206. Reim F, Dombrowski Y, Ritter C, Buttmann M, Hausler S, Ossadnik M, et al. Immunoselection of breast and ovarian cancer cells with trastuzumab and natural killer cells: selective escape of CD44high/CD24low/HER2low breast cancer stem cells. Cancer Res. 2009;69(20):8058-66.

207. Yan H, Chen X, Zhang Q, Qin J, Li H, Liu C, et al. Drug-tolerant cancer cells show reduced tumor-initiating capacity: depletion of CD44 cells and evidence for epigenetic mechanisms. PLoS One. 2011;6(9):e24397.

208. Guzman-Ramirez N, Voller M, Wetterwald A, Germann M, Cross NA, Rentsch CA, et al. In vitro propagation and characterization of neoplastic stem/progenitor-like cells from human prostate cancer tissue. Prostate. 2009;69(15):1683-93.

209. Tam WL, Weinberg RA. The epigenetics of epithelial-mesenchymal plasticity in cancer. Nat Med. 2013;19(11):1438-49.

210. Cheng SW, Tsai HW, Lin YJ, Cheng PN, Chang YC, Yen CJ, et al. Lin28B is an oncofetal circulating cancer stem cell-like marker associated with recurrence of hepatocellular carcinoma. PLoS One. 2013;8(11):e80053.

211. Vlachostergios PJ, Puca L, Beltran H. Emerging Variants of Castration-Resistant Prostate Cancer. Curr Oncol Rep. 2017;19(5):32.

212. Lee AR, Che N, Lovnicki JM, Dong X. Development of Neuroendocrine Prostate Cancers by the Ser/Arg Repetitive Matrix 4-Mediated RNA Splicing Network. Front Oncol. 2018;8:93.

213. Nadal R, Schweizer M, Kryvenko ON, Epstein JI, Eisenberger MA. Small cell carcinoma of the prostate. Nat Rev Urol. 2014;11(4):213-9.

214. Roos M, Pradere U, Ngondo RP, Behera A, Allegrini S, Civenni G, et al. A Small-Molecule Inhibitor of Lin28. ACS Chem Biol. 2016;11(10):2773-81.

215. Farrell AS, Joly MM, Allen-Petersen BL, Worth PJ, Lanciault C, Sauer D, et al. MYC regulates ductal-neuroendocrine lineage plasticity in pancreatic ductal adenocarcinoma associated with poor outcome and chemoresistance. Nat Commun. 2017;8(1):1728.

216. Little CD, Nau MM, Carney DN, Gazdar AF, Minna JD. Amplification and expression of the c-myc oncogene in human lung cancer cell lines. Nature. 1983;306(5939):194-6.

Appendices

Appendix A. LIN28B expression is positively correlated with t-NEPC

Beltran CRPC cohort

SU2C 2015 from cBioPortal

NPp53 GEMMs

Barretina Cell Line 2012
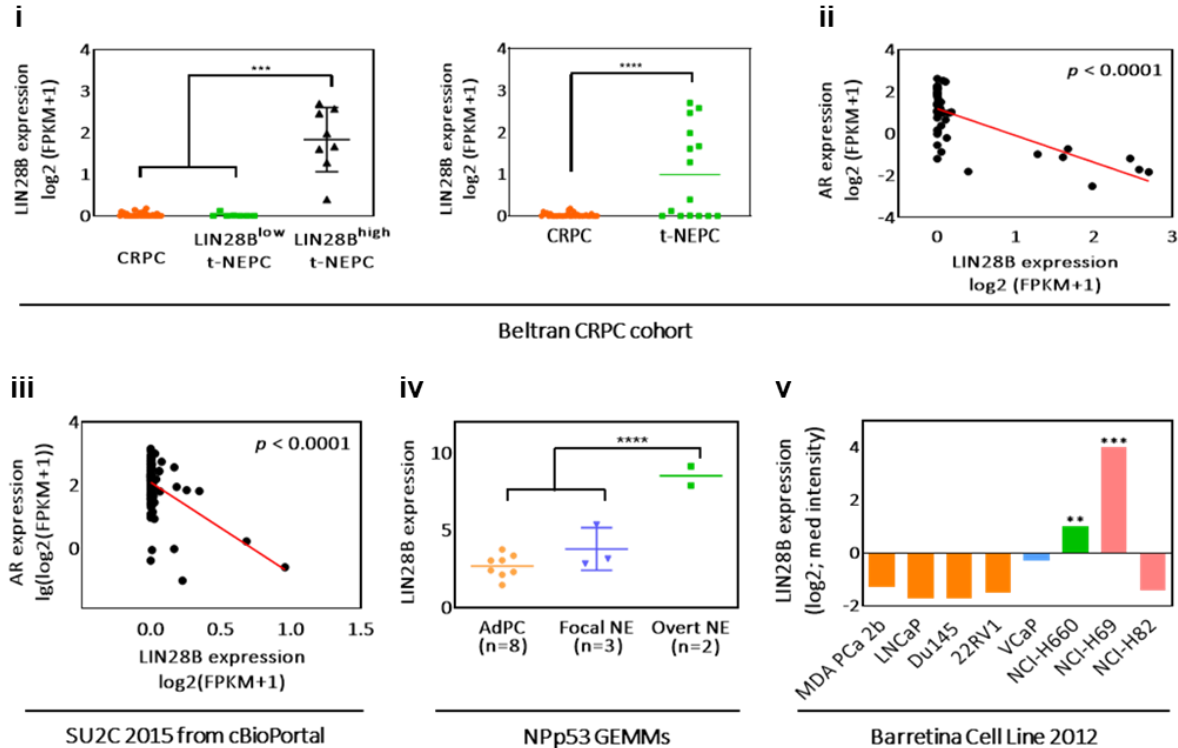
**Appendix A. LIN28B expression is positively correlated with t-NEPC progression.**
(i) LIN28B expression was compared among CRPC tumor samples from the Beltran *et al.* (2016) cohort and separated into three groups, CRPC-Ad (n=34), t-NEPC expressing low levels of LIN28B, t-NEPC(LIN28B^low) (n=7), and t-NEPC expressing high levels of LIN28B, t-NEPC(LIN28B^high) (n=8). **(ii)** LIN28B and AR are negatively correlated in human CRPC cohorts. Pearson's *r* coefficient (-0.70) between LIN28B and AR expressions was obtained from Beltran *et al.* (2016). **(iii)** LIN28B and AR are negatively correlated in human CRPC cohorts. Pearson's *r* correlation coefficient (-0.46) between LIN28B and AR expressions obtained from SU2C from cBioPortal (2015). **(iv)** LIN28B expression in different phenotypic subcategories of the NPp53 GEMMs (Zou *et al.* 2017) are shown. (AdPC, n=8; Focal NE, n=3; Overt NE, n=2). **(v)** LIN28B expression in different PCa cell lines from Barretina *et al.* (2016). All results are presented as mean ± SD. Statistical analyses were performed by one-way ANOVA or unpaired student's t test with **, ***, ****, denoting $P<0.01$, $P<0.001$, $P<0.0001$, respectively. AdPC, adenocarcinoma prostate cancer; CRPC-Ad, castration-resistant prostate adenocarcinoma; CRPC, castration-resistant prostate cancer; GEMMs, genetically engineered mouse models; NE, neuroendocrine; PCa, prostate cancer; t-NEPC, treatment-induced neuroendocrine prostate cancer.

Appendix B. *LIN28A* is not differentially expressed among CRPC and NEPC tumors
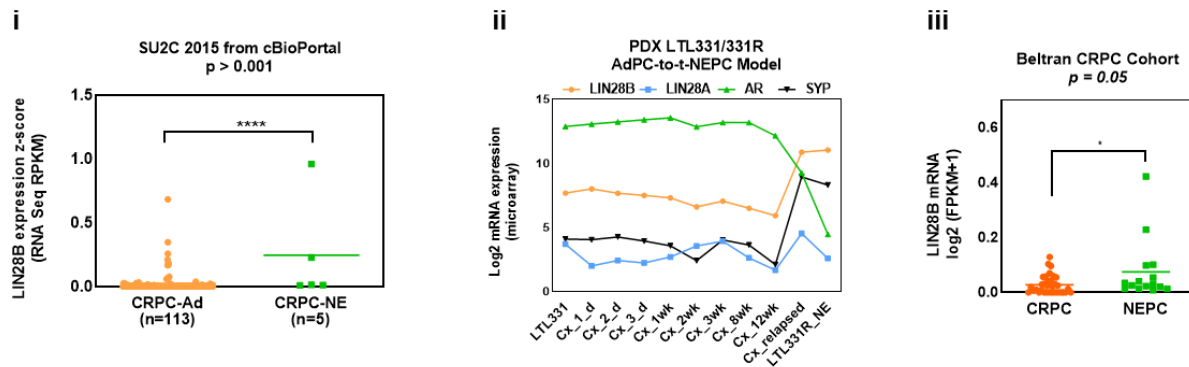

Appendix B. *LIN28A* is not differentially expressed among CRPC and NEPC tumors. (i) *LIN28B* expression was compared among CRPC tumor samples from SU2C from cBioPortal (2015) and separated into two groups, CRPC-Ad (n=113) and t-NEPC (n=5). **(ii)** The expressions of *LIN28A, LIN28B, SOX2, AR*, and *SYP* during the progression of AdPC (LTL331) to t-NEPC (LTL331R_NE) after castration in the PDX LTL331/331R model are shown. **(iii)** *LIN28A* expression was compared among CRPC tumor samples from the Beltran *et al.* (2016) cohort and separated into two groups, CRPC-Ad (n=34) and t-NEPC (n=15). Statistical analyses were performed by student's *t* test with *, **** denoting $P<0.05$, $P<0.0001$, respectively.

Appendix C. *LIN28B* and *SOX2* are positively correlated in CRPC cohorts
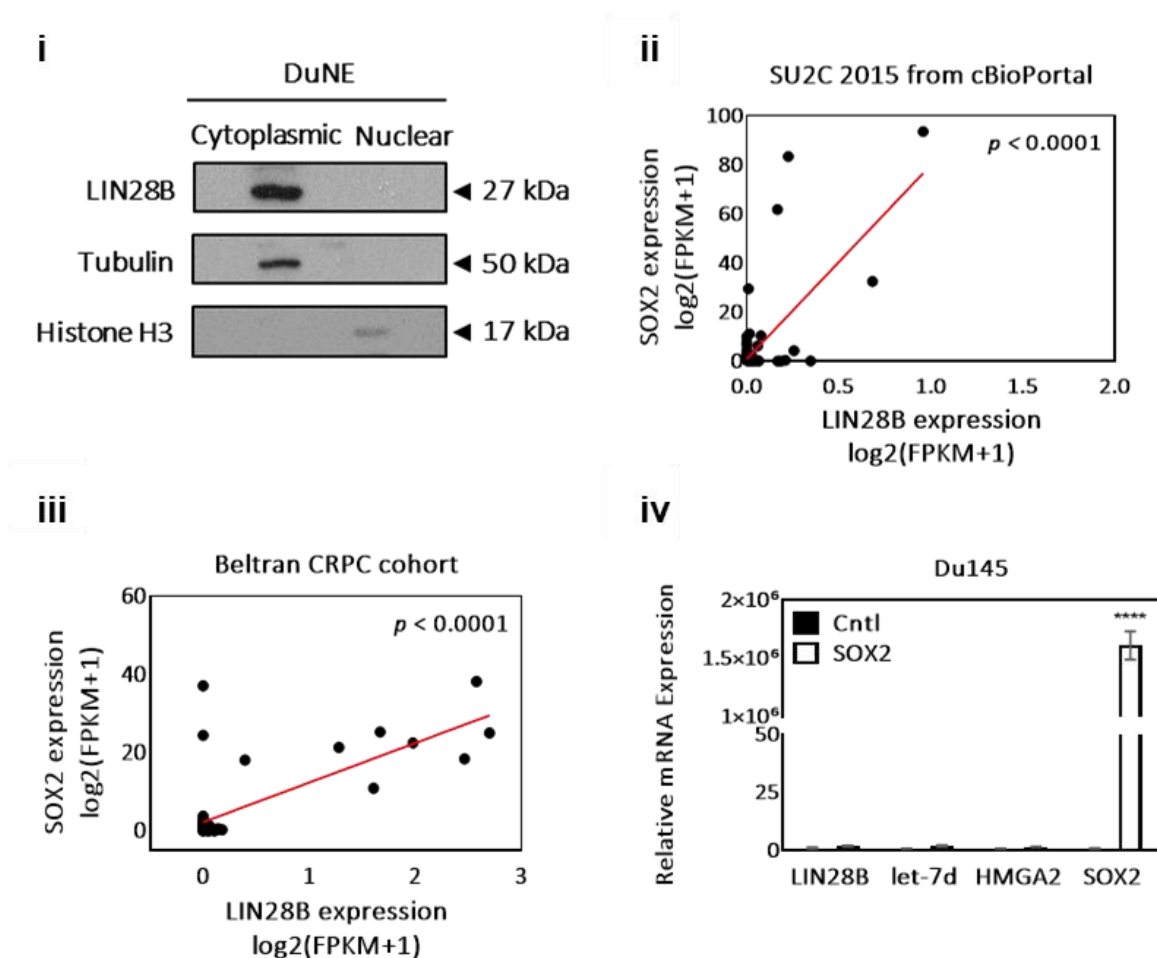
Appendix C. *LIN28B* and *SOX2* are positively correlated in CRPC cohorts. (i) DuNE cells were used to separate cytoplasmic and nuclear protein fractions. *LIN28B* protein was detected by immunoblotting. H3 and tubulin were used as markers to confirm the efficacy of protein fractionation. **(ii)** Pearson's *r* correlation coefficient (0.73) between *LIN28B* and *SOX2* expressions obtained from Beltran *et al.* (2016). **(iii)** Pearson's *r* correlation coefficient (0.71) between *LIN28B* and *SOX2* expressions obtained from SU2C from cBioPortal (2016). **(iv)** Du145 cells were transiently transfected with *SOX2*. Cells were then extracted for RNA. Relative quantifications of LIN28B, let-7d, HMGA2, and SOX2 were compared to GAPDH via qPCR. Three independent technical replicates were performed for each experiment. Only one set of the representative immunoblots is shown. All results are presented as mean ± SD. Statistical analyses were performed by one-way ANOVA with **** denotes *P*<0.0001.

Appendix D. LIN28B mediates stemness and tumorigenesis properties in NEPC
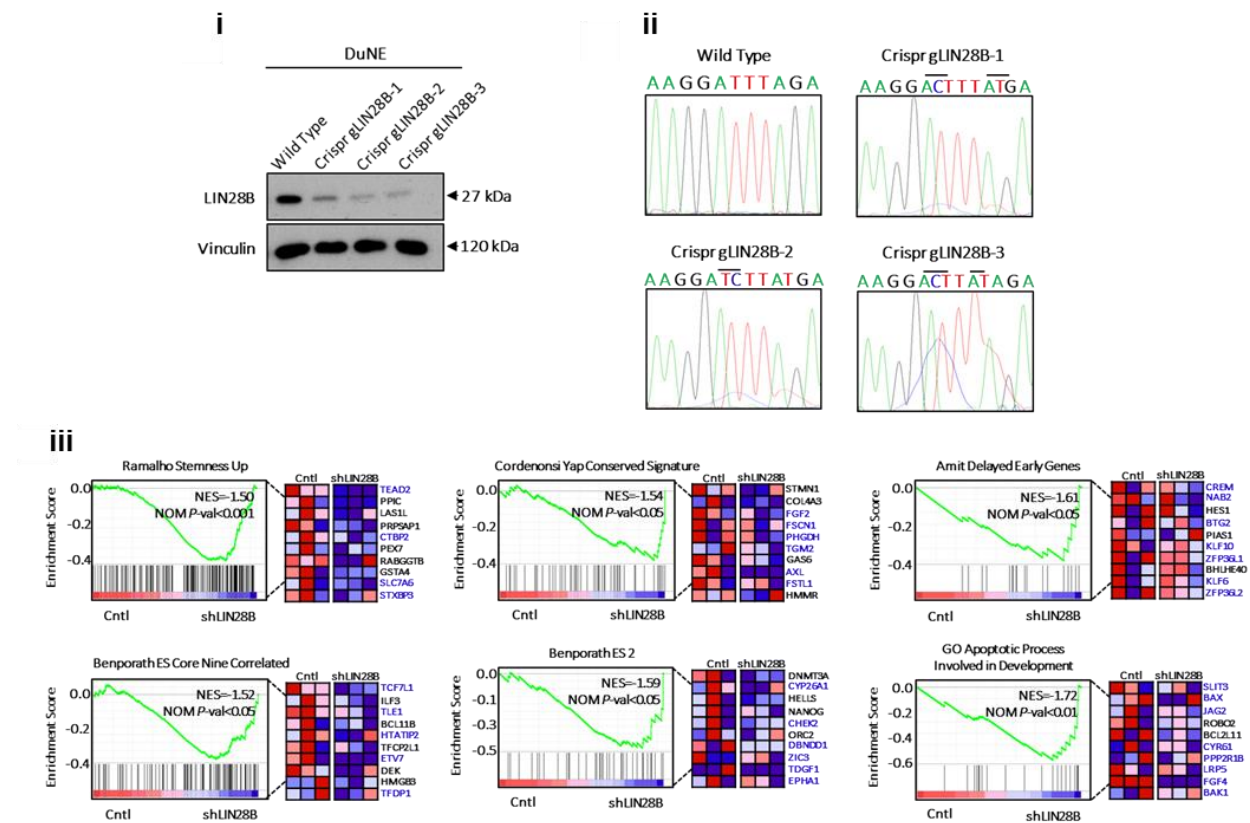
**Appendix D. LIN28B mediates stemness and tumorigenesis properties in NEPC.**
(i) GeneArt CRISPR technology was used to mutate and knockout the LIN28B gene in the DuNE cell line. **(ii)** Validation of CRISPR efficacy was confirmed by immunoblotting and Sanger sequencing. **(iii)** GSEA enrichment plots shows the correlation of DuNE(gLIN28B) dataset (n=3302) with the GSEA gene sets in the lineage plasticity/embryogeneis subgroup from subfigure 3A. Three independent technical replicates were performed for each experiment. Only one set of the representative immunoblots is shown. GSEA, gene set enrichment analysis; GO, gene ontology; NES, normalized enrichment score.

Appendix E. Let-7d is a negative downstream effector of LIN28B in NEPC
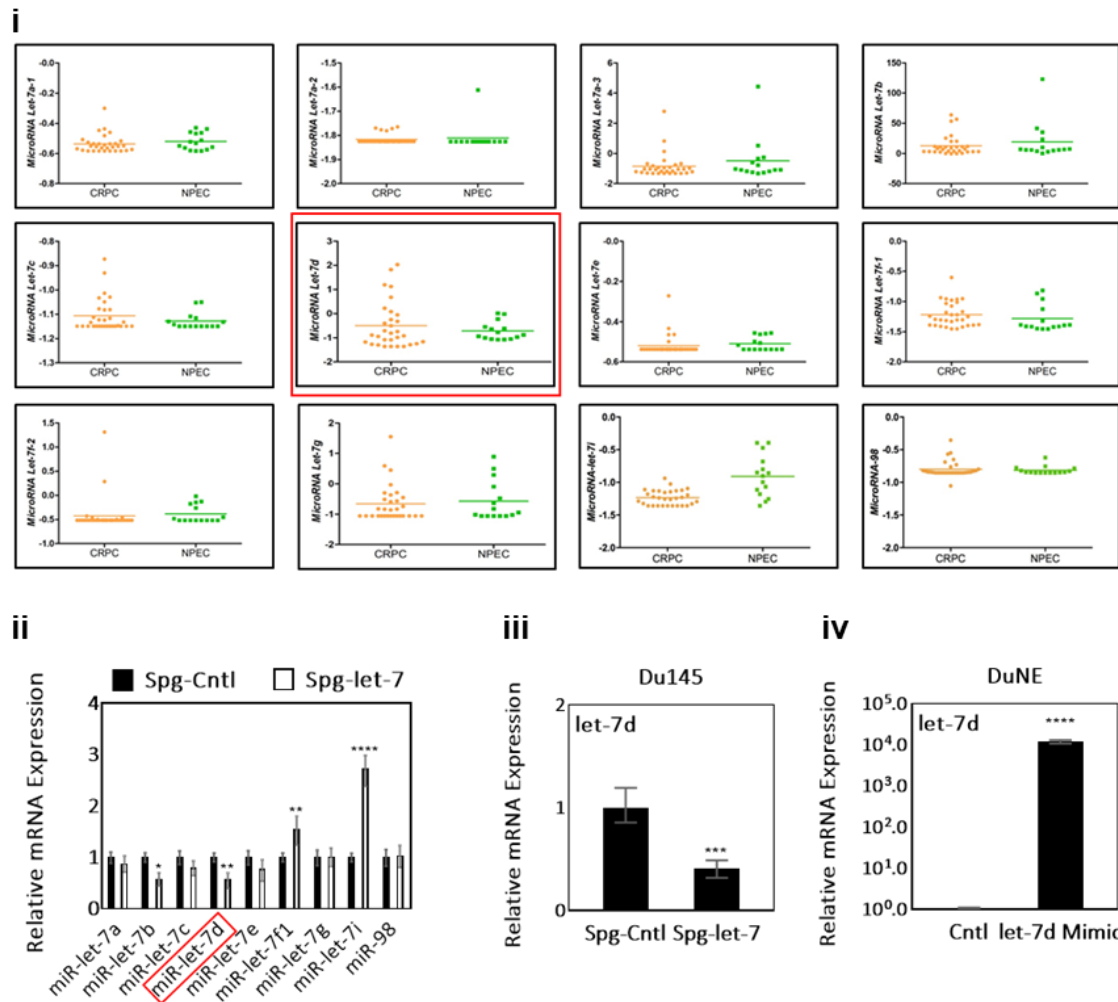
Appendix E. Let-7d is a negative downstream effector of LIN28B in NEPC. (i) The relative expression of mature miRNA levels of individual let-7 family members was profiled among CRPC tumor samples from SU2C from cBioPortal (2015) and separated into two groups, CRPC-Ad (n=113) and t-NEPC (n=5). **(ii)** Du145 cells were transfected with sponge-control or sponge-let-7 expression vector and extracted for RNA to detect the expression levels of individual let-7 family members using qPCR. **(iii)** Du145 cells were transfected with sponge-control or sponge-let-7 expression vector and extracted for RNA to detect the expression level of let-7d using qPCR. **(iv)** DuNE cells were transfected with control or let-7d mimic expression vector and extracted for RNA to detect the expression level let-7d using qPCR. Three independent technical replicates were performed for each experiment. All results are presented as mean ± SD. Statistical analyses were performed by student's t test with *, **, ***, ****, denoting $P<0.05$, $P<0.01$, $P<0.001$, $P<0.0001$, respectively.
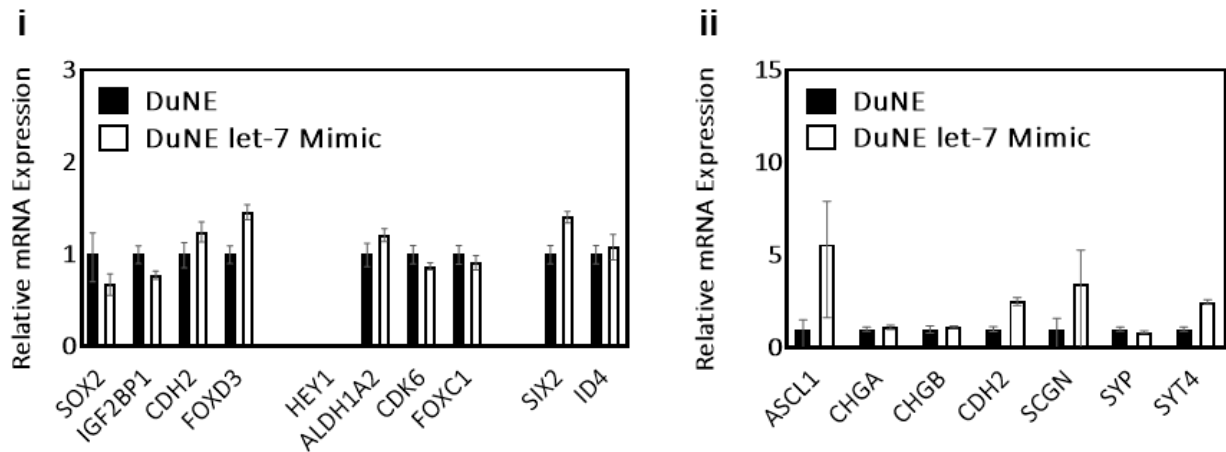
Appendix F. Altering LIN28B expression does not affect REST, NMYC, or EZH2 expression
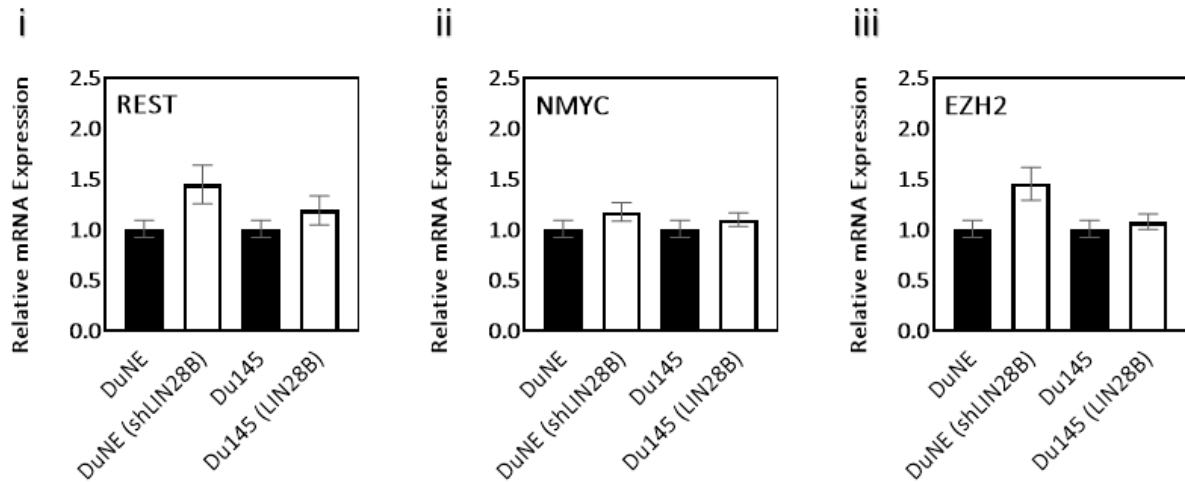
Appendix F. Altering LIN28B expression does not affect REST, NMYC, or EZH2 expression. Du145 and DuNE cells were transiently transfected with shLIN28B and LIN28B, respectively. RNA was extracted to measure the expression level of **(i)** REST, **(ii)** NMYC, and **(iii)** EZH2.Three independent technical replicates were performed for each experiment.

Appendix G. Altering let-7d expression does not affect stem cell or neuroendocrine markers

Appendix G. Altering let-7d expression does not affect stem cell or neuroendocrine markers. DuNE cells were transfected with Let-7-mimic and extracted for RNA to assess the expression level of **(i)** stem cell markers or **(ii)** neuroendocrine markers. Three independent technical replicates were performed for each experiment.